THE UNIVERSITY OF CALGARY

Maxima of Non-Stationary Gaussian Random Fields

by

Ingrid Farasyn

A THESIS

SUBMITTED TO THE FACULTY OF GRADUATE STUDIES

IN PARTIAL FULFILLMENT OF THE REQUIREMENTS FOR THE

DEGREE OF MASTER OF SCIENCE IN CIVIL ENGINEERING

DEPARTMENT OF CIVIL ENGINEERING

CALGARY, ALBERTA

APRIL, 1997

Abstract

In many structural reliability problems, the maxima of random fields are important. In most of the existing methods, those maxima are approximated using upcrossing techniques.

Sun's Tube Method uses a different approach. The method is based on geometrical concepts and it can be used to compute the maxima of both homogeneous and non-homogeneous Gaussian random fields.

Different discretizations to which this method is applicable are discussed. The special case of nonstationary stochastic processes is analyzed in detail. The method provides results that are in good agreement with simulation. The maxima of earthquake signals and structural responses to those signals are computed. Both linear and non-linear responses are discussed. It is indicated how the maxima of higher-dimensional random fields can be approximated.

Sun's Tube Method gives good results with little computational effort and there is hardly any restriction to the type of random fields that can be analyzed.

Acknowledgements

I would like to express my deep gratitude to all of those who supported me throughout my education and contributed in some way to the development of this research: my parents, my supervisor Dr. Maes and my fellow students Jim Gilliland and Luc Huyse.

Table of Contents

List of Tables

List of Figures

Chapter 1

Introduction

1.1 Scope

Stochastic processes and random fields are frequently used to model random influences on structures. A common feature of structural reliability techniques used in safety analysis is to reformulate the problem into a time-invariant one using the extreme value distribution of the random field or stochastic process. Therefore, it is important to have the best possible approximation of the maxima of these processes and fields. Most existing methods use some kind of upcrossing technique to establish those approximations. In this thesis a new method, first employed by Sun (1993), is studied. The method can be used to approximate the extreme value distribution of both homogeneous and non-homogeneous Gaussian random fields and processes. The main part of this thesis will focus on the application of Sun's Tube Method to stochastic processes.

In Chapter 2, the classical technique of upcrossings is discussed and some results from literature are given. In Chapter 3, different discretization methods are introduced. All those methods yield the format that is required to apply Sun's Tube Method. In Chapter 4, the method is introduced and discussed in detail. In Chapter 5, the results obtained using Sun's Tube Method are compared with simulation results for several random processes. In Chapter 6, two extensions of the method are given. It is discussed how the method can be used to compute the extreme value

distribution of non-linear responses and higher-dimensional random fields.

1.2 Objectives

The objectives of this thesis are to explore, test and implement the usage of Sun's Tube Method to compute the extreme value distribution of stochastic processes. The method will be tested by comparing the results of Sun's Tube Method with Monte Carlo simulation results. In order to fully understand the fundamentals of Sun's Method, the geometrical concepts on which the method is based, will be discussed in detail.

1.3 Preliminary Definitions

While 'random fields' are random functions defined over some Euclidean space, the term 'stochastic process' is used for the specific case where the random function is defined over a one-dimensional Euclidean space. An example of a stochastic process is the horizontal component of the ground acceleration during an earthquake. An example of a three-dimensional random field is the height of the ocean surface above a given point (t_1, t_2) at time t_3. In this Section, some definitions and properties of stochastic processes are given. A detailed study of the properties of stochastic processes can be found for instance in Lin (1967) or Papoulis (1991). For properties and definitions of higher-dimensional random fields, we refer to Section 6.2.

A stochastic process $X(t, \zeta)$ defined in an interval $[0, T]$ is a rule for assigning to every outcome ζ of an experiment S a function $X(t, \zeta)$. Thus a stochastic process is a family of time functions depending on the parameter ζ. The domain of ζ is the

set of all experimental outcomes and the domain of t is the interval $[0, T]$. A sample $x(t)$ of a stochastic process $X(t)$ is obtained by considering the function $X(t, \zeta)$ for a given outcome ζ. If t is fixed and all possible outcomes ζ are considered, then $X(t)$ is a random variable called the state of the given process at time t. In what follows, we shall use the notation $X(t)$ to represent a stochastic process, omitting its dependence on ζ.

A stochastic process $X(t)$ is a noncountable infinity of random variables, one for each t. To characterize this process completely in a probabilistic sense, it is necessary to establish $F(x_1, x_2, ..., x_m; t_1, t_2, ..., t_m)$, the joint distribution of the random variables $X(t_1), X(t_2), ...X(t_m)$:

$$F(x_1, x_2, ..., x_m; t_1, t_2, ..., t_m) = \Pr(X(t_1) < x_1, X(t_2) < x_2, ..., X(t_m) < x_m) \quad (1.1)$$

for every x_i, t_i and m. In Equation (1.1), $\Pr(A)$ denotes the probability that event A occurs. $F(x_1, x_2, ..., x_m; t_1, t_2, ..., t_m)$ is called the n^{th}-order distribution of the stochastic process $X(t)$. Usually in engineering fields, it is sufficient to establish only the first two of those distributions, i.e. $F(x_1; t_1)$ and $F(x_1, x_2; t_1, t_2)$.

The mean $\mu_X(t)$ of a stochastic process $X(t)$ is defined as:

$$\mu_X(t) = \mathbb{E}\{X(t)\} \quad (1.2)$$

In Equation (1.2), $\mathbb{E}\{X\}$ represents the expected value or mean of a random variable X defined by

$$\mathbb{E}\{X\} = \int_{-\infty}^{\infty} x f(x)\, dx \quad (1.3)$$

where $f(x)$ is the probability density function of the random variable X.

The autocorrelation function $R_{XX}(t_1, t_2)$ of the process $X(t)$ is given by

$$R_{XX}(t_1, t_2) = \mathbb{E}\{X(t_1) X(t_2)\} \tag{1.4}$$

When no confusion is possible, the notations $\mu(t)$ and $R(X_1, X_2)$ are used instead of $\mu_X(t)$ and $R_{XX}(t_1, t_2)$. The variance $\sigma_X^2(t)$ of a stochastic process is given by

$$\sigma_X^2(t) = \mathbb{E}\{X(t) X(t)\} = R(t, t) \tag{1.5}$$

A stochastic process $X(t)$ is called strict-sense stationary if its distributions (1.1) are invariant to a shift of the origin. This means that the processes $X(t)$ and $X(t + c)$ have the same distributions for any c.

A stochastic process $X(t)$ is called wide-sense stationary if the mean $\mu(t)$ of the process is constant and if the autocorrelation function depends only on the difference $\tau = t_2 - t_1$:

$$R(\tau) = \mathbb{E}\{X(t) X(t + \tau)\} \tag{1.6}$$

Notice that it follows from (1.5) and (1.6) that a wide-sense stationary process must have a constant variance.

A stochastic process is said to be a normal or Gaussian process if the random variables $X(t_1), X(t_2), ..., X(t_n)$ are jointly normal for any n and $t_1, t_2, ..., t_n$. A Gaussian process is completely determined in terms of its means and autocorrelation functions. Therefore, a wide-sense stationary normal process is also a strict-sense stationary process.

The power spectral density of a wide-sense stationary process $X(t)$ is the Fourier transform $S(\omega)$ of its autocorrelation function

$$S(\omega) = \frac{1}{2\pi} \int_{-\infty}^{\infty} R(\tau) e^{-j\omega\tau} d\tau \tag{1.7}$$

where j is the imaginary unit defined as $j^2 = -1$. The second order spectral moment λ_2 of a stochastic process $X(t)$ is given by:

$$\lambda_2 = 2 \int_0^{\infty} \omega^2 S(\omega)\, d\omega = -\left(\frac{d^2 R(\tau)}{d\tau^2} \right)_{\tau=0} \tag{1.8}$$

The maximum $M_X(T)$ of the stochastic process $X(t)$ in the interval $[0,T]$ is defined as:

$$M_X(T) = \max_{0 \le t \le T} (X(t)) \tag{1.9}$$

For a given process $X(t)$ and a specified interval $[0,T]$, $M_X(T)$ is a random variable. The distribution $P(\beta)$ of the maximum is called the extreme value distribution of the stochastic process $X(t)$ in the interval $[0,T]$:

$$P(\beta) = \Pr(M(T) > \beta) \tag{1.10}$$

where β is a specified level. If $X(t)$ represents for instance the load effect in a structural member and β is the structural resistance, then the structure will fail during $[0,T]$ with probability $P(\beta)$.

Chapter 2

Extremes of Stochastic Processes

2.1 Extremes Based on Level Upcrossings

Except for a few closed-form solutions discussed in Section 2.2, the large majority of approximate solutions to the problem of computing the maxima of stochastic processes is based on the concept of upcrossings. One uses the fact that the maximum of a process will exceed a level β if there is at least one upcrossing of that level. Several authors discuss this upcrossing technique in detail (Adler, 1981 - Breitung, 1994 - Papoulis, 1991). The fundamental ideas of this approach are given in this Section.

Let $X(t)$ be a stochastic process defined in the interval $[0,T]$. Then $X(t)$ is said to have an upcrossing of the level β at the point t_0 if there exists an $\varepsilon > 0$ such that $X(t) \leq \beta$ in $[t_0 - \varepsilon, t_0]$ and $X(t) \geq \beta$ in $[t_0, t_0 + \varepsilon]$. The number of such points t_0 in $[0,T]$ is called the number of upcrossings of β by $X(t)$ in $[0,T]$, and it is denoted $N_\beta(T)$. Note that this number $N_\beta(T)$ is a discrete random variable for a given level β and a specified length of time T. An example is given in Figure 2.1. For the process $X(t)$ in that Figure, $N_\beta(T)$ equals 3. The rate of upcrossings is defined as the number of upcrossings per unit time. A well know result by Rice (1944, 1945) gives the expected value $\upsilon(t)$ of the rate of upcrossing:

$$\upsilon(t) = \boldsymbol{E}\left\{\lim_{\Delta T \to 0} \frac{N_\beta(\Delta T)}{\Delta T}\right\} = \int_{-\infty}^{0} \dot{x} f_{x\dot{x}}(\beta, \dot{x}, t)\, d\dot{x} \tag{2.1}$$

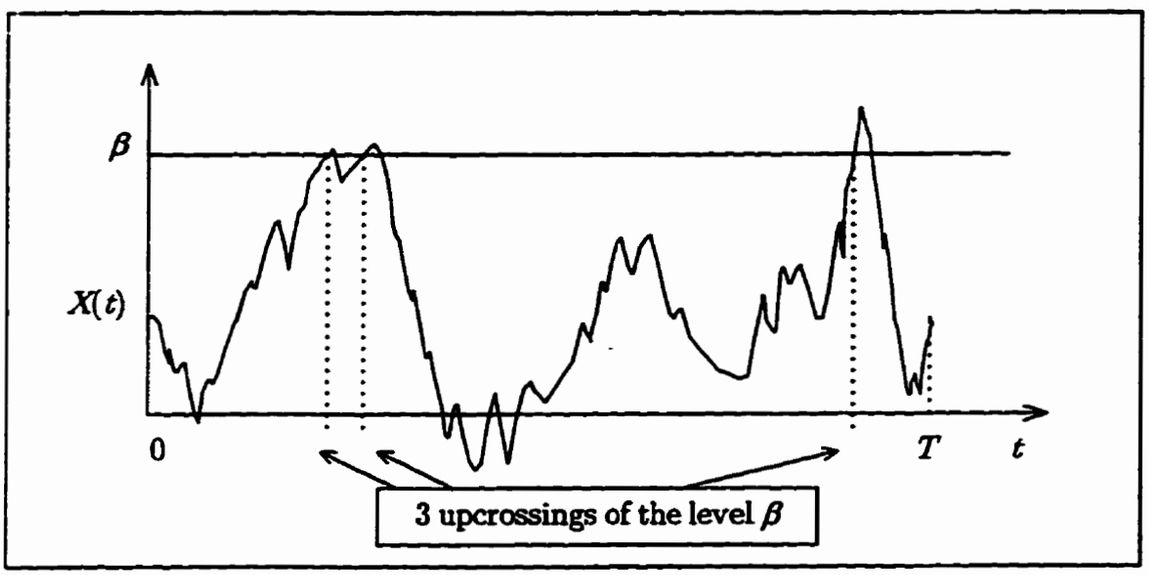

Figure 2.1: Upcrossings of the Level β by a Stochastic Process $X(t)$

where a superposed dot indicates the derivative with respect to time and $f_{x\dot{x}}(x, \dot{x}, t)$ is the joint probability density function of $x(t)$ and its derivative $\dot{x}(t)$ at time t.

In the case of a zero-mean, stationary, Gaussian process $X(t)$, we can use formula (2.1) to compute the expected number of upcrossings $N_\beta(T)$ of the level β in the interval $[0, T]$:

$$\mathbb{E}\{N_\beta(T)\} = \frac{1}{2\pi}\sqrt{\frac{-\ddot{R}(0)}{R(0)}}\exp\left(-\frac{\beta^2}{2R(0)}\right) \tag{2.2}$$

where $R(\tau)$ is the autocorrelation function of the stationary process $X(t)$ as defined in Section 1.3. This formula is now used to establish an upperbound for the extreme value distribution $M_X(T)$ (1.9) of a stationary Gaussian process $X(t)$:

$$\Pr(M_X(T) \geq \beta) \tag{2.3}$$

$$= \Pr(X(0) \geq \beta \text{ or } N_\beta(T) \geq 1) \tag{2.4}$$

$$= \Pr(X(0) \geq \beta) + \Pr P(N_\beta(T) \geq 1) - \Pr(X(0) \geq \beta \text{ and } N_\beta(T) \geq 1) \quad (2.5)$$

$$\leq \Pr(X(0) \geq \beta) + \Pr(N_\beta(T) \geq 1) \quad (2.6)$$

$$\leq \Pr(X(0) \geq \beta) + \mathbb{E}\{N_\beta(T)\} \quad (2.7)$$

Insertion of Rice's formula (2.2) in (2.7) yields an upperbound for the extreme value distribution $M_X(T)$ of a stationary Gaussian random process. It is clear that one would expect the upper bound to be very tight if β is a high level.

It can be proven that for some special processes, Equation (2.7) actually gives the exact extreme value distribution. One of those processes is the stationary normal process $\xi(t)$ defined in $[0, T]$ by

$$\xi(t) = X_1 \cos(\omega t) + X_2 \sin(\omega t) \quad (2.8)$$

where ω is a fixed constant and where X_1 and X_2 are independent, standard normal random variables. It is assumed that

$$0 < T < \frac{\pi}{\omega} \quad (2.9)$$

Due to this restriction on the length of the interval $[0, T]$, the probability

$$\Pr(X(0) \geq \beta \text{ and } N_\beta(T) \geq 1) \quad (2.10)$$

in Equation (2.5) is equal to zero. Furthermore, the random variable $N_\beta(T)$ can only take on the values 0 or 1 for values of T satisfying (2.9). Therefore, the upperbound

(2.7) is in fact the exact extreme value distribution for this specific process $\xi(t)$:

$$\Pr(M_\xi(T) \geq \beta) = \Pr(\xi(0) \geq \beta) + \boldsymbol{E}\{N_\beta(T)\} \tag{2.11}$$

$$= 1 - \Phi(\beta) + \frac{\omega T}{2\pi} \exp\left(-\frac{\beta^2}{2}\right) \tag{2.12}$$

where $\Phi(\cdot)$ denotes the standard normal distribution. This analytical result will be compared with the result obtained using Sun's Tube Method in Section 5.2.1.

2.2 Results in Literature

Exact formulas for the extreme value distribution of a stochastic process exist only for a limited number of processes. One of those processes is the process $\xi(t)$ defined in (2.8). Other examples can be found in Adler (1990). For several other cases, approximations exist. Those approximations are all derived on the basis of upcrossings as described in Section 2.1. Rather than listing the resulting formulas, we will indicate where they can be found.

Approximations for stationary processes with a finite second order spectral moment λ_2 (See Section 1.3) are given in Cramer and Leadbetter (1967) and Leadbetter et al. (1983). Approximations for maxima of functions of stationary Gaussian vector processes (vectors with components that are stochastic processes) are discussed in Breitung (1994, Chapter 8). Bounds for univariate non-stationary Gaussian processes and for functions of non-stationary Gaussian vector processes are derived in Breitung (1990).

The main problem of methods based on upcrossings is to prove that the obtained

approximations are not just upperbounds, but that they are also asymptotically correct. This is usually done by proving that the approximating point processes converge to a Poisson process which involves much more complicated mathematics than the derivation of the approximation itself.

The method discussed in this thesis uses a totally different approach, based on Sun's Tube Method (1993). A direct approximation of the maximum distribution is used so that assumptions about upcrossings are unnecessary. Derivation of the final formula is straightforward and the method can be applied to a wide range of discretizations.

Chapter 3

Discretization of Stochastic Processes

In order to use Sun's method to compute the extreme value distribution of a stochastic process, the process has to be represented in a specific discretized format. In Section 3.1, the discretized format, required to apply Sun's tube method is discussed. In Sections 3.2 through 3.4 different discretization methods that have the necessary format are introduced. The methods discussed in Section 3.2 and 3.3 can easily be adapted to higher dimensional random fields. Section 3.4 describes a discretization that is particularly well suited to model earthquake signals and their structural responses.

3.1 Format Required to Apply Sun's Method

Let $X(t)$ denote a zero-mean, Gaussian random process defined in $[0,T]$. This process is not necessary stationary. Since the process is Gaussian, it is completely defined by the autocorrelation function (ACF):

$$R_{XX}(t_1,t_2) = \mathbb{E}\{X(t_1)\,X(t_2)\} \tag{3.1}$$

and the variance function

$$\sigma_X^2(t) = R_{XX}(t,t) = \mathbb{E}\{X(t)\,X(t)\} \tag{3.2}$$

This process $X(t)$ is now discretized to $\hat{X}(t)$:

$$X(t) \rightarrow \hat{X}(t) = \sum_{i=1}^{N} X_i f_i(t) \tag{3.3}$$

The X_i's are a sequence of independent standard normal random variables (zero mean, unit variance and zero correlation) and the functions $f_i(t)$ are a set of deterministic functions. This specific format, basically a linear combination of standard normal random variables and deterministic functions, is the format that is required to apply Sun's Method. Several discretization methods yield this format, as is shown in the following Sections.

Note that due to the independence of the standard normal random variables X_i in (3.3):

$$R_{\hat{X}\hat{X}}(t_1, t_2) = \sum_{i=1}^{N} f_i(t_1) f_i(t_2) \tag{3.4}$$

and

$$\sigma^2_{\hat{X}}(t) = R_{\hat{X}\hat{X}}(t, t) = \sum_{i=1}^{N} f_i^2(t) \tag{3.5}$$

3.2 Truncated Karhunen-Loève Expansion

One possibility is to represent a Gaussian process $X(t)$ using an eigenfunction expansion. This expansion, the Karhunen-Loève Expansion, is discussed extensively in literature (Adler, 1981 - Papoulis, 1991 - Li and Der Kiureghian, 1993). The basic concepts are given here for the one-dimensional case of a stochastic process.

The random process is expressed in terms of its spectral decomposition:

$$X(t) = \sum_{i=1}^{\infty} X_i \left(\sqrt{\lambda_i} h_i(t) \right) \tag{3.6}$$

where the X_i's are independent standard normal random variables. λ_i and $h_i(t)$ are the eigenvalues and eigenfunctions respectively of the covariance function obtained from the integral equation

$$\int_0^T R(t_1, t_2) h_i(t_1) dt_1 = h_i(t_2) \qquad i = 1, 2, ... \tag{3.7}$$

The eigenfunctions $h_i(t)$ are normalized to satisfy:

$$\int_0^T h_i(t) h_j(t) dt = \delta_{ij} \tag{3.8}$$

Furthermore, it is assumed that the eigenvalue sequence λ_i is decreasing.

The random process $X(t)$ is represented by an infinite set of random variables $X_i, i = 1, 2, ...$ (3.6). However, usually only the few terms with the larger eigenvalues contribute significantly to the expansion. Since it is assumed that the eigenvalues are ordered in decreasing magnitude, the process $X(t)$ can be approximated by $\hat{X}(t)$:

$$X(t) \rightarrow \hat{X}(t) = \sum_{i=1}^{N} X_i \left(\sqrt{\lambda_i} h_i(t) \right) \tag{3.9}$$

where N is the number of terms that are included in the discretization. This is a discretization which meets the requirements set out in Section 3.1. Provided that the exact eigenfunctions of the autocovariance function are available, this method

is the most efficient method for discretizing a random process, i.e. it requires the smallest number of random variables to describe the process within a given level of accuracy (Li and Der Kiureghian, 1993). Unfortunately, for most autocorrelation functions, the exact solutions of the integral (3.8) are not available in closed form In this case, approximate methods have to be used. Basically, the integral problem (3.8) can be converted into a matrix eigenvalue problem using a discrete integration rule or a Galerkin-type approximation (See Mura and Koya, 1992). However, Li and Der Kiureghian (1993) prove that these approximate implementations of the Karhunen-Loève expansion are inferior to the method described in Section 3.3.

3.3 Expansion Optimal Linear Estimation Method

Li and Der Kiureghian (1993) suggest the use of the Expansion Optimal Linear Estimation Method to discretize non-homogeneous Gaussian random fields. In this Section, the fundamental concepts of this method are described for the case of a zero-mean Gaussian random process. In Section 3.3.1, the Optimal Linear Estimation Method is discussed. While the discretizations obtained with this method do not satisfy the requirements set out in Section 3.1, they are the starting point for the Expansion Optimal Linear Estimation Method (See Section 3.3.2). It will be shown that this expansion method yields discretizations that do satisfy the necessary requirements for Sun's Tube Method.

3.3.1 Optimal Linear Estimation Method

The stochastic process $X(t)$ in $[0,T]$ is described as the scalar product of a vector of M nodal values

$$\mathbf{V} = (V_1, V_2, ..., V_M) = (X(t_1), X(t_2), ..., X(t_M)) \tag{3.10}$$

and a vector of deterministic functions

$$\mathbf{b}(t) = (b_1(t), b_2(t), ..., b_M(t)) \tag{3.11}$$

Writing $\langle \mathbf{x}, \mathbf{y} \rangle$ for the scalar product of two vectors $\mathbf{x}$ and $\mathbf{y}$, we have:

$$X(t) \rightarrow \hat{X}(t) = \langle \mathbf{V}, \mathbf{b}(t) \rangle = \sum_{i=1}^{M} V_i b_i(t) \tag{3.12}$$

in which M is the number of nodal points in the interval $[0,T]$. The functions $b_i(t)$ are to be determined by minimizing the variance of the discretization error subject to $\hat{X}(t)$ being an unbiased estimator of $X(t)$ in the mean. Therefore we minimize

$$\mathbb{E}\left\{\left|X(t) - \hat{X}(t)\right|^2\right\} \tag{3.13}$$

subject to

$$\mathbb{E}\left\{\hat{X}(t)\right\} = 0 \tag{3.14}$$

The solution is (Li and Der Kiureghian, 1993):

$$\mathbf{b}(t) = \mathbf{C}^{-1}\mathbf{a}(t) \tag{3.15}$$

In Equation (3.15), $\mathbf{a}(t)$ is the vector containing the covariances of $X(t)$ with the elements of the vector $\mathbf{V}$:

$$\mathbf{a}(t) = \begin{pmatrix} \mathbb{E}\{X(t) \cdot V_1\} \\ \mathbb{E}\{X(t) \cdot V_2\} \\ \vdots \\ \mathbb{E}\{X(t) \cdot V_M\} \end{pmatrix} = \begin{pmatrix} R_{XX}(t, t_1) \\ R_{XX}(t, t_2) \\ \vdots \\ R_{XX}(t, t_M) \end{pmatrix} \tag{3.16}$$

and $\mathbf{C}$ is the covariance matrix:

$$\mathbf{C} = \begin{bmatrix} R(t_1, t_1) & R(t_1, t_2) & \cdots & (t_1, t_M) \\ R(t_1, t_2) & R(t_2, t_2) & & \\ \vdots & & \ddots & \\ R(t_1, t_M) & & & (t_M, t_M) \end{bmatrix} \tag{3.17}$$

Among all linear representations of $X(t)$ in terms of the nodal random variables $X(t_i) = V_i$, the preceding representation is optimal in the sense that it minimizes the error in the variance (3.13) at any given time. This is particularly desirable for the Gaussian distribution, which is completely defined by means of its mean and variance. The Optimal Linear Estimation Method constructs the random process by employing shape functions that take into account the correlation structure of the process. This is the key to the superior accuracy of this method, as is illustrated in Li and Der Kiureghian (1993).

The random variables V_i are dependent and do not have unit variance. Hence, the method as explained in this section does not satisfy the requirements set out in Section 3.1. The Expansion Optimal Linear Estimation Method offers a remedy

to this problem and, in addition, it improves the efficiency of the Optimal Linear Estimation Method.

3.3.2 Expansion Optimal Linear Estimation Method

Assuming that **C** is non-singular, the M-dimensional vector **V** can be expressed in terms of its spectral decomposition:

$$\mathbf{V} = \sum_{i=1}^{M} X_i \sqrt{\theta_i} \mathbf{\Phi}_i \tag{3.18}$$

where the X_i's are independent standard normal random variables. θ_i and $\mathbf{\Phi}_i$ are the eigenvalues and eigenvectors of the covariance matrix **C** (3.17) obtained by solving the eigenvalue problem

$$\mathbf{C}\mathbf{\Phi}_i = \theta_i \mathbf{\Phi}_i \qquad\qquad i = 1, 2, ..., M \tag{3.19}$$

The eigenvectors are normalized such that

$$\langle \mathbf{\Phi}_i, \mathbf{\Phi}_j \rangle = \delta_{ij} \tag{3.20}$$

Furthermore, it is assumed that the eigenvalues in (3.18) are ordered by decreasing magnitude. Equations (3.18) and (3.19) are now combined with (3.12). This gives the following discretization for the random process $X(t)$:

$$X(t) \rightarrow \hat{X}(t) = \sum_{i=1}^{M} \frac{X_i}{\sqrt{\theta_i}} \langle \mathbf{\Phi}_i, \mathbf{a}(t) \rangle \tag{3.21}$$

where $\mathbf{a}(t)$ is defined in (3.16). We have now established a discretization (3.21) that meets the requirements discussed in Section 3.1.

The efficiency of this method can be improved by using a subset $N < M$ of the terms in (3.21) corresponding to the largest eigenvalues:

$$X(t) \rightarrow \hat{X}^*(t) = \sum_{i=1}^{N} \frac{X_i}{\sqrt{\theta_i}} \langle \Phi_i, \mathbf{a}(t) \rangle \tag{3.22}$$

This enables us to reduce the number of random variables that describe the stochastic process $X(t)$. Li and Der Kiureghian (1993) prove that the error resulting from this truncation is non-oscillatory, i.e. the truncation of each term further reduces the variance of the discretization error.

3.4 Discretization of an Earthquake Signal

3.4.1 Introduction

In this Section, an approach that is particularly well suited to model earthquake ground motions and responses to ground motions is discussed. This approach was first introduced by Der Kiureghian and Li (1996). It will be shown how both temporal and spectral non-stationarity can be modeled.

Although the Karhunen-Loève expansion offers the most efficient discretization in terms of error variance,

$$\boldsymbol{E}\left(\left|X(t) - \hat{X}(t)\right|^2\right) \tag{3.23}$$

it requires the solution of an integral eigenvalue problem (3.8) that can be very large for broad-band processes, such as earthquake ground motions. Typically, such

motions have a zero mean and are approximately Gaussian. Therefore, the ground motion $X(t)$ can be represented in the following discretized form:

$$\hat{X}(t) = \sum_{i=1}^{N} W_i a_i(t) \tag{3.24}$$

N represents the number of discretization functions. The coefficients W_i, $i = 1, 2, ..., N$ are Gaussian random variable with zero mean and variance σ_i^2. The functions $a_i(t)$ are a set of deterministic functions that will be determined in this Section.

$X(t)$ can now be considered as the response of a linear filter to a white noise excitation $W(t)$. The white noise can be thought of as the broad-band excitation at the bedrock level and the filter can be imagined to represent the local soil system or wave propagation path. Instead of discretizing $X(t)$ directly, the trick is to discretize $W(t)$.

Let t_i, $i = 0, 1, ..., N$, denote a set of closely and equally spaced time points at intervals $\Delta t = t_i - t_{i-1}$. We can now define a sequence of random pulses with magnitudes

$$W_i = \int_{t_{i-1}}^{t_i} W(t)\, dt \qquad i = 1, 2, ..., N \tag{3.25}$$

It can now be shown (See Appendix A) that W_i are statistically independent Gaussian random variables with zero mean and constant variance

$$\sigma_i^2 = \sigma^2 = 2\pi\Phi_0\Delta t \tag{3.26}$$

where the intensity Φ_0 is the constant power spectral density (See Section 1.3) of the white noise $W(t)$. The sequence W_i, $i = 1, 2, ..., N$ represents $W(t)$ in the discrete

form of a random pulse train.

Expression for the Unit-Impulse Response Function $h_f(t)$

A natural choice for the deterministic function $a_i(t)$ in (3.24) is

$$a_i(t) = h_f(t - t_i) \tag{3.27}$$

where $h_f(t)$ is the unit-impulse response function of the filter. $h_f(t)$ can be obtained by considering a second order linear filter (the local soil) subjected to a white noise input (the wide band excitation at the bedrock level). The equation of motion can be expressed as:

$$\ddot{u}_f(t) + 2\zeta_f\omega_f\dot{u}_f(t) + \omega_f^2 u_f(t) = -W(t) \tag{3.28}$$

In (3.28), ω_f represents the natural frequency of the soil and ζ_f represents its damping ratio. So ω_f and ζ_f respectively control the predominant frequency and the bandwidth of the motion. u_f is the displacement of the soil layer relative to the bedrock. The above concepts are illustrated in Figure 3.1. Of interest is the absolute acceleration $X(t)$ of the filter, which with the above interpretation is the same as the absolute acceleration at the ground surface (See Figure 3.1):

$$X(t) = \ddot{u}_f(t) + W(t) \tag{3.29}$$

It can be verified (Der Kiureghian and Li, 1996) that the unit-impulse-response function for the absolute acceleration of the ground surface is given by:

$$h_f(t) = -\left(C_1 \sin(\omega_d t) + C_2 \cos(\omega_d t)\right) \exp\left(-\zeta_f \omega_f t\right) \tag{3.30}$$

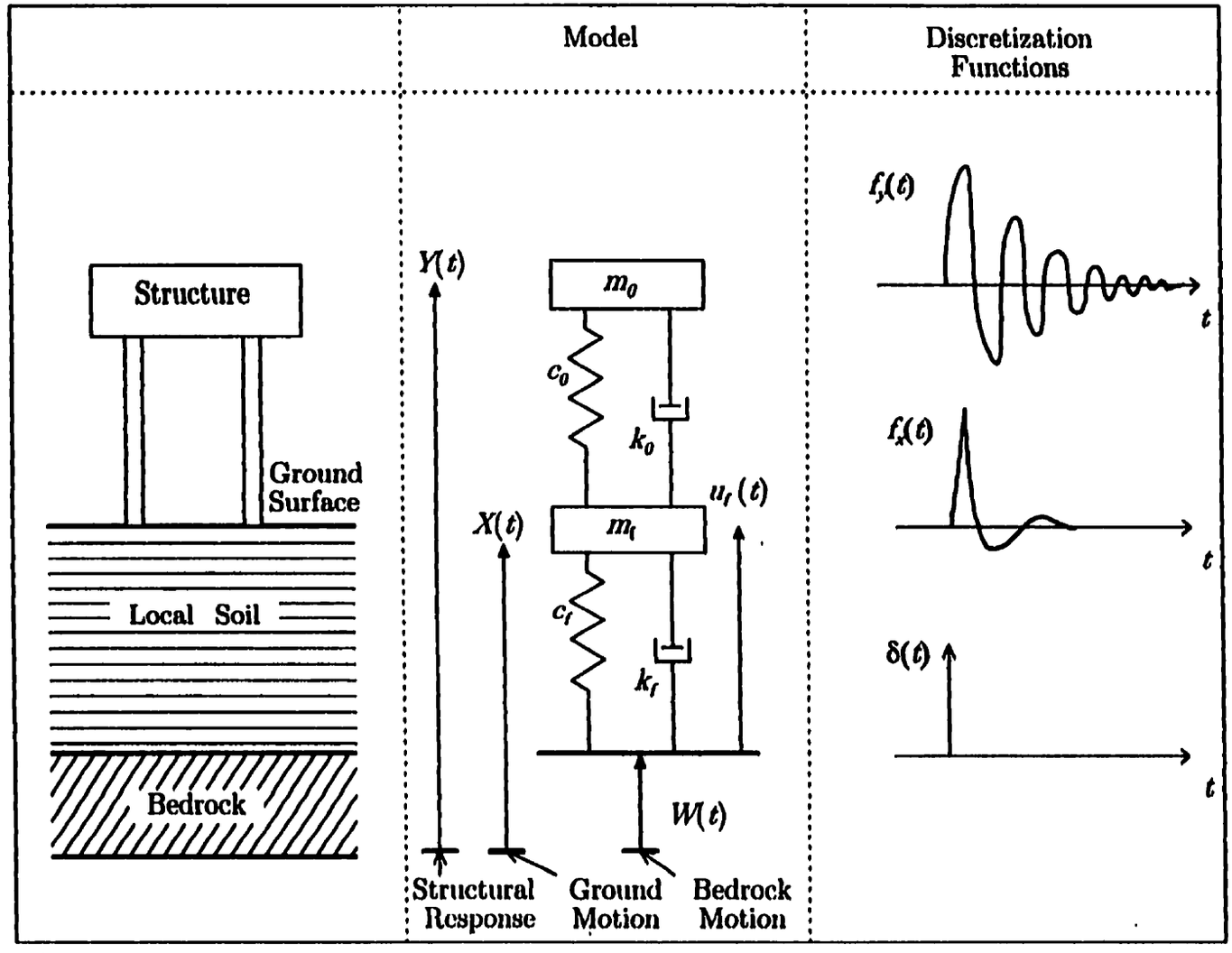

Figure 3.1: Model Used to Discretize Earthquake Signals and Stochastic Responses to Earthquake Signals

with

$$\omega_d = \omega\sqrt{1-\zeta_f^2} \tag{3.31}$$

$$C_1 = \frac{\omega_f\left(1-2\zeta_f^2\right)}{\sqrt{1-\zeta_f^2}} \tag{3.32}$$

$$C_2 = 2\zeta_f\omega_f \tag{3.33}$$

Optimal Choice for the Discretization Function $a_i(t)$

While the unit-impulse response function is a natural choice for the discretization functions $a_i(t)$ in (3.24), it is not the best choice. A better choice is obtained by minimizing the variance of the discretization error (3.23) relative to $a_i(t)$, with $X(t)$ denoting the exact solution of the filter response to the white noise input. It can be proven (See Appendix A) that minimization of (3.23) leads to:

$$a_i(t) = \frac{1}{\Delta t}\int_{\min(t,t_{i-1})}^{\min(t,t_i)} h(t-\tau)\,d\tau \tag{3.34}$$

where $h(t)$ is defined in (3.30). Insertion of (3.30) in (3.34) gives the following expression for $a_i(t)$:

$$a_i(t) = \begin{cases} 0 & t < t_{i-1} \\ \frac{1}{\Delta t\sqrt{1-\zeta_f^2}}\left\{\exp\left(-\zeta_f\omega_f\left(t-t_{i-1}\right)\right)\sin\left(\omega_d\left(t-t_{i-1}\right)-\theta\right)\right\} & \\ +\frac{1}{\Delta t} & t_{i-1} \le t \le t_i \\ \frac{1}{\Delta t\sqrt{1-\zeta_f^2}}\left\{\exp\left(-\zeta_f\omega_f\left(t-t_{i-1}\right)\right)\sin\left(\omega_d\left(t-t_{i-1}\right)-\theta\right)\right. & \\ \left.-\exp\left(-\zeta_f\omega_f\left(t-t_i\right)\right)\sin\left(\omega_d\left(t-t_i\right)-\theta\right)\right\} & t_i < t \end{cases} \tag{3.35}$$

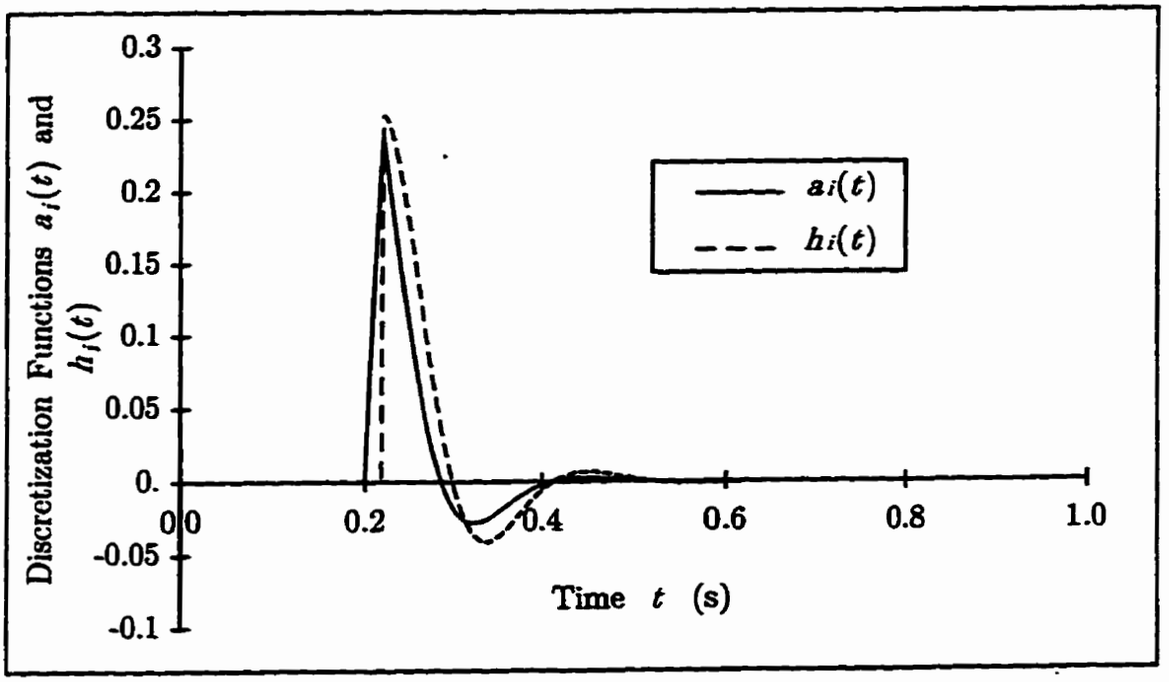

Figure 3.2: Two Options for the Discretization Functions of a Ground Acceleration Process

with

$$\theta = \arccos(\zeta_f) \tag{3.36}$$

Both options for the discretization functions ($h(t-t_i)$ and $a_i(t)$ as defined in respectively (3.30) and (3.35)) are plotted in Figure 3.2. The difference between the two functions is minimal for small values of Δt. However, one important difference between the two functions is that the function $a_i(t)$ as defined in (3.35) is continuous. As is discussed in Section 4.3, this property simplifies the use of Sun's Tube Method significantly.

3.4.2 Modeling of Non-Stationarity

The above discretization defines a stationary process. Earthquake motions, however, are typically nonstationary in both the time and frequency domain.

To account for temporal nonstationarity, the pulse train (3.25) is multiplied by a deterministic modulation function $q(t)$. The discrete representation (3.24) then becomes:

$$\hat{X}(t) = \sum_{i=1}^{N} W_i q(t_i) a_i(t) \tag{3.37}$$

The following modulation function is used:

$$q(t) = \begin{cases} 0 & t_0 \geq t \\ q_0 \left\{ \exp\left[-a(t-t_0)\right] - \exp\left[-b(t-t_0)\right] \right\} & \\ & t_0 < t \end{cases} \tag{3.38}$$

where q_0, a, b and t_0 are constants. For $a < b$, the above function is non-negative and, as is typical of the intensity of earthquake motions, it gradually increases from zero at $t = t_0$ to a peak value at $t = t_0 + (\ln b - \ln a) / (b - a)$ and then decays towards zero for large t. An example of such a modulation function is given in Figure 3.3.

To account for spectral nonstationarity, 2 filters, each with their own modulation function $q_k(t)$ are considered.

$$\hat{X}(t) = \sum_{i=1}^{N} W_i \sum_{k=1}^{2} q_k(t_i) a_{ik}(t) \tag{3.39}$$

In (3.39), $a_{ik}(t)$ denotes the deterministic function obtained from (3.35) in terms of the unit-impulse-response function of the k^{th} filter.

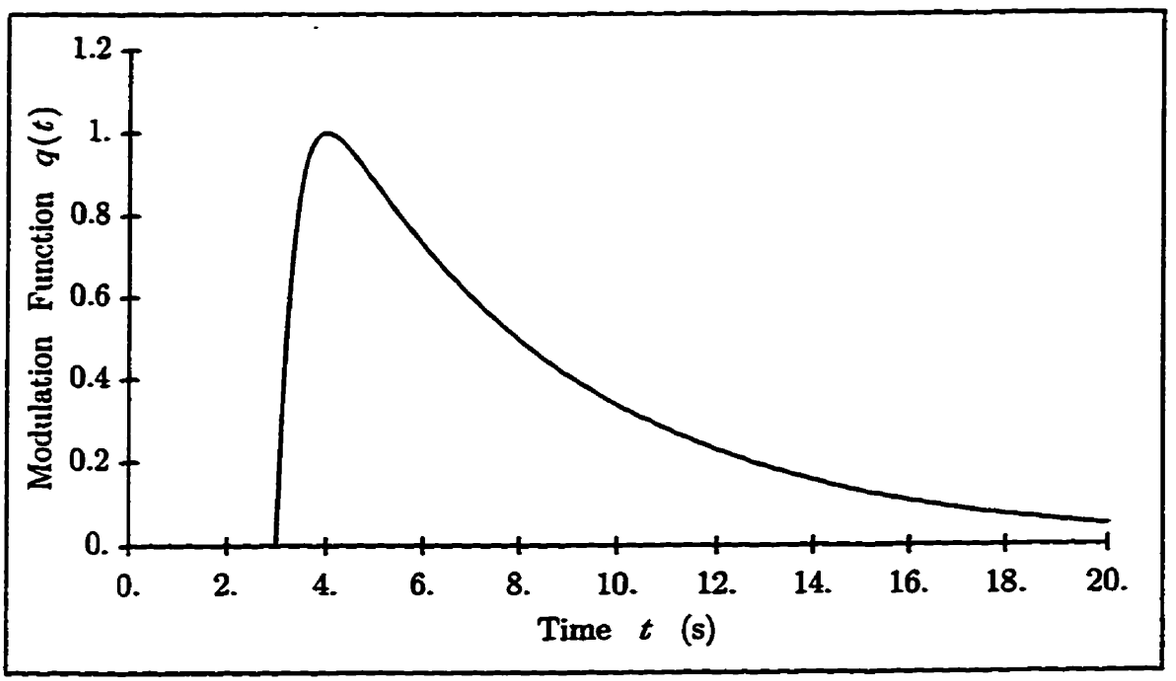

Figure 3.3: Modulation Function $q(t)$

By choosing appropriate values for the filter properties and for the parameters in the modulation function, any type of spectral and temporal nonstationarity can be accounted for.

If we introduce

$$W_i = X_i \sigma \tag{3.40}$$

where σ is defined in Equation (3.26) and X_i is a standard normal random variable, we can write Equation (3.39) as

$$\hat{X}(t) = \sum_{i=1}^{N} X_i f_i(t) \tag{3.41}$$

In expression (3.41) f_i is defined by

$$f_i(t) = \sum_{k=1}^{2} \sigma q_k(t_i)\, a_{ik}(t) \tag{3.42}$$

Note that this is exactly the format (3.3) required to apply Sun's Tube Method.

3.4.3 Linear Stochastic Structural Responses

The previous discussion illustrates how the required discrete format can be constructed for a seismic ground motion process. However, it should be emphasized that any stochastic response $\hat{Y}(t)$ of a linear system subject to this ground motion process $\hat{X}(t)$ can be obtained in the same discrete format. Let $h_Y(t)$ be the unit-impulse-response function of the linear filter to which the earthquake signal is applied and $f_{iY}(t)$ the response of the linear filter to an input function $f_i(t)$ (3.42). Since linear systems are considered, the response $f_{iY}(t)$ to one of the functions $f_i(t)$ can be computed using convolution (Clough and Penzien, 1975):

$$f_{iY}(t) = \int_0^t f_i(\tau)\, h_Y(t-\tau)\, d\tau \tag{3.43}$$

The stochastic response $\hat{Y}(t)$ can now be written as

$$\hat{Y}(t) = \sum_{i=1}^{N} X_i f_{iY}(t) \tag{3.44}$$

which is exactly the format required to apply Sun's Tube Method. In Section 5.4.1, the above technique is used to model the displacement of a linear filter subjected to an earthquake ground motion.

3.4.4 Non-Linear Stochastic Structural Responses

In Section 6.1, it will be shown how Sun's Tube Method can be applied to non-linear responses.

3.5 Linear Combination of Sine and Cosine Functions

A special kind of cyclic process results from the linear combination of sine and cosine functions.

$$\hat{X}(t) = \sum_{i=1}^{N} (X_{1k} a_k \sin(\omega_k t) + X_{2k} b_k \cos(\omega_k t)) \tag{3.45}$$

with X_{1i} and X_{2i}, $i = 1,..N$ standard normal random variables and a_i and b_i, the coefficient of respectively the sine and cosine functions. Note that the discretization (3.45) has the format needed to apply Sun's Tube Method.

A stationary process can be obtained by choosing:

$$a_k = b_k = c_k \qquad\qquad k = 1, 2, ..., N \tag{3.46}$$

and then

$$\sigma^2_{\hat{X}}(t) = \sum_{i=1}^{N} c_k^2 \tag{3.47}$$

Although the processes resulting from (3.45) do not have direct practical applications, these processes are a good tool to understand the principles of Sun's Tube method and the geometry of the N-dimensional unit sphere, as is described in Section 5.2.

Chapter 4

Sun's Tube Method

In this Chapter, the fundamentals of Sun's Method are discussed. In Section 4.1, a spherical representation of discretized stochastic processes is introduced. This representation is the starting point for the derivation of Sun's Formula in Section 4.2. Section 4.3 deals with the probabilities associated with endpoints and discontinuities. In Section 4.4, Sun's Formula is discussed. Section 4.5 illustrates how other statistics associated with the extreme value can be computed using Sun's Formula. In Section 4.6, it is shown how Sun's Formula can easily be used to compute the extreme value distribution of non-zero-mean Gaussian Processes.

Sun's Tube Method is mostly based on geometrical principles. While it is tedious to interpret the derivation in higher dimensions, it is intuitive if one thinks about it in three dimensions ($N = 3$). To facilitate this interpretation, several Figures are included. Those Figures are purely indicative and do not have the pretention of being exact.

4.1 Spherical Representation of a Discretized Random Process

It is assumed that the random process $\hat{X}(t)$ is represented in the discretized format discussed in Section 3.1:

$$\hat{X}(t) = \sum_{i=1}^{N} X_i f_i(t) \tag{4.1}$$

with $X_i,\ i = 1, 2, ..., N$ a sequence of independent standard normal random variables and the functions $f_i(t)$ a set of deterministic functions. Different types of discretization that yield this format, have been discussed in the previous chapter.

Without loss of generality, it is assumed that the process is scaled in such a way that

$$0 < \sigma_{\hat{X}}^2 \leq 1 \tag{4.2}$$

over the entire time interval $[0, T]$ and that its peak value in this interval is exactly equal to 1. Note that this requirement can always be met by considering the scaled process

$$\hat{X}_S(t) = \frac{\hat{X}(t)}{\sqrt{\max_{t\in[0,T]} \sigma_{\hat{X}}^2}} \tag{4.3}$$

The discretized process (4.1) can be rewritten as the scalar product of a constant random vector

$$\mathbf{X} = (X_1, X_2, ..., X_N) \tag{4.4}$$

and a deterministic, time-dependent vector

$$\mathbf{f}(t) = (f_1(t), f_2(t), ..., f_N(t)) \tag{4.5}$$

to yield

$$\hat{X}(t) = \langle \mathbf{X}, \mathbf{f}(t) \rangle \tag{4.6}$$

The vector $\mathbf{X}$ is a standard normal random vector and it can therefore be written as the following product:

$$\mathbf{X} = |\mathbf{X}| \cdot \frac{\mathbf{X}}{|\mathbf{X}|} = R_N \cdot \mathbf{U} \tag{4.7}$$

- The random variable R_N in Equation (4.7) represents the length of the random vector $\mathbf{X}$:

$$R_N = \sqrt{|\mathbf{X}|^2} \tag{4.8}$$

From Equation (4.8), it is clear that R_N is the square root of a χ^2-random variable with N degrees of freedom (Wiley, 1972). Therefore, R_N is said to be a χ_N-random variable. The probability density function of this χ_N-random variable is

$$f_{\chi_N}(r) = \begin{cases} 0 & r < 0 \\ \frac{2^{1-\frac{N}{2}} r^{N-1}}{\Gamma\left(\frac{N}{2}\right)} \exp\left(-\frac{r^2}{2}\right) & r \geq 0 \end{cases} \tag{4.9}$$

This density function is plotted for 5, 20 and 100 degrees of freedom in Figure 4.1.

- The random vector $\mathbf{U}$ in Equation (4.7) is defined by:

$$\mathbf{U} = \left(\frac{X_1}{|\mathbf{X}|}, \frac{X_2}{|\mathbf{X}|}, ..., \frac{X_N}{|\mathbf{X}|}\right) \tag{4.10}$$

$\mathbf{U}$, a vector with unit length, has a uniform distribution on the N-dimensional unit sphere. The N-dimensional unit sphere S^N in the N-dimensional space $\mathcal{R}^N$ is the locus of a point $\mathbf{y}$ which is at a constant distance 1 from the origin:

$$S^N = \left\{\mathbf{y} : \mathbf{y} = (y_1, y_2, ..., y_N), \sum_{i=1}^{N} y_i^2 = |\mathbf{y}|^2 = 1\right\} \tag{4.11}$$

Furthermore, it can be proven that the random vector $\mathbf{U}$ is independent of

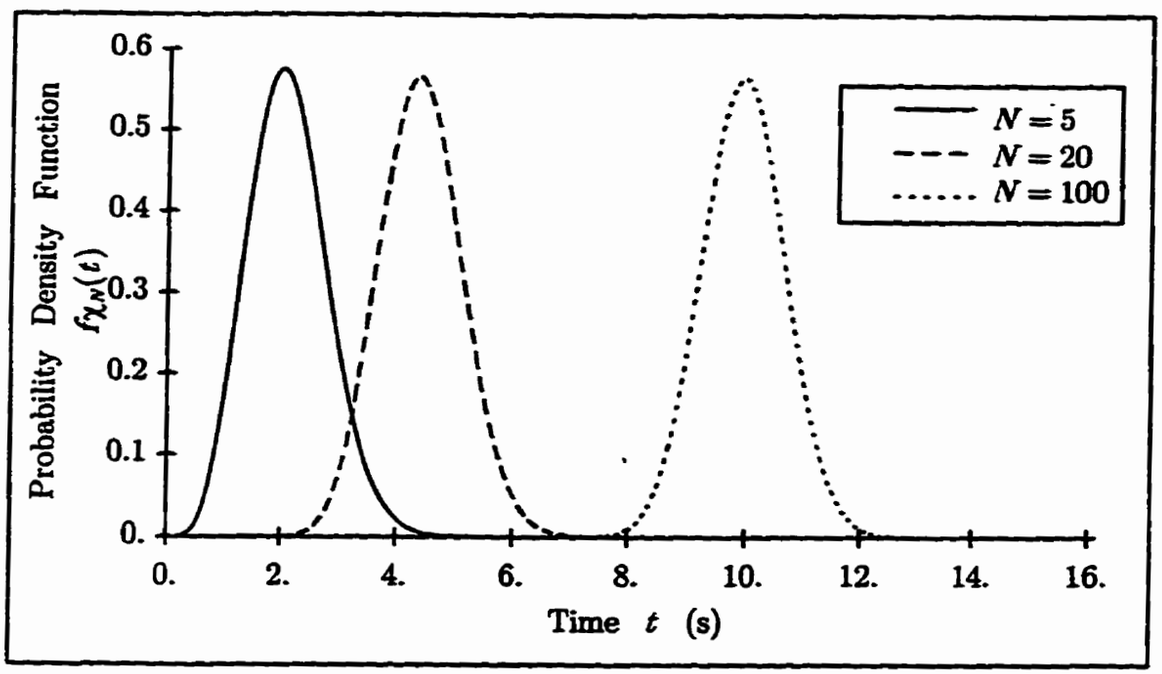

Figure 4.1: Probability Density Function of a χ-Random Variable with 5, 20 and 100 Degrees of Freedom

$$R_N = |\mathbf{X}|.$$

After scaling the vector $\mathbf{f}(t)$ to unit length, the random process $\hat{X}(t)$ (5.32) can be expressed as

$$\hat{X}(t) = R_N |\mathbf{f}(t)| \left\langle \mathbf{U}, \frac{\mathbf{f}(t)}{|\mathbf{f}(t)|} \right\rangle \tag{4.12}$$

The importance of the above expression can hardly be overstated: according to (4.12), each sample $\hat{x}(t)$ of the stochastic process $\hat{X}(t)$ can be represented as $(r_N |\mathbf{f}(t)|)$ times the scalar product of two vectors with unit length. The first vector is the realization $\mathbf{u}$, which is constant in time for a given sample. The second vector is a deterministic vector $\mathbf{f}(t) / |\mathbf{f}(t)|$, which, in time, describes a path on the surface of the N-dimensional unit sphere.

The spherical representation of two such samples $\hat{x}(t)$ is given in Figure 4.2. The

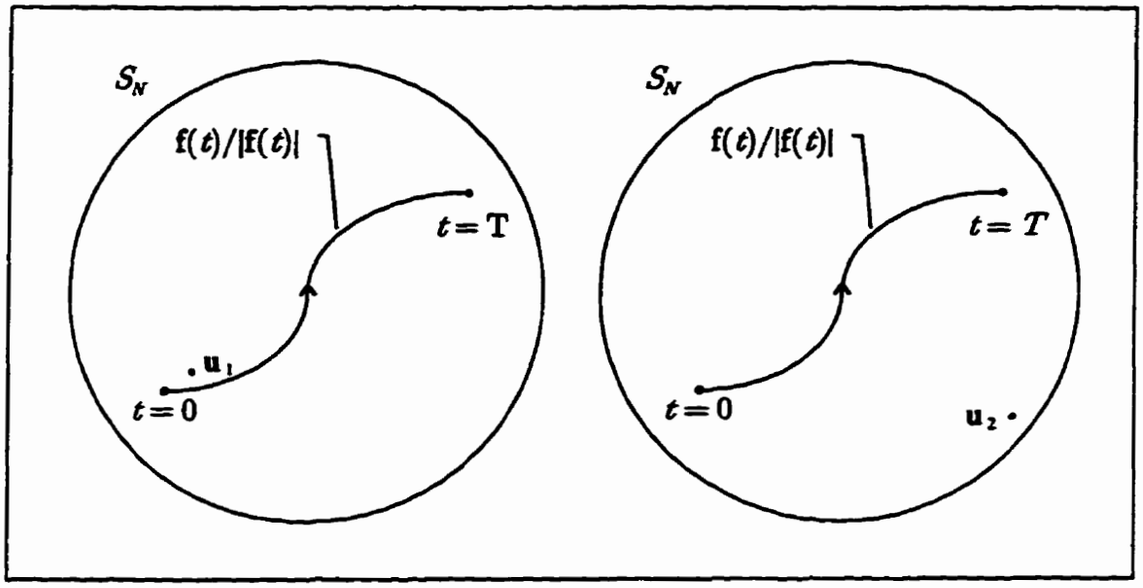

Figure 4.2: Spherical Representation of Two Samples $\hat{x}(t)$ of the Random Process $\hat{X}(t)$

vector $\mathbf{f}(t) / |\mathbf{f}(t)|$ is deterministic. Therefore, the path described by this vector is the same for all samples. Samples only differ in the position of the random vector $\mathbf{u}$.

4.2 Sun's Formula without Endpoint Probabilities

In this Section, the main term of Sun's Formula (4.44) is computed. In Section 4.2.1, the exceedance probability $P(\beta)$ is rewritten to yield a format to which the relative frequency approach can be applied (Section 4.2.2). In Section 4.2.3, the integral expression is derived.

4.2.1 Introduction

The probability of interest is

$$P(\beta) = \Pr\left(\max_{t\in[0,T]} \hat{X}(t) > \beta\right) \tag{4.13}$$

Insertion of (4.12) and division by $(R_N |f(t)|)$ yields:

$$P(\beta) = \Pr\left(\max_{t\in[0,T]} \left\langle \mathbf{U}, \frac{\mathbf{f}(t)}{|\mathbf{f}(t)|} \right\rangle > \frac{\beta}{R_N |\mathbf{f}(t)|}\right) \tag{4.14}$$

If R_N takes on a particular value r, it is useful to introduce the conditional probability $P(\beta|\, R_N = r)$ defined as

$$\begin{aligned} P(\beta|\, R_N = r) &= \Pr\left(\max_{t\in[0,T]} \hat{X}(t) > \beta \,\middle|\, R_N = r\right) && (4.15)\\ &= P\left(\max_{t\in[0,T]} \left\langle \mathbf{U}, \frac{\mathbf{f}(t)}{|\mathbf{f}(t)|} \right\rangle > \frac{\beta}{R_N |\mathbf{f}(t)|} \,\middle|\, R_N = r\right) && (4.16)\\ &= P\left(\max_{t\in[0,T]} \left\langle \mathbf{U}, \frac{\mathbf{f}(t)}{|\mathbf{f}(t)|} \right\rangle > \frac{\beta}{r |\mathbf{f}(t)|}\right) && (4.17) \end{aligned}$$

$P(\beta)$ is computed by integration of the conditional probability $P(\beta|\, R_N = r)$ over all possible values of the random variable R_N:

$$P(\beta) = \int_0^\infty P(\beta|\, R_N = r)\, f_{\chi_N}(r)\, dr \tag{4.18}$$

where $f_{\chi_N}(r)$ is the probability density function of a χ_N-distribution as defined in (4.9). Since

$$\max_{t\in\{0,T\}} \left\langle \mathbf{U}, \frac{\mathbf{f}(t)}{|\mathbf{f}(t)|} \right\rangle \leq |\mathbf{U}| \left|\frac{\mathbf{f}(t)}{|\mathbf{f}(t)|}\right| = 1 \tag{4.19}$$

the probability $P(\beta|\, R_N = r)$ can only contribute to $P(\beta)$ if (See (4.17):

$$\frac{\beta}{r\,|\mathbf{f}(t)|} < 1 \tag{4.20}$$

$$\Updownarrow$$

$$r > \frac{\beta}{|\mathbf{f}(t)|} \tag{4.21}$$

Since

$$\frac{\beta}{|\mathbf{f}(t)|} \geq \beta \qquad \text{for all } t \in [0,T] \tag{4.22}$$

the lower endpoint of the integral in (4.18) can be changed to β:

$$P(\beta) = \int_{\beta}^{\infty} P(\beta|\, R_N = r)\, f_{\chi_N}(r)\, dr \tag{4.23}$$

4.2.2 Relative Frequency Approach

The probability $P(\beta|\, R_N = r)$ as defined in equation (4.17) is now computed using the relative frequency approach (Sun, 1993). Of all possible realizations $\mathbf{u}$ of the random vector $\mathbf{U}$ on the unit sphere, only a specific set of random vectors will result in a scalar product $\left\langle \mathbf{U}, \frac{\mathbf{f}(t)}{|\mathbf{f}(t)|} \right\rangle$ that satisfies the inequality

$$\max_{t\in[0,T]} \left\langle \mathbf{U}, \frac{\mathbf{f}(t)}{|\mathbf{f}(t)|} \right\rangle > \frac{\beta}{r\,|\mathbf{f}(t)|} \tag{4.24}$$

These are the random vectors $\mathbf{U}$ that contribute to the conditional probability $P(\beta|\, R_N = r)$ (4.17). From (4.24), it is clear that the area on the N-dimensional unit sphere covered by those random vectors $\mathbf{U}$ is dependent on β and r. Therefore, the surface area of that part of the N-dimensional unit sphere that is spanned by the

endpoints of those random vectors $\mathbf{U}$ is represented by $A(\beta, r)$. Once an expression is derived for this surface area, the conditional probability $P(\beta | R_N = r)$ can be computed as this surface area $A(\beta, r)$ divided by the total area of the unit sphere.

Tube Around Curve on Unit Sphere

First, the inequality (4.24) is further examined. Introducing $\Theta(t)$ as the angle between the two vectors $\mathbf{U}$ and $\mathbf{f}(t) / |\mathbf{f}(t)|$, we can express the left-hand-side in inequality (4.24) as follows:

$$\max_{t\in[0,T]} \left\langle \mathbf{U}, \frac{\mathbf{f}(t)}{|\mathbf{f}(t)|} \right\rangle = \max_{t\in[0,T]} \left(\underbrace{|\mathbf{U}|}_{=1} \underbrace{\left| \frac{\mathbf{f}(t)}{|\mathbf{f}(t)|} \right|}_{=1} \cos(\Theta(t)) \right) = \max_{t\in[0,T]} \cos(\Theta(t)) \tag{4.25}$$

From (4.25), it is obvious that the inequality (4.24) cannot be satisfied for values of $\beta / (r |\mathbf{f}(t)|)$ that are greater than 1. In Figure 4.3, the angle $\theta(t)$ is sketched for the two samples given in Figure 4.2. Therefore, only the cases where

$$\frac{\beta}{r |\mathbf{f}(t)|} \leq 1 \tag{4.26}$$

are considered. The inequality (4.24) can now be written as

$$\max_{t\in[0,T]} \cos(\Theta(t)) > \frac{\beta}{r |\mathbf{f}(t)|} \tag{4.27}$$

$$\Updownarrow$$

$$\min_{t\in[0,T]} \Theta(t) < \arccos\left(\frac{\beta}{r |\mathbf{f}(t)|} \right) \tag{4.28}$$

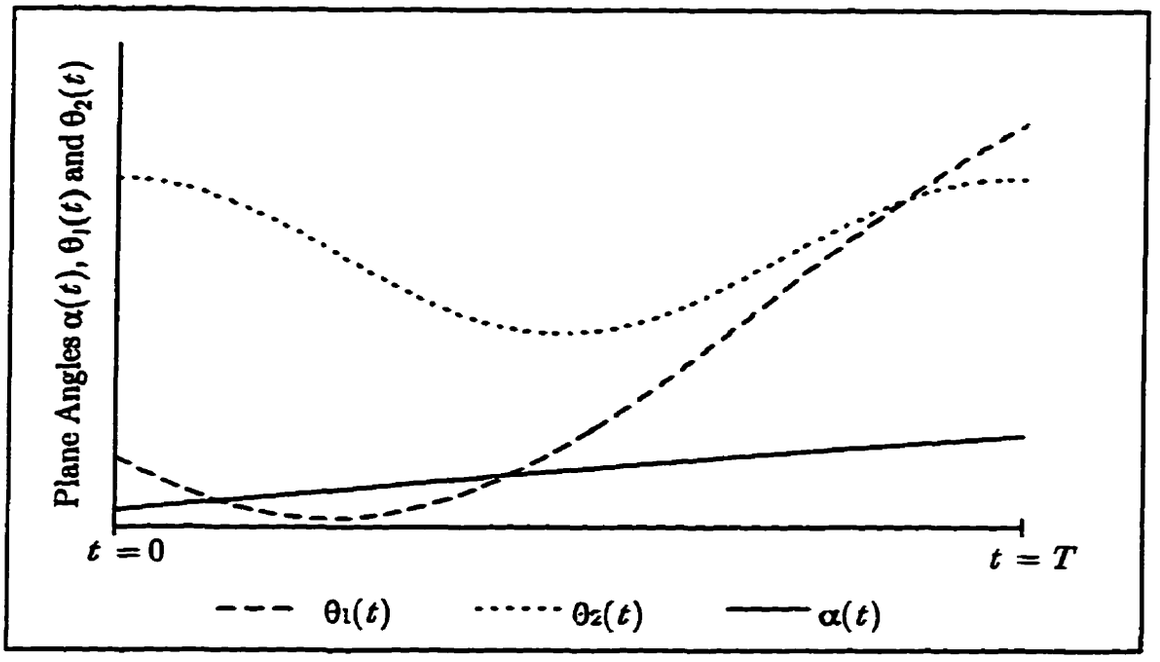

Figure 4.3: Plane Angles $\theta_1(t)$, $\theta_2(t)$ and $\alpha(t) = \arccos(\beta/(r|f(t)|))$ for the Random Process $\hat{X}(t)$

The right-hand-side of inequality (4.28) is plotted in Figure 4.3. For this purpose, it is assumed that $\hat{X}(t)$ is a random process that has an increasing variance in the interval $[0,T]$ and the maximum of the variance is reached at time $t = T$. We can conclude that for Sample I, inequality (4.28) is satisfied, while this is not the case for Sample II. In general, only those realizations u of the random vector U that lie sufficiently close to the path of $\mathbf{f}(t) / |\mathbf{f}(t)|$ will at some point in the interval $[0,T]$ result in an angle $\theta(t)$ that satisfies the inequality (4.28). Those vectors u are enclosed in a tube around the path of $\mathbf{f}(t) / |\mathbf{f}(t)|$. The word "tube" is used in higher-dimensional geometry to refer to the area around a manifold. The width of this tube is variable in time. A measure for this width is the plane angle $\alpha(t)$ - measured in a plane perpendicular to the path - between the path and the outer

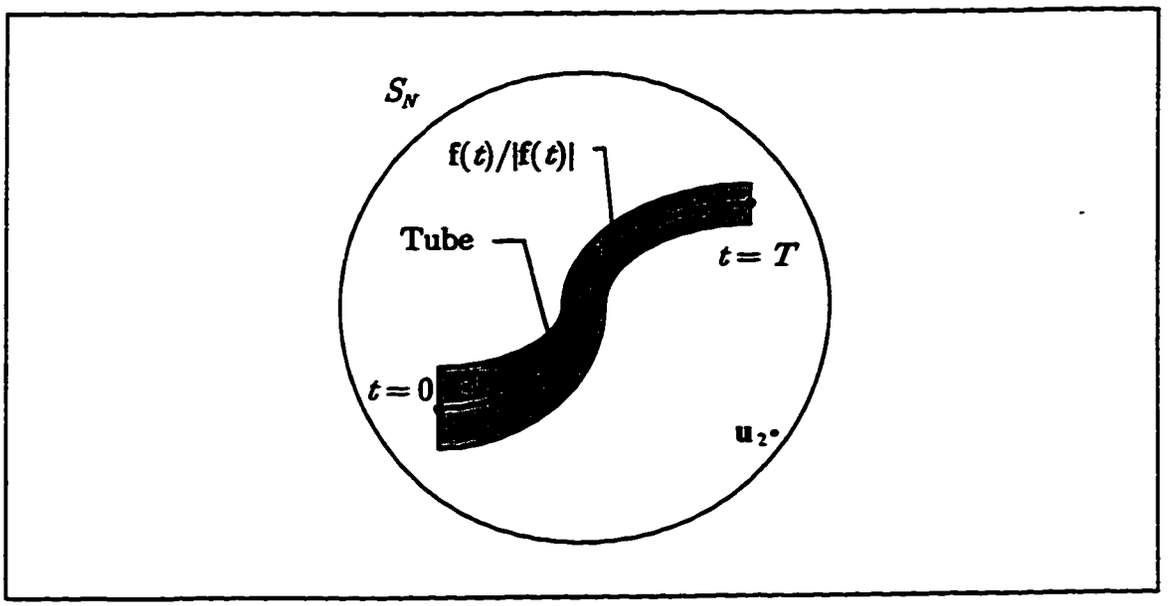

Figure 4.4: Tube around the path of the vector $\mathbf{f}(t) / |\mathbf{f}(t)|$ on the unit sphere

bound of the tube. From (4.28), it follows that this angle is given by:

$$\alpha(t) = \begin{cases} \arccos\left(\frac{\beta}{r|\mathbf{f}(t)|}\right) & (\beta/(r|\mathbf{f}(t)|)) \leq 1 \\ 0 & (\beta/(r|\mathbf{f}(t)|)) > 1 \end{cases} \tag{4.29}$$

In Figure 4.4, this tube is sketched together with the two realizations $\mathbf{u}^{\mathrm{I}}$ and $\mathbf{u}^{\mathrm{II}}$ of the random vector $\mathbf{U}$. It can be observed that realization $\mathbf{u}^{\mathrm{I}}$ corresponding to Sample I lies within the tube around the path of the vector $\mathbf{f}(t) / |\mathbf{f}(t)|$, while this is not the case for the realization $\mathbf{u}^{\mathrm{II}}$ corresponding to Sample II. In general, if the realization $\mathbf{u}$ of the random vector $\mathbf{U}$ lies within the tube with width $\alpha(t)$, it will satisfy (4.28), which means that it will indeed result in a stochastic process $\hat{X}(t)$ with a maximum greater that β. Notice that the tube has zero-width at the time-instances for which $\beta/(r|\mathbf{f}(t)|) > 1$.

Surface Area of Tube Around Path on Unit Sphere

Hotelling (1939) determined that the surface area dA of a tube around a curve of elementary arclength ds on the N-dimensional unit sphere is given by

$$dA = \frac{\pi^{\frac{N-2}{2}}}{\Gamma\left(\frac{N}{2}\right)} \sin^{N-2}(\alpha)\, ds \tag{4.30}$$

with α the plane angle, measured in a plane perpendicular to the curve, between the curve and the outer bound of the tube. $\Gamma(\cdot)$ is the Gamma-function (Abramowitz and Stegun, 1972), defined by

$$\Gamma(z) = \int_0^\infty t^{z-1} e^{-t} dt \tag{4.31}$$

Hotelling (1939) indicates that (4.30) takes no account of overlapping of the tube with itself. This overlapping will occur if the curvature of the curve on the unit sphere is excessive in relation to the width of the tube. An example where such overlap will occur is if there are sharp turns in the curve. This is the case in the application discussed in Section 5.3.3.

The total area $A(\beta, r)$ of the tube determined by β and r is given by integration over the path of $\mathbf{f}(t) / |\mathbf{f}(t)|$:

$$A(\beta, r) = \frac{\pi^{\frac{N-2}{2}}}{\Gamma\left(\frac{N}{2}\right)} \int_{s(t=0)}^{s(t=T)} \sin^{N-2}(\alpha(t))\, ds(t) \tag{4.32}$$

where $\alpha(t)$ is defined in (4.29) and $s(t)$ is the arclength of the path described by the vector $\mathbf{f}(t) / |\mathbf{f}(t)|$ on the N-dimensional unit sphere. We emphasize that expression (4.30) only takes into account the area perpendicular to the path of the vector

$\mathbf{f}(t) / |\mathbf{f}(t)|$. How the areas at the endpoints of the curve can be taken into account is discussed in Section 4.3.

The surface area A_N of the N-dimensional unit sphere S^N is given by (Kendall, 1961)

$$A_N = \frac{2\pi^{\frac{N}{2}}}{\Gamma\left(\frac{N}{2}\right)} \tag{4.33}$$

4.2.3 Derivation of the Integral Expression

The relative frequency approach as described in Section 4.2.2 can now be used to compute the probability in the integrand of (4.23) as the ratio of the surface area of the tube divided by the surface area of the N-dimensional unit sphere:

$$P(\beta | R_N = r) = \frac{A(\beta, r)}{A_N} \tag{4.34}$$

$$= \frac{1}{2\pi} \int_{s(t=0)}^{s(t=T)} \sin^{N-2}(\alpha(t))\, ds(t) \tag{4.35}$$

Insertion of (4.35) in (4.23) and changing the order of integration results in:

$$P(\beta) = \frac{1}{2\pi} \int_{s(t=0)}^{s(t=T)} \int_{\beta}^{\infty} \sin^{N-2}(\alpha(t))\, f_{\chi_N}(r)\, dr\, ds(t) \tag{4.36}$$

The definition for $\alpha(t)$ (4.29) can now inserted in (4.36):

$$P(\beta) = \frac{1}{2\pi} \int_{s(t=0)}^{s(t=T)} \underbrace{\int_{\beta/|\mathbf{f}(t)|}^{\infty} \sin^{N-2}\left(\arccos\left(\frac{\beta}{r\,|\mathbf{f}(t)|}\right)\right) f_{\chi_N}(r)\, dr}_{=I(\beta,t)}\, ds(t) \tag{4.37}$$

In what follows, it will be shown that the asymptotic approximation ($\beta \rightarrow \infty$) for (4.37) derived in Maes and Breitung (1996), is actually the exact solution for all β.

First the integral $I(\beta,t)$ will be computed. Noting that

$$\arccos(x) = \arcsin\left(\sqrt{1-x^2}\right) \qquad \text{for} \qquad 0 \le x \le 1 \tag{4.38}$$

$I(\beta,t)$ can be written as

$$I(\beta,t) = \int_{\beta/|\mathbf{f}(t)|}^{\infty} \sin^{N-2}\left(\arcsin\left(\sqrt{1-\left(\frac{\beta}{r\,|\mathbf{f}(t)|}\right)^2}\right)\right) f_{\chi N}(r)\,dr \tag{4.39}$$

$$= \int_{\beta/|\mathbf{f}(t)|}^{\infty} \left(1-\left(\frac{\beta}{r\,|\mathbf{f}(t)|}\right)^2\right)^{\frac{N-2}{2}} f_{\chi N}(r)\,dr \tag{4.40}$$

If we now make the substitution

$$r \to y = \frac{r^2 - \left(\frac{\beta}{r|\mathbf{f}(t)|}\right)^2}{2} \tag{4.41}$$

we obtain that

$$I(\beta,t) = \int_0^{\infty} \left(\frac{2y}{2y+\frac{\beta^2}{|\mathbf{f}(t)|^2}}\right)^{\frac{N-2}{2}} f_{\chi N}\left(\sqrt{2y+\frac{\beta^2}{|\mathbf{f}(t)|^2}}\right)\left(\frac{1}{\sqrt{2y+\frac{\beta^2}{|\mathbf{f}(t)|^2}}}\right) dy \tag{4.42}$$

The probability density function $f_N(\cdot)$ (4.9) is inserted in (4.42):

$$I(\beta,t) = \frac{2^{1-\frac{N}{2}}}{\Gamma\left(\frac{N}{2}\right)} \int_0^{\infty} \left(\frac{2y}{2y+\frac{\beta^2}{|\mathbf{f}(t)|^2}}\right)^{\frac{N-2}{2}} \left(2y+\frac{\beta^2}{|\mathbf{f}(t)|^2}\right)^{\frac{N-1}{2}} \cdot \exp\left(-\frac{2y+\frac{\beta^2}{|\mathbf{f}(t)|^2}}{2}\right)\left(\frac{1}{\sqrt{2y+\frac{\beta^2}{|\mathbf{f}(t)|^2}}}\right) dy$$

Further simplification gives:

$$\begin{aligned} I(\beta,t) &= \frac{\exp\left(-\frac{\beta^2}{2|\mathbf{f}(t)|^2}\right)}{\Gamma\left(\frac{N}{2}\right)} \underbrace{\int_0^{\infty} y^{\frac{N-2}{2}} \exp(-y)\, dy}_{=\Gamma\left(\frac{N}{2}\right)} \\ &= \exp\left(-\frac{\beta^2}{2|\mathbf{f}(t)|^2}\right) \end{aligned}$$

Equation (4.37) can now be written as

$$P(\beta) = \frac{1}{2\pi} \int_{s(t=0)}^{s(t=T)} \exp\left(-\frac{\beta^2}{2|\mathbf{f}(t)|^2}\right) ds(t) \tag{4.43}$$

with $s(t)$ the arclength of the path described on the unit sphere by the vector $\mathbf{f}(t) / |\mathbf{f}(t)|$.

Introducing the function $c(t)$ defined by

$$c(t) = \left|\frac{ds(t)}{dt}\right| \tag{4.44}$$

equation (4.43) can be written as:

$$P(\beta) = \frac{1}{2\pi} \int_0^T \exp\left(-\frac{\beta^2}{2|\mathbf{f}(t)|^2}\right) c(t)\, dt \tag{4.45}$$

An expression for $c(t)$ in terms of the discretization functions $f_i(t)$ and the derivatives of those discretization functions $f_i'(t)$ can be obtained by observing that the elementary arclength $ds(t)$ is given by:

$$ds(t) = \sqrt{\sum_{i=1}^{N} \left(d\left(\frac{f_i(t)}{|f(t)|}\right)\right)^2} \tag{4.46}$$

Therefore, $c(t)$ can be computed as

$$c(t) = \left|\frac{ds(t)}{dt}\right| = \sqrt{\sum_{i=1}^{N}\left(\frac{d}{dt}\left(\frac{f_i(t)}{|f(t)|}\right)\right)^2} \tag{4.47}$$

$$= \sqrt{\frac{\sum_{i=1}^{N} f_i'(t)^2}{\sum_{i=1}^{N} f_i(t)^2} - \left(\frac{\sum_{i=1}^{N} f_i'(t)\, f_i(t)}{\sum_{i=1}^{N} f_i(t)^2}\right)^2} \tag{4.48}$$

The first term in the square-root in expression (4.48) can be simplified to yield

$$\frac{\sum_{i=1}^{N} f_i'(t)^2}{\sum_{i=1}^{N} f_i(t)^2} = \frac{\sigma_{\dot{X}}^2(t)}{\sigma_X^2(t)} \tag{4.49}$$

Similarly, the second term of the square-root in expression (4.48) can be re-interpreted. Since

$$\frac{1}{\sigma}\left(\frac{d\sigma}{dt}\right) = \frac{1}{2\sigma^2}\frac{d}{dt}\left(\sigma^2\right) \tag{4.50}$$

$$= \frac{1}{2\sum_{i=1}^{N} f_i(t)^2}\frac{d}{dt}\left(\sum_{i=1}^{N} f_i(t)^2\right) \tag{4.51}$$

$$= \frac{\sum_{i=1}^{N} f_i'(t)\, f_i(t)}{\sum_{i=1}^{N} f_i(t)^2} \tag{4.52}$$

the second term in the square-root in expression (4.48) can be written as

$$\left(\frac{\sum_{i=1}^{N} f_i'(t)\, f_i(t)}{\sum_{i=1}^{N} f_i(t)^2}\right)^2 = \left(\frac{1}{\sigma}\left(\frac{d\sigma}{dt}\right)\right)^2 \tag{4.53}$$

We now insert (4.49) and (4.53) in the expression for $c(t)$ (4.47). This results in a

definition for $c(t)$ in terms of the variances:

$$c(t) = \sqrt{\frac{\sigma_{\dot{X}}^2(t)}{\sigma_X^2(t)} - \left(\frac{1}{\sigma_X(t)}\frac{d\sigma_X(t)}{dt}\right)^2} \qquad (4.55)$$

4.3 Probability Associated with Endpoints and Discontinuities

The probabilities discussed in this Section are not considered by Sun (1993). Taking into account the probabilities associated with the endpoints improves the accuracy of the method, as is illustrated in Section 5.2.1. The probabilities associated with discontinuities enable the use of discontinuous discretization functions.

The expression given by Hotelling to compute the surface area of a tube around a curve on a sphere includes only the area perpendicular to the curve. The surface area of the hemi-spherical caps over the endpoints of the tube has to be accounted for separately. This is indicated in Figure 4.5. The additional probability associated with these endpoints is:

$$\frac{1}{2}\Phi\left(-\frac{\beta}{|f(0)|}\right) + \frac{1}{2}\Phi\left(-\frac{\beta}{|f(T)|}\right) \qquad (4.56)$$

where $\Phi(\cdot)$ denotes the standard normal distribution. A mathematical derivation of (4.56) is given in Appendix B.

For certain types of discretization, the discretization functions are discontinuous. In that case, the path of the vector $\mathbf{f}(t)/|\mathbf{f}(t)|$ consists of non-consecutive arcs, since each discontinuity causes a "jump" in the path of $\mathbf{f}(t)/|\mathbf{f}(t)|$. Two hemi-

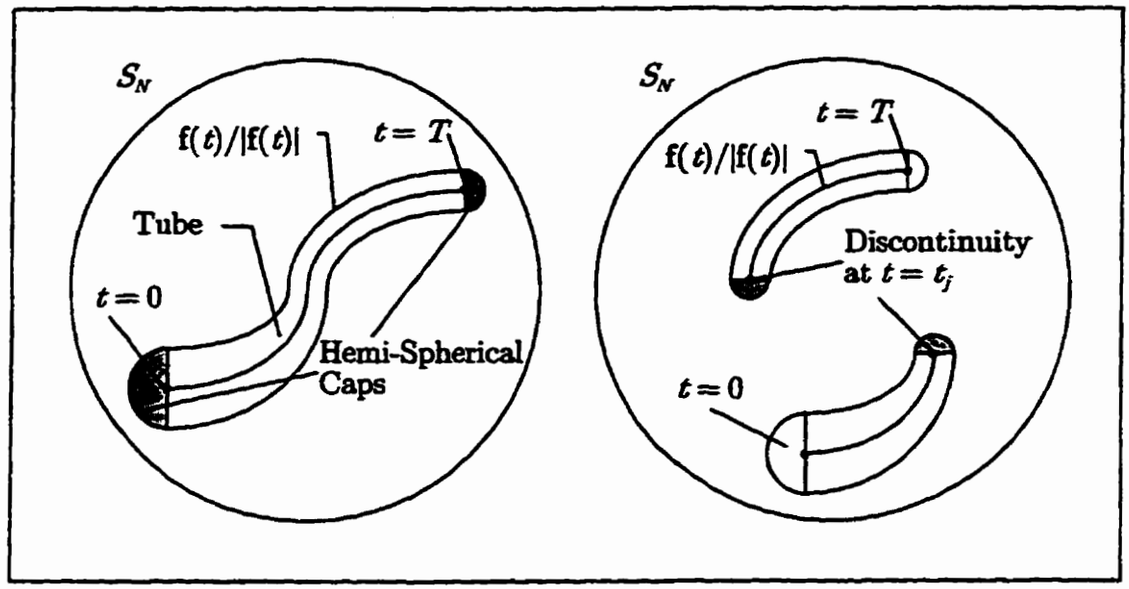

Figure 4.5: Hemi-Sperical Caps Associated with Endpoints and Discontinuities

spherical caps have to be added in the computation of the area of the tube for each discontinuity (See Figure 4.5). Assuming that the discretization functions in (4.1) are discontinuous at M points t_j, the additional probability is given by:

$$\sum_{j=1}^{M} \Phi\left(-\frac{\beta}{|f(t_j)|}\right) \tag{4.57}$$

Adding the terms (4.57) gives an approximate solution for the problem of discontinuities in the path of $\mathbf{f}(t) / |\mathbf{f}(t)|$. The two hemi-spherical areas added on both sides of the discontinuity may overlap if the "jump" caused by the discontinuity is small (See Figure 4.6). Other problems of self-overlap of the tube with itself occur if the path described by $\mathbf{f}(t) / |\mathbf{f}(t)|$ passes more than once through the same point. Self-overlap may also be a local phenomenon (Hotelling, 1939) resulting from the curvature of the curve being greater than some critical radius or from a sudden

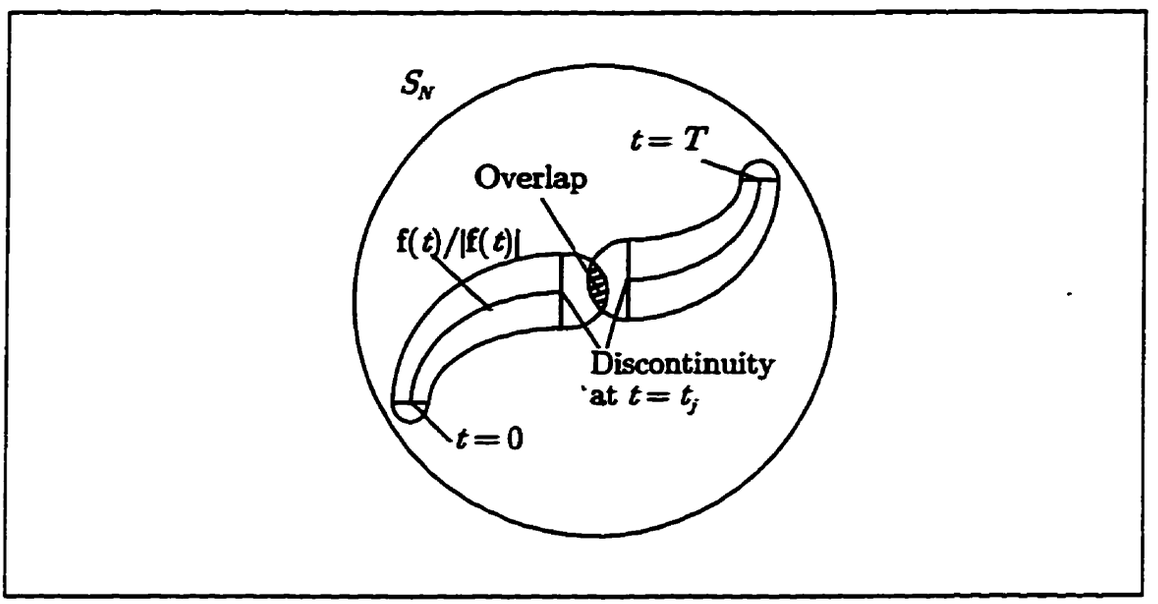

Figure 4.6: Self-Overlap Caused by a 'Small' discontinuity in the Path of the Vector $\mathbf{f}(t) / |\mathbf{f}(t)|$ on the Unit Sphere

change in direction of the path of $\mathbf{f}(t) / |\mathbf{f}(t)|$, caused by a discontinuity in the first derivative of the discretization functions $f_i(t)$ (See Figure 4.7). The latter possibility is discussed in Section 5.3.3.

By adding the probabilities in expressions (4.56) and (4.57) to the probability in expression (4.46), the following approximation is obtained for the extreme value distribution:

$$\begin{aligned} P(\beta) &= \frac{1}{2\pi}\int_0^T \exp\left(-\frac{\beta^2}{2\,|\mathbf{f}(t)|^2}\right) c(t)\,dt \\ &\quad + \frac{1}{2}\Phi\left(-\frac{\beta}{|\mathbf{f}(0)|}\right) + \frac{1}{2}\Phi\left(-\frac{\beta}{|\mathbf{f}(T)|}\right) + \sum_{j=1}^{M}\Phi\left(-\frac{\beta}{|\mathbf{f}(t_j)|}\right) \end{aligned} \tag{4.58}$$

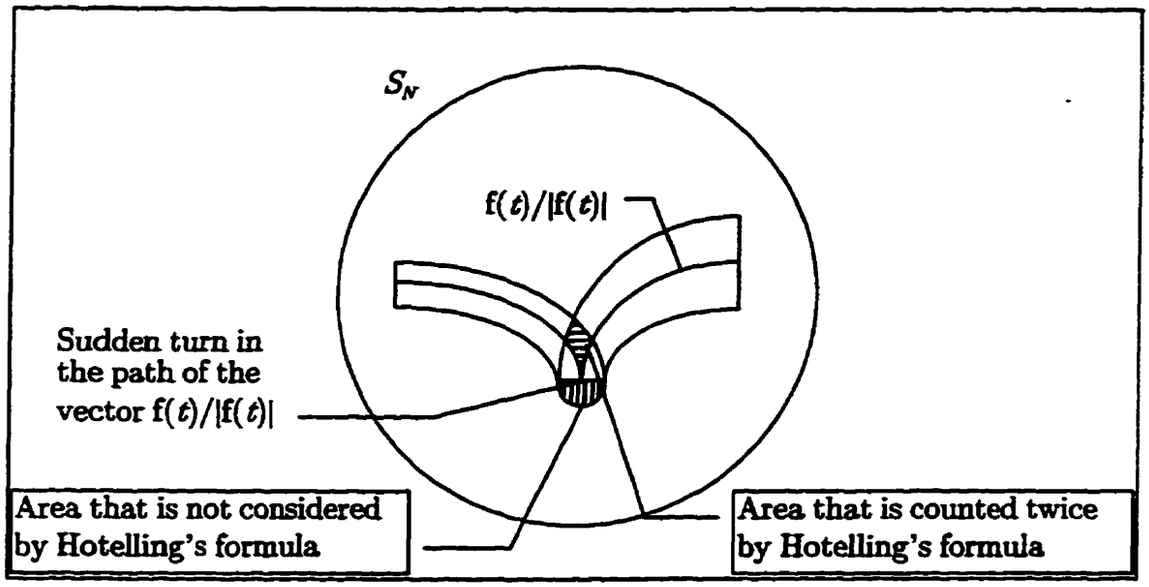

Figure 4.7: Self-Overlap Caused by a Sudden Change in Direction of the Path of the Vector $\mathbf{f}(t) / |\mathbf{f}(t)|$ on the Unit Sphere

4.4 Discussion of Sun's Formula

The extreme value distributions of both stationary and non-stationary Gaussian processes can be obtained using equation (4.58) with little computational effort. Once $c(t)$ is computed, the first integral in (4.58) can be computed using numerical integration.

For a stationary process, with no discontinuities in the discretization functions, (4.58) can be simplified to yield:

$$P(\beta) = \frac{T\sigma_{\dot{X}}}{2\pi} \exp\left(-\frac{\beta^2}{2}\right) + \Phi(-\beta) \tag{4.59}$$

which is the well known formula for exceedance probabilities of stationary Gaussian processes with unit variance (See Section 2.1). In Section 5.2.1, the extreme value

distribution of such a process is computed using (4.59).

It should be noted that equation (4.58) cannot be applied blindly. As is discussed in Section 4.3, the user should pay attention to possible problems of self-overlap.

4.5 Other Statistics Based on Sun's Formula

The purpose of this Section is to indicate how Sun's Method can be employed to compute some other useful results related to the extreme value distribution of a stochastic process.

In this Section $S_\theta^N(t)$ denotes the spherical cap around the point $\mathbf{f}(t) / |\mathbf{f}(t)|$ on the N-dimensional unit sphere S^N (See Appendix B). $\overline{L}$ denotes that part of the unit-sphere S^N that does not belong to the area L:

$$\begin{cases} L \cup \overline{L} = S^N \\ L \cap \overline{L} = \emptyset \end{cases} \tag{4.60}$$

The operator $\mathbf{A}(L)$ is used to represent the surface area of the area L on the N-dimensional unit sphere S^N.

4.5.1 Exceedance Probability at a Given Time

The probability that at specified time t the value of the stochastic process will be greater than a given level β is simply the exceedance probability:

$$\Pr\left(\hat{X}(t) > \beta\right) = \Phi\left(-\frac{\beta}{\sigma_{\hat{X}}(t)}\right) \tag{4.61}$$

4.5.2 Conditional Probabilities of Exceedance

We will now compute the conditional probability

$$\Pr\left(\hat{X}(t_2) > \beta \middle| \hat{X}(t_1) > \beta\right) \tag{4.62}$$

For this purpose, we use the formula

$$\Pr\left(\hat{X}(t_2) > \beta \middle| \hat{X}(t_1) > \beta\right) = \frac{\Pr\left(\left(\hat{X}(t_2) > \beta\right) \cap \left(\hat{X}(t_1) > \beta\right)\right)}{\Pr\left(\hat{X}(t_1) > \beta\right)} \tag{4.63}$$

The probability in the denominator of (4.63) is given in (4.61). For the computation of the numerator, we use the same technique as we employed for the derivation of Sun's Formula. Using the relative frequency approach, the conditional probability

$$\Pr\left(\left(\hat{X}(t_2) > \beta\right) \cap \left(\hat{X}(t_1) > \beta\right) \middle| R_N = r\right) \tag{4.64}$$

is given by the surface area of the intersection of the spherical caps around the points t_1 and t_2 divided by the surface area of the unit sphere:

$$\Pr\left(\left(\hat{X}(t_2) > \beta\right) \cap \left(\hat{X}(t_1) > \beta\right) \middle| R_N = r\right) = \frac{\mathbf{A}\left(S_\theta^N(t_1) \cap S_\theta^N(t_2)\right)}{\mathbf{A}(S^N)} \tag{4.65}$$

This intersection area is plotted in Figure 4.8. This can be explained by observing that samples $\mathbf{u}$ of the random vector $\mathbf{U}$ in that intersection area will result in a value for $\hat{x}(t)$ that is greater than β both at time t_1 and time t_2. An estimate for the surface area can be obtained by simulation. Once the conditional probability (4.64) is computed, the probability in the numerator of (4.63) can be computed by

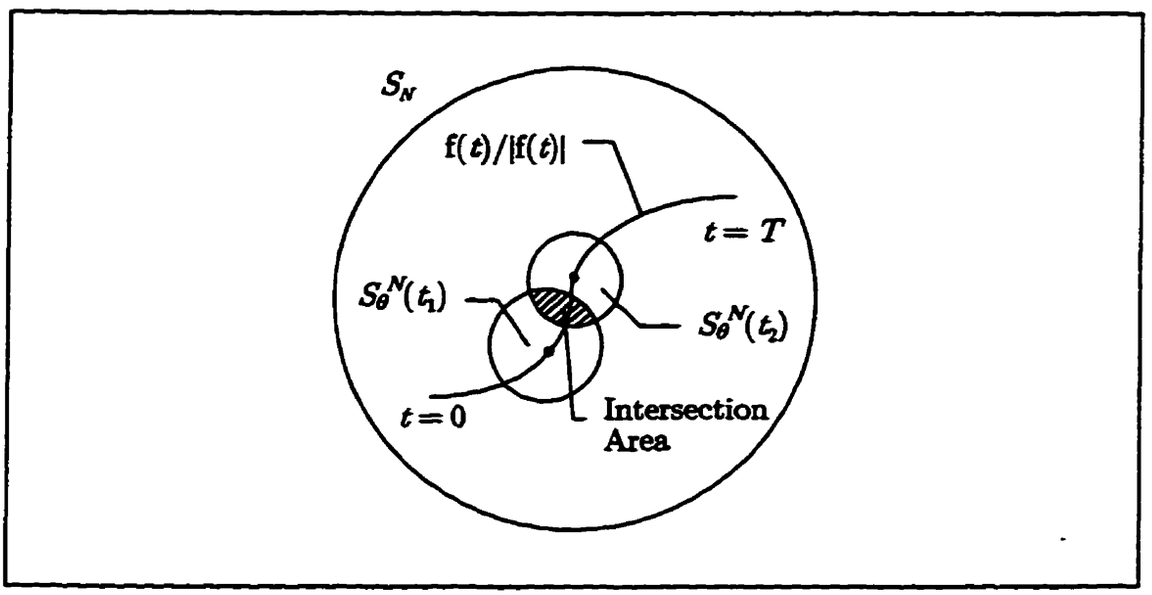

Figure 4.8: Spherical Representation of Conditional Probability of Exceedance

integration over all possible values of the random variable R_N (See Section 4.2.1).

4.5.3 Rate of Upcrossings

The mean rate of upcrossings $\upsilon(t)$ of $\hat{X}(t)$ above a level β is defined as

$$\upsilon(t) = \lim_{\Delta t \to 0} \frac{\mathbb{E}\left(N_\beta(\Delta t)\right)}{\Delta t} \tag{4.66}$$

where $N_\beta(\Delta t)$ is the number of upcrossings as defined in Chapter 2. Hagen and Tvedt (1991) prove that $\upsilon(t)$ can be written in the limiting form

$$\upsilon(t) = \lim_{\Delta t \to 0} \frac{\Pr\left(\left(\hat{X}(t) < \beta\right) \cap \left(\hat{X}(t + \Delta t) > \beta\right)\right)}{\Delta t} \tag{4.67}$$

The numerator denotes the probability that the process $\hat{X}(t)$ has a value smaller than β at time t and a value greater than β at a slightly later time $t+\Delta t$. If this is the case, one or more up-crossings must have occurred during the interval Δt. Der Kiureghian and Li (1996) show that for sufficiently small values Δt, the probability of more than one up-crossing can be neglected. The conditional probability

$$\Pr\left(\left(\hat{X}(t) < \beta\right) \cap \left(\hat{X}(t+\Delta t) > \beta\right) \middle| R_N = r\right) \tag{4.68}$$

can again be computed using the relative frequency approach:

$$\Pr\left(\left(\hat{X}(t) < \beta\right) \cap \left(\hat{X}(t+\Delta t) > \beta\right) \middle| R_N = r\right) = \frac{\mathbf{A}\left(\overline{S_\theta^N(t)} \cap S_\theta^N(t+\Delta t)\right)}{\mathbf{A}(S^N)} \tag{4.69}$$

A representation of the area $\left(\overline{S_\theta^N(t)} \cap S_\theta^N(t+\Delta t)\right)$ in Equation (4.69) is given in Figure 4.9. Realizations $\mathbf{u}$ of the vector $\mathbf{U}$ that lie within this area contribute to the probability in (4.69). Since those vectors $\mathbf{u}$ do not lie in the spherical cap around the point $\mathbf{f}(t)/|\mathbf{f}(t)|$, they will result in a process $\hat{x}(t)$ that has a value smaller than β at time t. However, those vectors $\mathbf{u}$ do lie in the spherical cap around the point $\mathbf{f}(t+\Delta t)/|\mathbf{f}(t+\Delta t)|$. Therefore, the value $\hat{x}(t+\Delta t)$ will be greater than β. Integration of the conditional probability (4.69) over all possible values of the χ_N-random variable yields the probability in the numerator of (4.67).

4.5.4 Cumulative Excursion Time

The length of time in the interval $[0,T]$ during which the stochastic process $\hat{X}(t)$ takes on a value greater than β is called the cumulative excursion time $\eta(T)$. Der

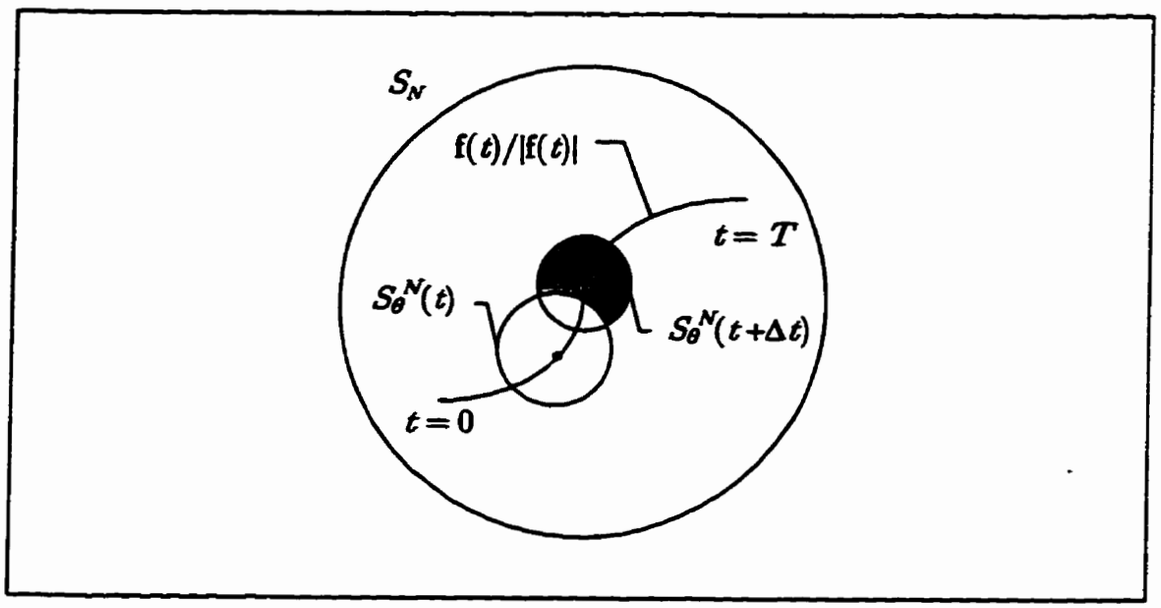

Figure 4.9: Computation of Rate of Upcrossings Using Spherical Representation

Kiureghian and Li (1996) indicate how the first two moments of this random variable can be computed:

$$\mathbb{E}(\eta(T)) = \int_0^T \Pr\left(\hat{X}(t) > \beta\right) dt \tag{4.70}$$

$$\mathbb{E}\left(\eta^2(T)\right) = \int_0^T \int_0^T \Pr\left(\left(\hat{X}(t_1) > \beta\right) \cap \left(\hat{X}(t_2) > \beta\right)\right) dt_1 dt_2 \tag{4.71}$$

The probability in the integrand of expression (4.70) can be computed using (4.61) and the probability in the integrand of expression (4.71) is computed in Section 4.5.2 (See equation (4.65)). Subsequently, numerical evaluation of the integrals in (4.70) and (4.71) is employed to determine the first and second moment of the random

variable $\eta(t)$. The variance can then be computed using

$$Var(\eta(T)) = \mathbf{E}\left(\eta^2(t)\right) - \mathbf{E}^2(\eta(t)) \tag{4.72}$$

4.5.5 Duration of a Single Excursion

The duration $D(t)$ of an excursion following the occurrence of an upcrossing of the level β at time t is defined as:

$$D(t) = \inf_{\tau} \left[\tau > t \text{ and } \hat{X}(\tau) < \beta\right] \tag{4.73}$$

In Equation (4.73), $\inf_{\tau}[\cdot]$ denotes the smallest value of τ for which the argument is true. For a given t, $D(t)$ is a random variable. Der Kiureghian and Li (1996) show that the mean value of this random variable $D(t)$ can be approximated by:

$$\mathbf{E}(D(t)) \cong \frac{\Pr\left(\hat{X}(t) > \beta\right)}{\upsilon(t)} \tag{4.74}$$

Notice that the computation of the numerator and the denominator in (4.74) are discussed respectively in (4.5.1) and (4.5.4).

4.6 Sun's Tube Method Applied to Non-Zero-Mean Gaussian Processes

So far, it has been assumed that the random process $X(t)$ has a constant zero mean. Suppose now that we want to use Sun's Method to compute the extreme value distribution of a process $Y(t)$ having a non-zero mean function $\mu_Y(t)$. Instead

of discretizing the process $Y(t)$, we discretize the zero-mean random process $Z(t)$:

$$Z(t) = (Y(t) - \mu_Y(t)) \tag{4.75}$$

Further we notice that

$$P(\beta) = \Pr\left(\max_{t\in[0,T]} \hat{Y}(t) > \beta\right) = \Pr\left(\max_{t\in[0,T]} \hat{Z}(t) > (\beta - \mu_{\hat{Y}}(t))\right) \tag{4.76}$$

Sun's Formula then becomes

$$\begin{aligned} P(\beta) &= \frac{1}{2\pi}\int_0^T \exp\left(-\frac{\beta(t)^2}{2\left|\mathbf{f}_Z(t)\right|^2}\right) c(t)\, dt \\ &\quad + \frac{1}{2}\Phi\left(-\frac{\beta(0)}{|\mathbf{f}_Z(0)|}\right) + \frac{1}{2}\Phi\left(-\frac{\beta(T)}{|\mathbf{f}_Z(T)|}\right) + \sum_{j=1}^{M}\Phi\left(-\frac{\beta(t_j)}{|\mathbf{f}_Z(t_j)|}\right) \end{aligned} \tag{4.77}$$

where $\beta(t)$ is defined as:

$$\beta(t) = \beta - \mu_{\hat{Y}}(t) \tag{4.78}$$

The vector $\mathbf{f}_Z(t)$ in Equation (4.77) lists the discretization functions of the zero-mean process $Z(t)$ (4.75):

$$\mathbf{f}_Z(t) = (\mathbf{f}_{Z_1}(t),\ \mathbf{f}_{Z_2}(t), ..., \mathbf{f}_{Z_N}(t)) \tag{4.79}$$

From (4.77), it is clear that the assumption of a zero-mean stochastic process in the derivation of Sun's Formula does not affect the generality of the method. Strongly fluctuating means could however affect the quality of Sun's Method.

Chapter 5

Applications of Sun's Tube Method

In this Chapter, the formula to approximate extreme value distributions is applied to several stochastic processes. The results of Sun's method are compared with extreme value distributions obtained by means of simulation. In Section 5.1, it is indicated how the simulation is performed. Results of two discretizations described in Chapter 3 are discussed. In Section 5.2, stochastic processes that are the sum of sine and cosine functions are considered. In Section 5.3, Sun's Tube method is applied to an earthquake signal and to a stochastic response to this signal.

5.1 Exceedance Probabilities Obtained by Simulation

In Monte Carlo simulation, a number N_S of independent samples $x(t)$ of the random process $X(t)$ are generated. An estimator $\hat{P}(\beta)$ for the exceedance probability $P(\beta)$ is obtained by checking if the generated sample $x(t)$ has a maximum that is greater than β:

$$\hat{P}(\beta) = \frac{1}{N_S} \sum_{i=1}^{N} \mathbf{1}\left(\max_{x \in T} x(t) > \beta \right) \tag{5.1}$$

where $\mathbf{1}(\cdot)$ is the indicator function that is equal to one when its argument is true and equal to zero otherwise. This estimator is unbiased:

$$\mathbf{E}\left(\hat{P}(\beta)\right) = P(\beta) \tag{5.2}$$

and asymptotically exact: as the number of samples N_S goes to infinity, the estimator $\hat{P}$ converges to the true exceedance probability $P(\beta)$. However, the convergence rate is slow. As discussed in Rubenstein (1981), this way of sampling can be compared to a sequence of N_S Bernoulli trials with probability of success $p = P(\beta)$. Hence, the Coefficient of Variation (COV) of estimator $\hat{P}(\beta)$ is equal to

$$COV\left(\hat{P}(\beta)\right) = \sqrt{\frac{1}{N_s P(\beta)\left(1 - P(\beta)\right)}} \approx \sqrt{\frac{1}{N_s \hat{P}(\beta)\left(1 - \hat{P}(\beta)\right)}} \tag{5.3}$$

The accuracy of the estimator is proportional to the COV. This means that 10^7 simulations are necessary to estimate an exceedance probability $P(\beta)$ of 10^{-5} with a COV of 0.1. In structural reliability problems, one is typically interested in small probabilities, which implies that simulation is a very expensive method to compute extreme value distributions. However, if no analytical solution is known, it is the only possible way to verify results obtained with approximation methods.

The discrete format required to apply Sun's method (3.3), makes simulation relatively simple. To generate a sample $x(t)$, N independent standard normal random variables x_i are generated using the polar method, as described in Ross (1990). Values for $x(t_i)$ at discrete times $t_i \in [0, T]$ can then easily be computed using equation (3.3).

5.2 Extreme Value Distribution of Linear Combination of Sine and Cosine Functions

In this Section, the extreme value distribution of process of the form (3.45) will be discussed. This type of processes is very instructive to understand the concepts of geometry in N-dimensions and the problems with overlap.

5.2.1 Stationary Process

In this Section, we compute the maximum of the special process

$$\xi(t) = X_1 \cos \omega t + X_2 \sin \omega t \tag{5.4}$$

where ω is a fixed positive constant. There are three reasons why this process is chosen as a first example. The extreme value distribution of this process can be computed analytically (See Chapter 2). It will be shown that Sun's formula yields the same result. The simple form of the process makes it easy to verify its representation on the unit sphere. Finally, some interesting observations about the problem of self-overlap can be made.

First, note that the process $\xi(t)$ is already in the form (3.3) with

$$\begin{cases} N = 2 \\ f_1(t) = \cos \omega t \\ f_2(t) = \sin \omega t \end{cases} \tag{5.5}$$

The variance of the process is constant:

$$\sigma_\xi^2(t) = \cos^2 \omega t + \sin^2 \omega t = 1 \tag{5.6}$$

Since the process is stationary, the expression for $c(t)$ (4.48) in Sun's Formula (4.58) can be simplified to yield:

$$c(t) = \sqrt{\sum_{i=1}^{2} f_i'(t)^2} = \omega \tag{5.7}$$

Insertion of (5.7) and (5.5) in Sun's formula (4.58) gives:

$$P(\beta) = \frac{1}{2\pi} \int_0^T \omega \exp\left(-\frac{\beta^2}{2}\right) dt + \frac{1}{2}\Phi(-\beta) + \frac{1}{2}\Phi(-\beta) \tag{5.8}$$

$$= \frac{\omega T}{2\pi} \exp\left(-\frac{\beta^2}{2}\right) + \Phi(-\beta) \tag{5.9}$$

This is exactly the analytical result derived in Section 2.1 with the restriction that this result (5.9) is only valid for values of T satisfying

$$0 < T < \frac{\pi}{\omega} \tag{5.10}$$

While the result obtained with Sun's Formula do not implicitly carry this restriction, it will be proven that (5.10) is necessary to avoid overlap. In order to explain this, we go back to the basic principles on which Sun's Method is based. Since there are only two discretization functions, the process $\xi(t)$ can be represented on a circle with radius 1. The vector $f(t)/|f(t)|$ is travelling with constant velocity on the perimeter of this circle. The representation is given in Figure 5.1. For the time

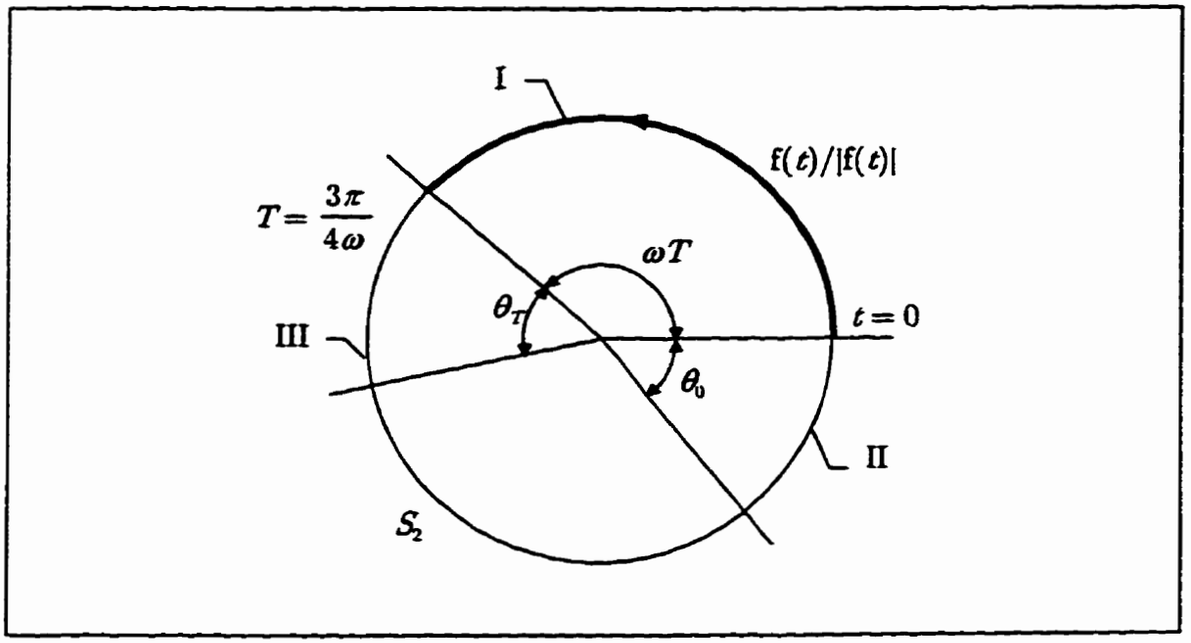

Figure 5.1: Representation of the Process $\xi(t)$ on the Unit Circle

being, we assume that

$$T = \frac{3}{4}\frac{\pi}{\omega} < \frac{\pi}{\omega} \tag{5.11}$$

Sun's formula was derived by integration of the conditional exceedance probability $P(\beta|\, R_N = r)$ cover all possible values of the random variable R_N (See Section 4.2.1):

$$P(\beta) = \int_0^\infty P(\beta|\, R_N = r)\, f_{\chi_2}(r)\, dr \tag{5.12}$$

where $f_{\chi_2}(r)$ is the probability density function of a χ_2-random variable with 2 degrees of freedom as defined in (4.9). For each value of R_N, the conditional probability $P(\beta|\, R_N = r)$ can be computed using the relative frequency approach. (See Section 4.2.2 and Appendix B). Rewriting equation (B.8) for the special case $N = 2$, we

obtain:

$$\int_0^\infty P(\beta|\, R_N = r) = \frac{1}{2\pi}\left(\underbrace{\omega T}_{\text{I}} + \underbrace{\theta_0}_{\text{II}} + \underbrace{\theta_T}_{\text{III}}\right) \tag{5.13}$$

with

$$\theta_0 = \theta_T = \begin{cases} \arccos(\beta/r) & \beta/r \leq 1 \\ 0 & \beta/r > 1 \end{cases} \tag{5.14}$$

Term I in equation (5.13) is the arclength associated with the path of the vector $f(t)/|f(t)|$. Term II and III represent arcs that are the two-dimensional equivalent of the N-dimensional hemi-spherical caps. Term I, II and III are represented in Figure 5.1.

It can now be explained why restriction (5.10) is necessary. From (5.14), it follows that

$$r \to \infty \qquad \Rightarrow \qquad \theta_0, \theta_T \to \frac{\pi}{2} \tag{5.15}$$

For values of $T > \frac{\pi}{\omega}$, the two angles θ_0 and θ_T will start to overlap as r increases. This is illustrated in Figure 5.2. As a consequence, the arclength associated with the overlap would be counted twice in the computation of $P(\beta|\, R_N = r)$. This can also be concluded from equation (5.13), which yields values for the conditional probability that are greater than one. This example illustrates a weakness of Sun's Method. Restrictions to avoid overlap are not an automatic result of the method. One has to look carefully into the geometrical representation on the unit-sphere to detect possible problems of overlap. This is relatively easy for the problem discussed here, but it is much more cumbersome when there are more than two discretization functions.

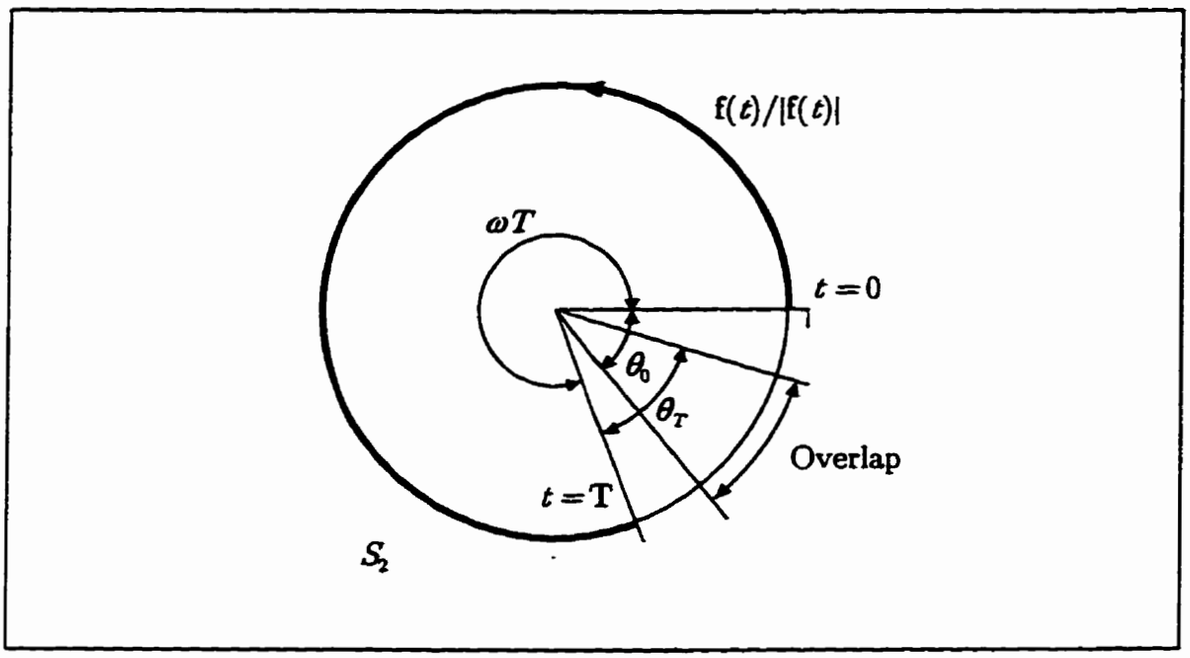

Figure 5.2: Overlap for Values of $T > \pi/\omega$

If restriction (5.10) is used with $\omega_{\max}$ the highest frequency in the discretization, i.e.

$$0 < T < \frac{\pi}{\omega_{\max}} \tag{5.16}$$

then, we can conclude with absolute certainty that there will be no overlaps. It should be noted however that (5.16) is a rather severe requirement.

As an example, the following process is studied:

$$X(t) = \sum_{i=1i}^{5} c_i \left(X_{1i} \cos \omega_i t + X_{2i} \sin \omega_i t\right) \qquad \text{for } t \in [0, 0.3] \tag{5.17}$$

with

$$\begin{aligned} c_i &= \tfrac{4+i}{\sqrt{510}} \\ \omega_i &= \pi \left(\tfrac{9+i}{5}\right) \end{aligned} \qquad i = 1, 2, ..., 5 \tag{5.18}$$

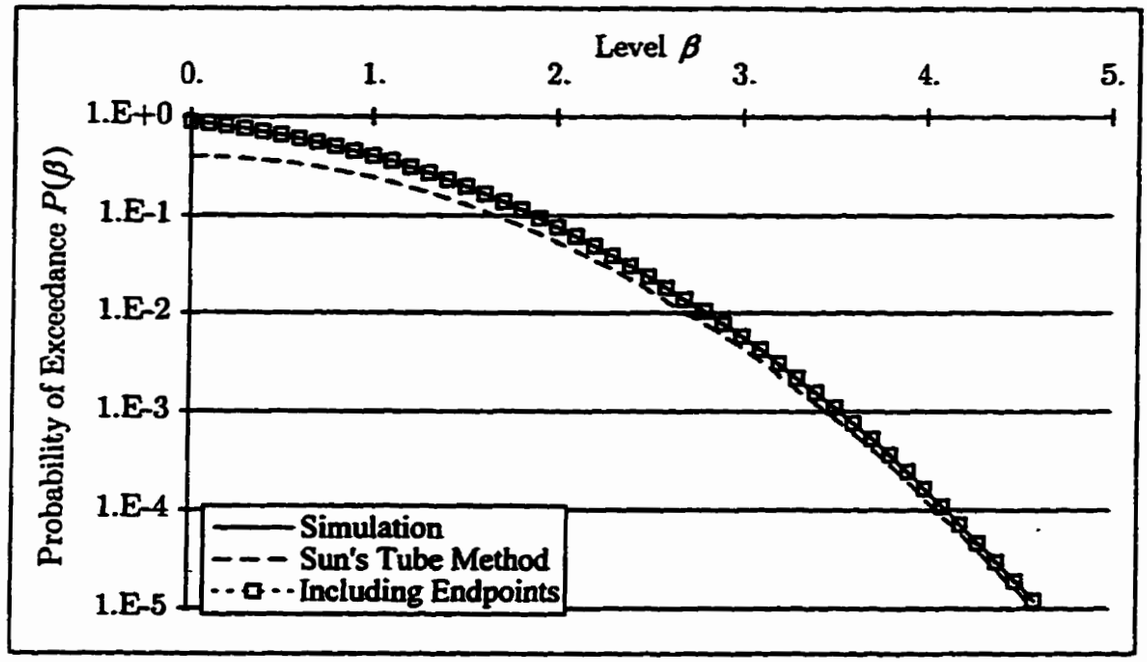

Figure 5.3: Extreme Value Distribution of the Stationary Process $X(t)$

Note that this is a stationary process with unit variance. The results obtained with Sun's method are compared with simulation results in Figure 5.3. The simulation results are based on 10^8 simulations. The graph shows clearly that neglecting the endpoint probabilities seriously underestimates the exceedance probability.

5.2.2 Non-Stationary Process

As discussed in Section 3.5, non-stationary processes can be obtained by taking different coefficients for the sine and cosine functions in the discretization. Sun's method is applied to a non-stationary process $Y(t)$:

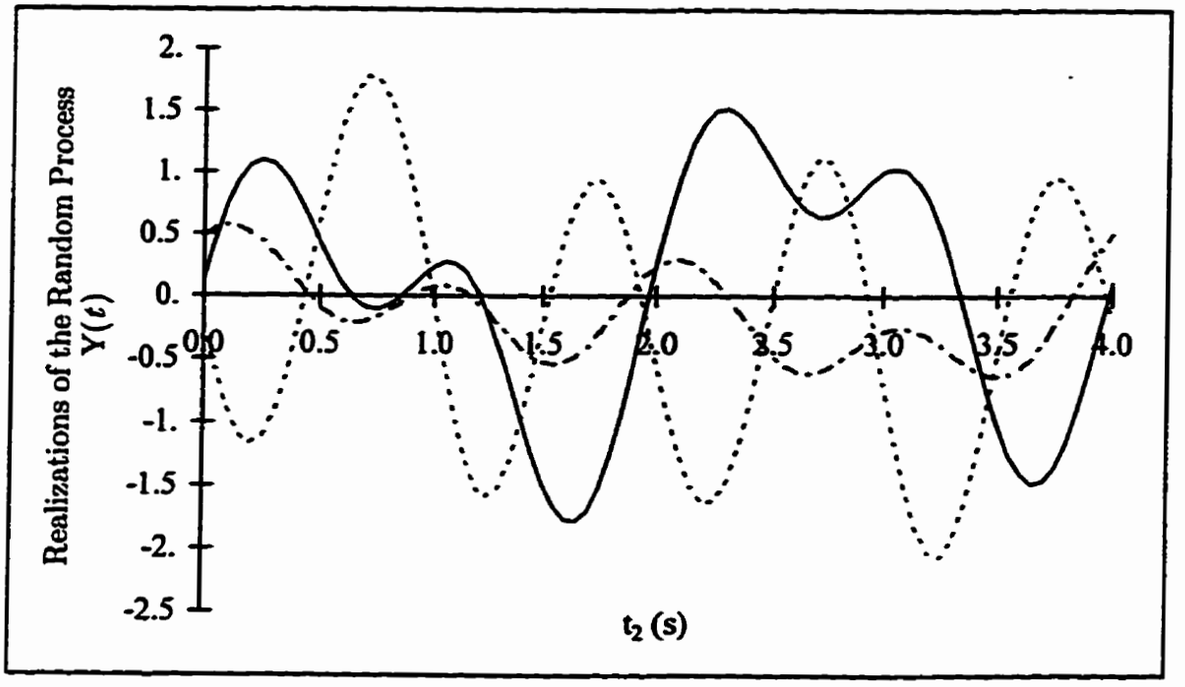

Figure 5.4: Samples of the Non-Stationary Process $Y(t)$

$$Y(t) = \tfrac{X_1}{2}\sin\left(\tfrac{\pi}{4}t\right) + X_2\sin\left(\tfrac{\pi}{2}t\right) + X_3\sin(\pi t) + X_4\sin(\pi t) + X_5\cos(\pi t) + X_6\cos(\pi t) \quad \text{for } t \in [0,4] \tag{5.19}$$

In Figure 5.4, 3 samples of this process are given. In Figure 5.5, the variance of the processes is plotted, together with the autocorrelation function at time-instances $t = 1$ s, 2 s and 3 s. As can be concluded from Figure 5.6, the results obtained with Sun's method are in good agreement with the exceedance probabilities obtained with simulation.

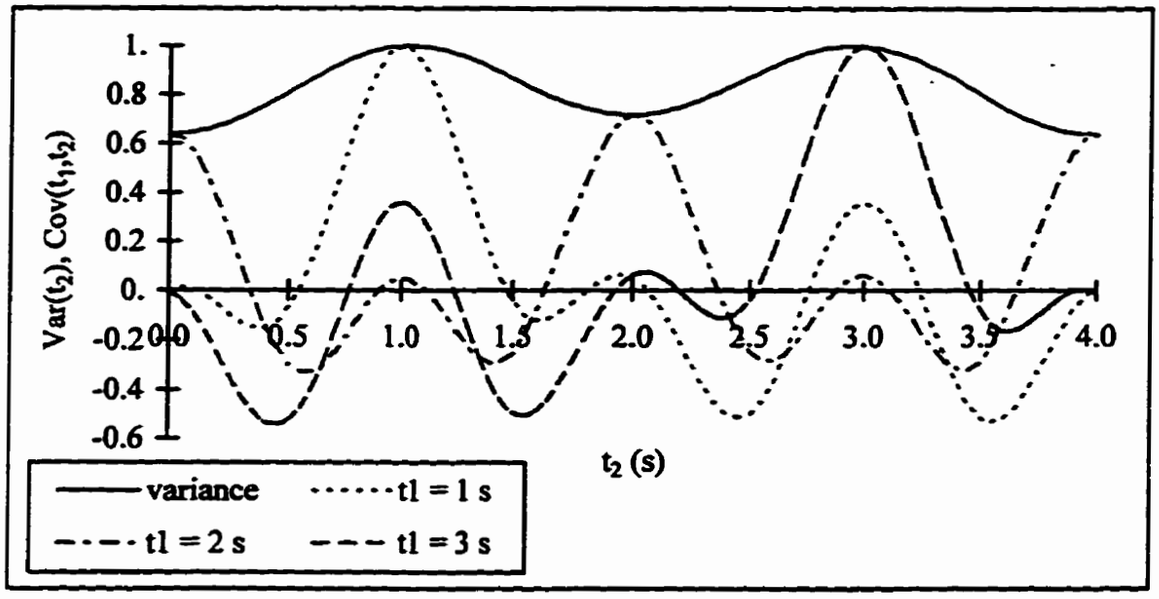

Figure 5.5: Variance and ACF of the Non-Stationary Process $Y(t)$

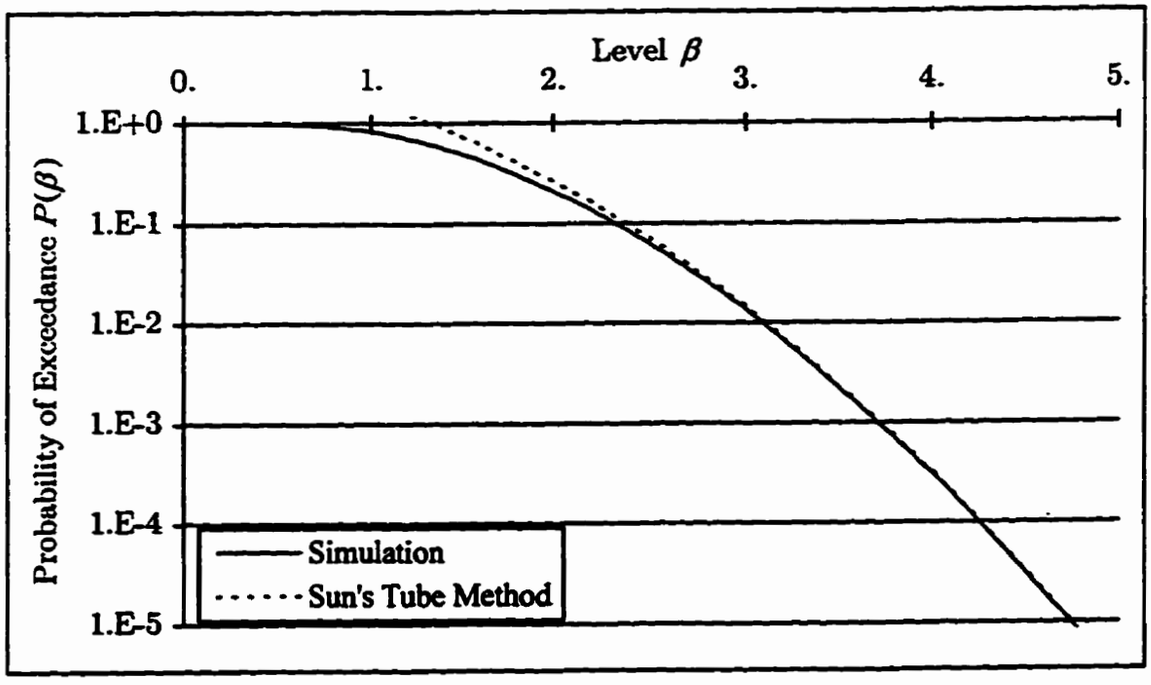

Figure 5.6: Extreme Value Distribution of the Non-Stationary Process $Y(t)$

5.3 Extreme Value Distribution of an Earthquake Signal

In order to apply Sun's Method to an earthquake signal, the discretization described in Section 3.4 is used. In Section 5.3.1, the two ground acceleration models proposed by Der Kiureghian and Li (1996) are introduced. In Section 5.3.2, some aspects of the simulation of such signals is discussed. In Section 5.3.3, Sun's Method is used to compute the extreme value distribution of a motion on firm ground.

5.3.1 Two Ground Acceleration Models

Der Kiureghian and Li (1996) use the discretization discussed in Section 3.4 to describe two ground motion processes. In both motions, the predominant frequency corresponds to the second filter. The first process describes a motion on a firm ground, and has a predominant frequency of 5π rad/s and the other, with a predominant frequency of 2π rad/s describes a motion on a soft ground or deep alluvial deposit. The assumed values of the parameters Φ_0, ω_f, ζ_f, q_0, a, b and t_0 for each filter of the two models are listed in Table 5.1.

Sample realizations of the two processes are shown in Figures 5.7 and 5.8. For these representation $\Delta t = 0.02$ s is used, which means that 20 s duration of each motion is described by 1000 random variable. The intensity parameter Φ_0 is selected such that for $q_k(t) = 1$ each acceleration record has a stationary root-mean-square value equal to $0.2g$ ($g = 9.81$ m/s^2). Note that the processes are distinctly nonstationary in both time and frequency domains. Consistent with typical ground motions, each process is initially rich in high frequencies and then it becomes richer in lower frequencies, which are dominant during the strong motion and coda phases

Parameter	$\Phi_0\,(m^2/s^3)$	$\omega_f\,(rad/s)$	ζ_f	q_0	$a\,(s^{-1})$	$b\,(s^{-1})$	t_0
Acceleration Process on Firm Ground							
Filter 1	0.0233	10π	0.6	0.718	0.256	2.568	0.0
Filter 2	0.0233	5π	0.4	1.300	0.193	2.901	3.0
Acceleration Process on Soft Ground							
Filter 1	0.0509	5π	0.4	0.718	0.256	2.568	0.0
Filter2	0.0509	2π	0.2	1.300	0.193	2.901	3.0

Table 5.1: Selected Parameter Values for Two Models of Ground Acceleration Process

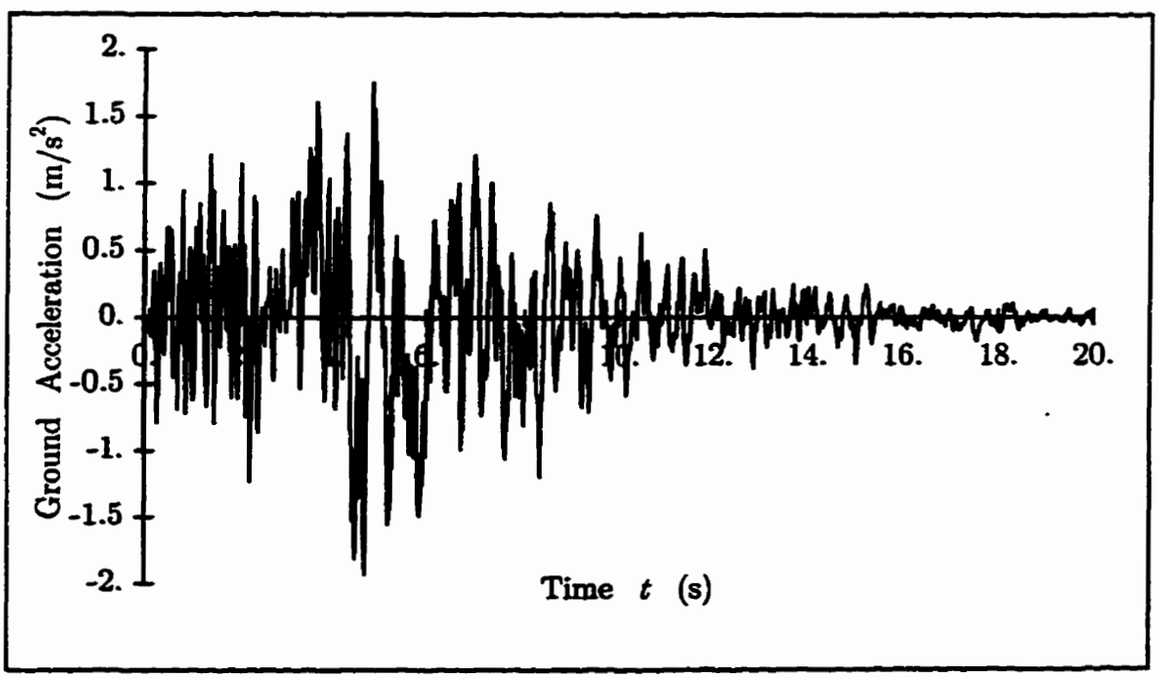

Figure 5.7: Realization of a Ground Acceleration Process on Firm Ground

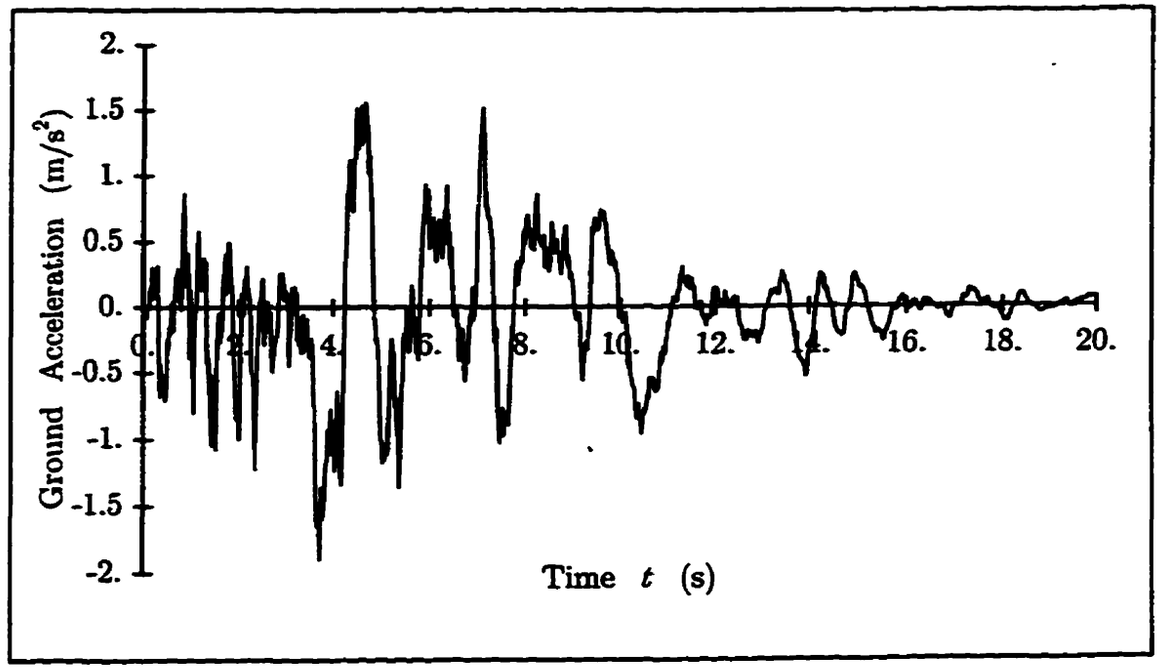

Figure 5.8: Realization of a Ground Acceleration Process on Soft Ground

of the record. The motion in Figure 5.7 is typical of acceleration records on firm ground, whereas the motion in Fugure 5.8 is typical of ground accelerations on deep soil deposits such as in Mexico city. In Figure 5.9, the variance of the ground motion process on firm ground is given, together with the Auto Covariance Function at time-instances $t = 2$ s, 5 s and 10 s. Figure 5.10 shows variance and covariances for the ground motion process on soft ground. Note how the correlation-length for the motion of soft ground is much larger than for the motion of soft ground. This can be explained by the fact that the damping ratio for firm ground motions is greater than for soft ground motions (See Table 5.1).

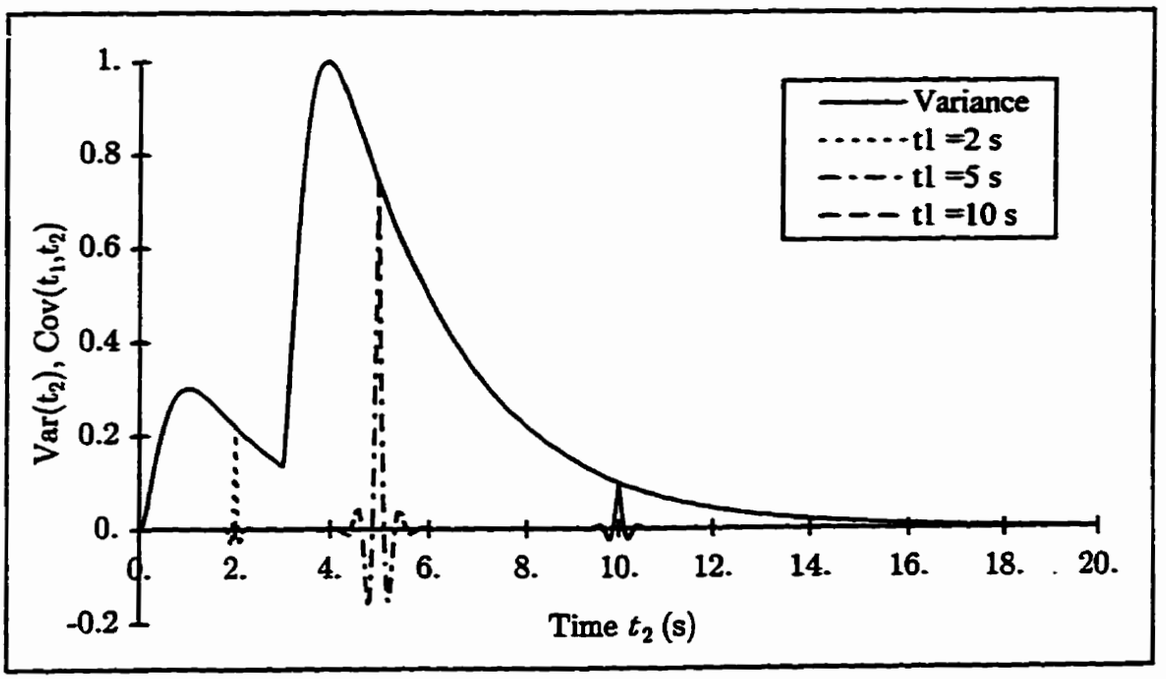

Figure 5.9: Variance and ACF of a Ground Acceleration Process on Firm Ground

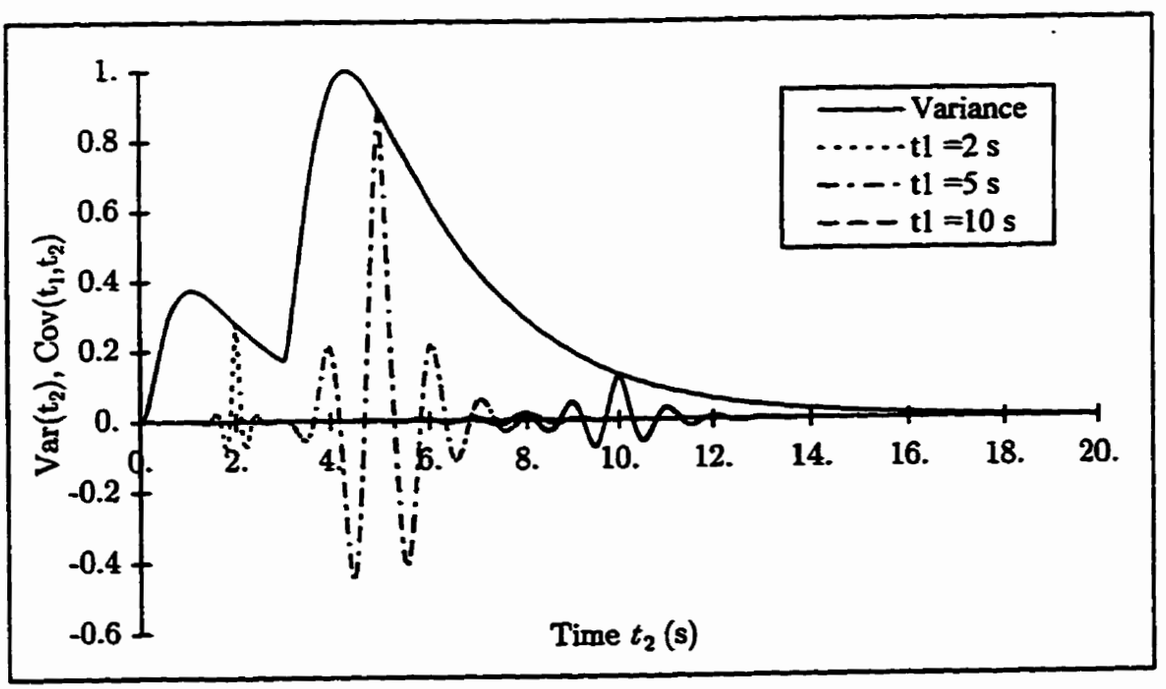

Figure 5.10: Variance and ACF of a Ground Acceleration Process on Soft Ground

5.3.2 Simulation of Earthquake Signals

We repeat the formula for the discretization of earthquake signals given in Section 3.4:

$$\hat{X}(t) = \sum_{i=1}^{N} X_i f_i(t) \tag{5.20}$$

with

$$f_i(t) = \sum_{k=1}^{2} \sigma q_k(t_i)\, a_{ik}(t) \tag{5.21}$$

where the summation is over the two filter considered in the models. Equation (5.20) and (5.21) can be combined to yield

$$\hat{X}(t) = \sigma \sum_{i=1}^{N} X_i \left(\sum_{k=1}^{2} q_k(t_i)\, a_{ik}(t) \right) \tag{5.22}$$

Simulation of the earthquake signal (5.22) is computationally cumbersome. With $\Delta t = 0.02$ s and $T_{total} = 20$ s, 1000 random variables have to be generated for each realization. Furthermore, hundreds of discretization functions have to be added to find the value of $\hat{x}(t)$ at a given time instance t. However, generating samples can be made more efficient by noting that (See equation (3.35)):

$$a_{ik}(t) = 0 \qquad \text{if} \qquad t < t_{i-1} \tag{5.23}$$

Therefore, N in expression (5.22) can be replaced by

$$N(t) = int\left(\frac{t}{\Delta t}\right) + 2 \tag{5.24}$$

Next, it can be observed that

$$a_{ik}(t) = \begin{cases} 0 & t < t_{i-1} \\ a_{1k}(t - t_i) & t \geq t_{i-1} \end{cases} \tag{5.25}$$

This means that the function $a_{ik}(t)$ as defined in (3.35) has to be computed only once for both filters. The process (5.22) can now be written as

$$\hat{X}(t) = \sigma \sum_{i=1}^{N(t)} X_i \left(\sum_{k=1}^{2} q_k(t_i)\, a_{1k}(t - t_i) \right) \tag{5.26}$$

Finally, we can observe that, due to the relatively large damping ratio, the values for the discretization function $a_{1k}(t)$ become small after a short length of time. This is illustrated in Figure 5.11 , where the discretization function $f_{10}(t)$ for an acceleration process on firm ground is plotted. As a consequence, the contribution of a specific discretization function $f_i(t)$ to the value of $\hat{x}(t)$ can be neglected for values

$$t \gg t_i \tag{5.27}$$

While all the foregoing observations enable us to improve the efficiency of sampling significantly, simulation remains computationally demanding.

5.3.3 Results of Sun's Method

In this Section, Sun's Method is used to compute the extreme value distribution of a ground acceleration process on firm ground. The results are given in Figure 5.12. The results are in good agreement with Monte Carlo simulation. For the level

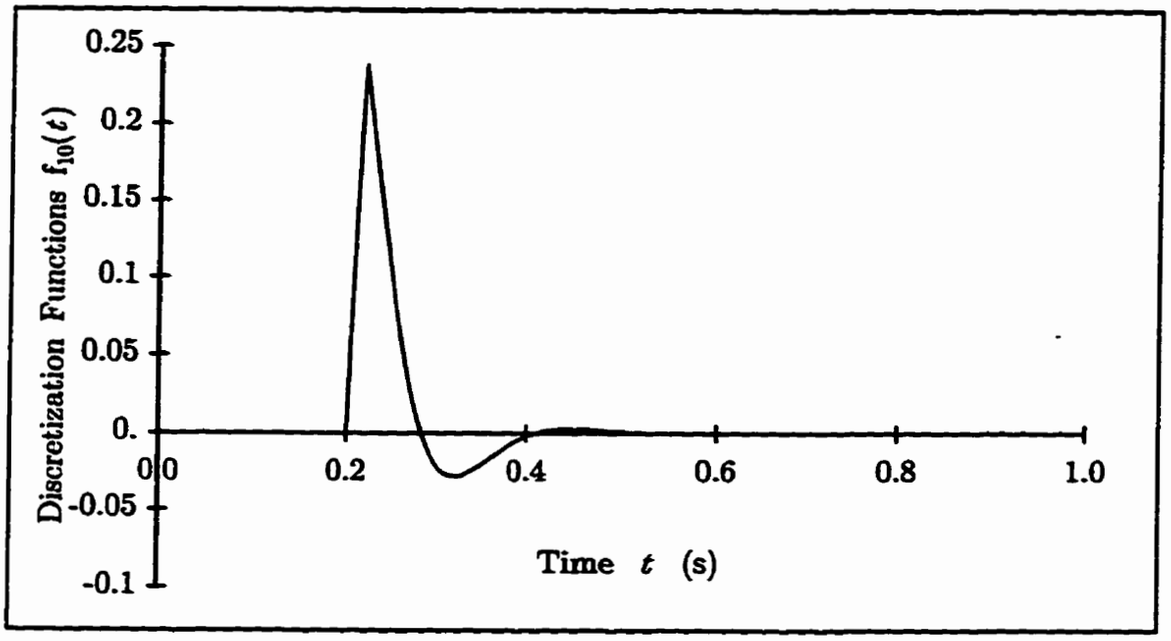

Figure 5.11: Discretization Function $f_{10}(t)$ of a Ground Motion on Firm Ground

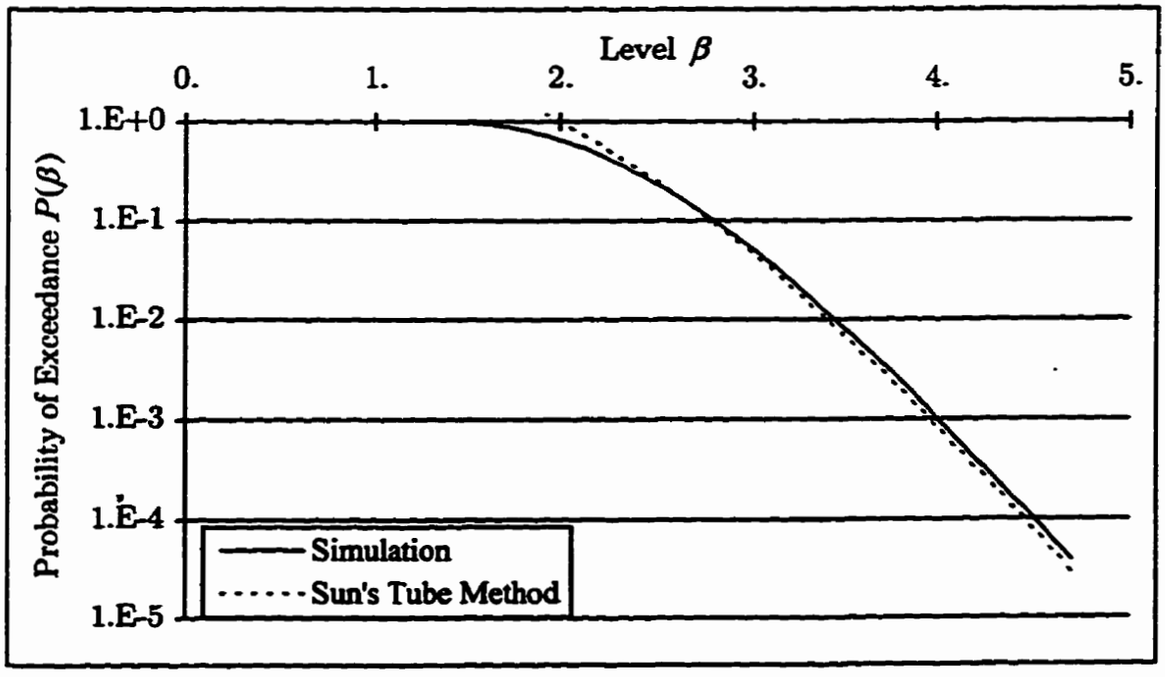

Figure 5.12: Extreme Value Distribution of a Ground Acceleration Process on Firm Ground

$\beta = 4.5$, Sun's Method underestimates the log(exceedance probability) = $(log(P(\beta))$ obtained using simulation by 2.5 %. This difference can be explained by the nature of the discretization functions. One of those discretization functions is plotted in Figure 5.11. The function is continuous in time but, due to the way $f_i(t)$ is defined in Equation (3.35), its first derivative has a discontinuity at $t = t_{i-1}$ and at $t = t_i$. This means that the path, described on the unit sphere by the vector $\mathbf{f}(t) / |\mathbf{f}(t)|$, is continuous, but that there is a sudden change in direction after every time-interval Δt. At those points, the tube around the path of $\mathbf{f}(t) / |\mathbf{f}(t)|$ has self-overlap (See Figure 4.7 in Section 4.3). This self-overlap decreases with increasing β. To obtain a more accurate estimation of the area of the tube at those points, higher order terms should be considered.

5.4 Extreme Value Distribution of a Stochastic Response

As discussed in Section 3.4.3, discretized stochastic responses are obtained by applying the earthquake signal (5.22) to a filter. In Section 5.4.1, a specific stochastic response is introduced. In Section 5.4.2, some observations about the discretization and simulation of stochastic responses are made. In Section 5.4.3, Sun's Method is used to compute the extreme value distribution of the stochastic response defined in Section 5.4.1. Finally, in Section 6.1, it is explained how Sun's Method can be used to compute the response of non-linear systems.

5.4.1 Stochastic Responses

The acceleration process of a motion on firm ground is now considered as the input signal to a single-degree-of-freedom linear oscillator whose motion is governed by the following dynamic equation of motion:

$$\ddot{u}(t) + 2\zeta_0\omega_0\dot{u}(t) + \omega_0^2 u(t) = -\hat{X}(t) \tag{5.28}$$

$\hat{X}(t)$ is the absolute acceleration of the ground in a discretized form as defined in equation (5.22). $u(t)$ is the displacement of the mass relative to the ground and ω_0 and ζ_0 are the natural frequency and viscous damping ratio of the oscillator. These concepts are given in Figure 3.1 on page 21. In this example, the following values are assumed for the oscillator properties:

$$\zeta_0 = 0.05 \tag{5.29}$$

$$\omega_0 = 2\pi \text{ rad/s} \tag{5.30}$$

Note that this represents a case where the oscillator frequency is less than the predominant frequency of the ground motion, which is 5π rad/s for a motion on firm ground. As discussed in Section 3.4.3, the resulting stochastic response $\hat{Y}(t)$ can be computed in the following discretized form:

$$\hat{Y}(t) = \sum_{i=1}^{N} X_i f_{iY}(t) \tag{5.31}$$

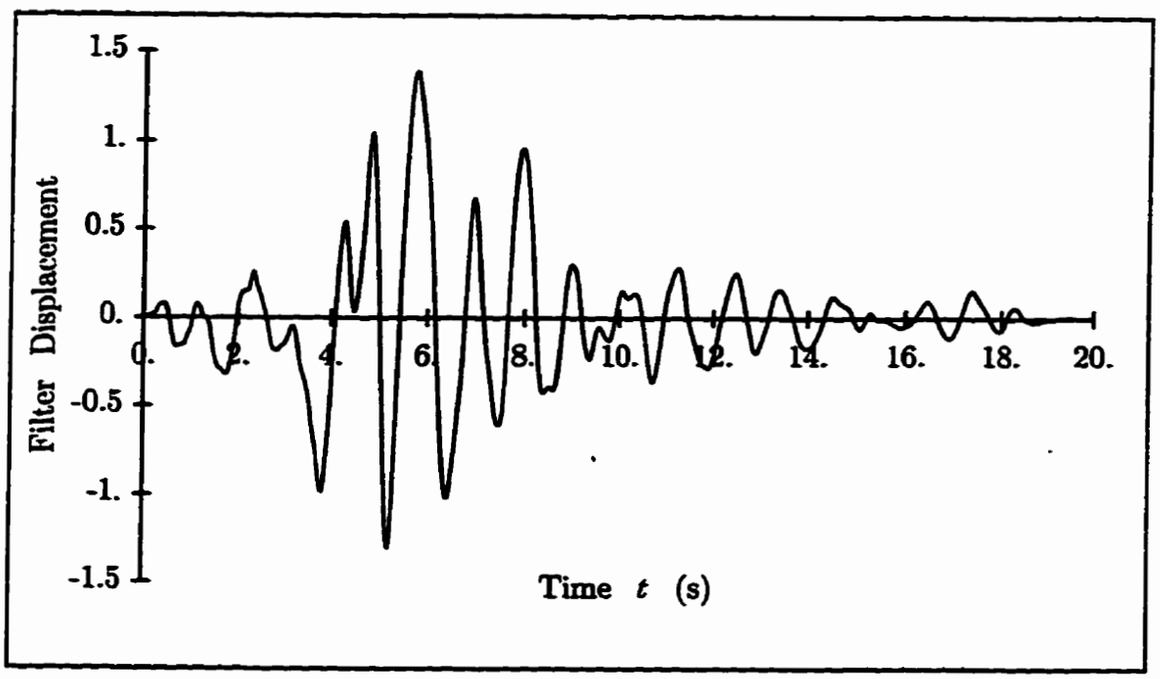

Figure 5.13: Realization of the Filter Displacement $\hat{Y}(t)$

with $f_{iY}(t)$ the response to the discretization function $f_i(t)$, which is now considered as an input signal:

$$f_{iY}(t) = \int_0^t f_i(\tau)\, h_Y(t-\tau)\, d\tau \tag{5.32}$$

with $h_Y(t)$ the unit-impulse-response functions of the linear oscillator (Clough and Penzien, 1975) defined by the governing equation (5.28):

$$h_Y(t) = \frac{1}{\omega_0\sqrt{1-\zeta_0^2}} \sin\left(\omega_0\sqrt{1-\zeta_0^2}t\right) \tag{5.33}$$

5.4.2 Simulation of Stochastic Responses

A sample of the stochastic response $\hat{Y}(t)$ is given in Figure 5.13. In Figure 5.14, the variance of the response is given, together with the autocorrelation function at times $t = 2$ s, 5 s and 10 s. The same observations that were made for the simulation of

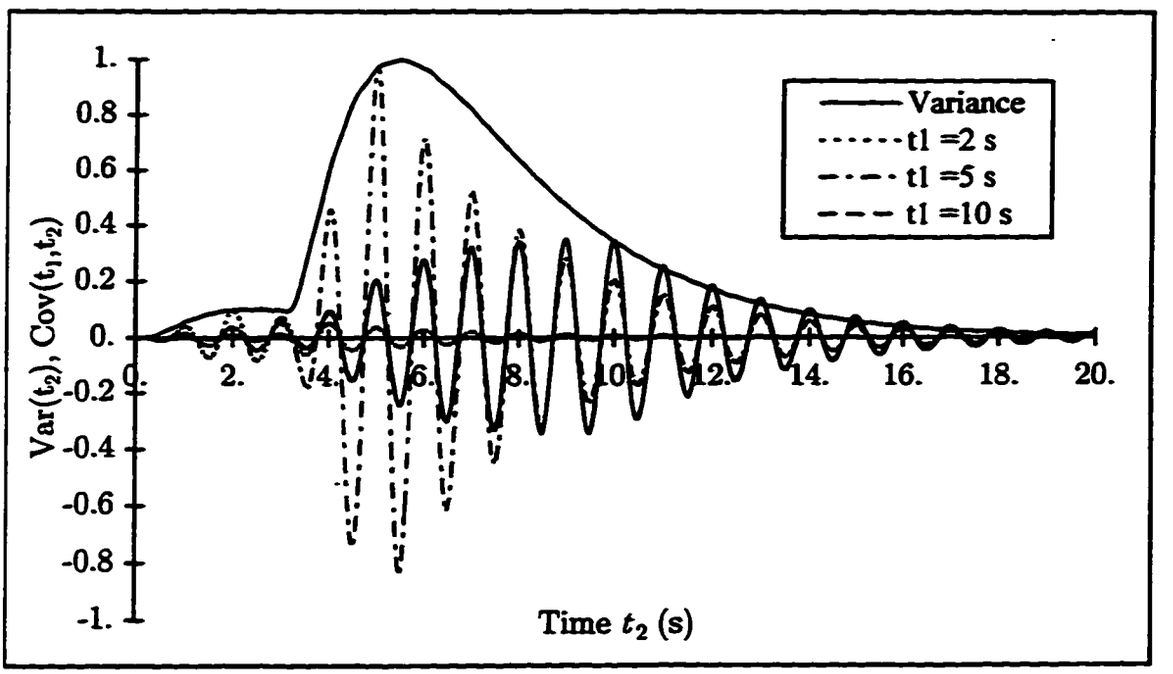

Figure 5.14: Variance and ACF of the Stochastic Response $\hat{Y}(t)$

earthquake signals (See Section 5.3.2), are valid for the simulation of stochastic responses, except for the fact that in this case, the value of the discretization functions does not decrease as rapidly as in the case of earthquake-signals. This is illustrated in Figure 5.15, where the discretization function $f_{10Y}(t)$ of the stochastic response $\hat{Y}(t)$ (5.31) is plotted. This can be explained by the small damping ratio of the linear oscillator ($\zeta_0 = 0.05$). As a consequence, simulation of stochastic responses is even more computationally demanding than the simulation of earth-quake signals.

5.4.3 Results of Sun's Method

In this section, Sun's Method is used to compute the extreme value distribution of the stochastic response defined in 5.4.1. These results are given in Figure 5.16. The results obtained using Sun's Method are exceptionally good. For the level $\beta = 4.5$,

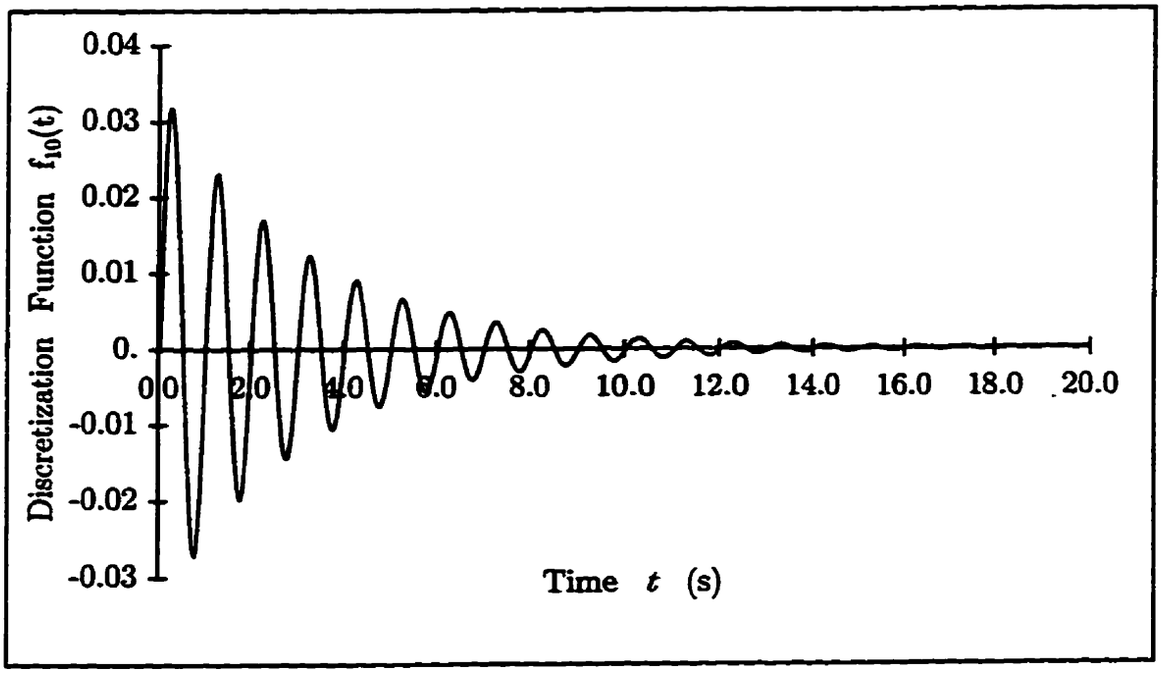

Figure 5.15: Discretization Function $f_{10Y}(t)$ of the Stochastic Response $\hat{Y}(t)$

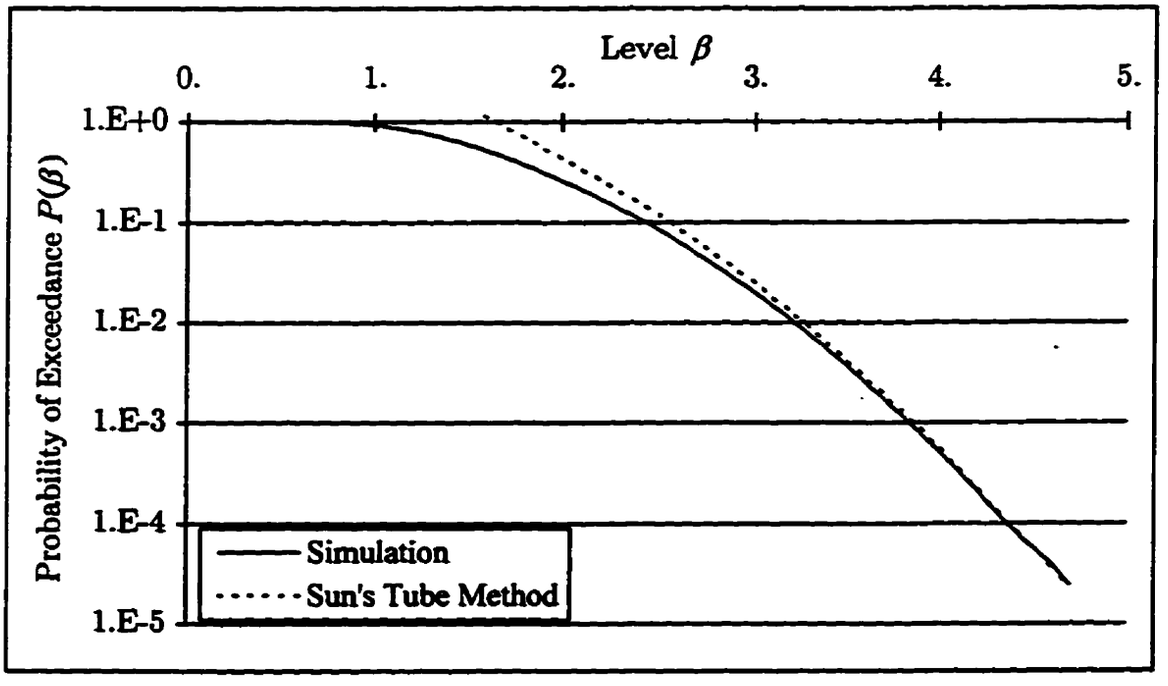

Figure 5.16: Extreme Value Distribution of the Stochastic Response $\hat{Y}(t)$

Sun's Method underestimates the log(exceedance probability) obtained using simulation by about 0.6 %. The fact that the method gives better results for a stochastic response to an earthquake signal than for the earthquake signal itself can be explained by the nature of the discretization functions. Unlike the discretization functions $f_i(t)$ for the earthquake signal (See Figure 5.11), the discretization functions $f_{iY}(t)$ for the stochastic response $\hat{Y}(t)$ (Figure 5.31) do not have discontinuities in the first derivative (See Section 5.3.3). The functions $f_{iY}(t)$ are the result of a convolution (4.6) of the functions $f_i(t)$ (which are discontinuous in the *first* derivative) and $h_Y(t)$. Therefore, the functions $f_{iY}(t)$ are discontinous in the *second* derivative. As a consequence, there are no sharp turns in the path of the vector $\mathbf{f}(t) / |\mathbf{f}(t)|$ in the case of stochastic responses. The 'smoothness' of the curve prevents problems with self-overlap.

Chapter 6

Extensions of Sun's Tube Method

In this Chapter, two interesting extensions of Sun's Method are discussed. In Section 6.1, it is shown how Sun's Method can be applied to non-linear stochastic responses. In Section 6.2, it is discussed how Sun's Method can be applied to higher-dimensional random fields.

6.1 Non-Linear Stochastic Structural Responses

6.1.1 Introduction

In this Section, it will be shown how Sun's Method can be used to compute the extreme value distribution of non-linear responses. In the case of a non-linear filter, the convolution technique discussed in Section 3.4.3 can no longer be used since convolution is based on the principle of superposition. There are however many important structural dynamics problems which cannot assumed to be linear, e.g. the response of a building to an earthquake motion severe enough to cause serious damage (Clough and Penzien, 1975).

In Sections 6.1.2 and 6.1.3, we assume that the system parameters, such as the damping ratio ζ and the natural frequency ω are fixed. In Section 6.1.4, it is shown how the following approach can be adapted to also deal with stochastic system parameters.

The equation of motion for a non-linear filter can be written as

$$\ddot{u}(t) + 2\zeta\omega\dot{u}(t) + S(u(t), \dot{u}(t))\, u(t) = -\hat{X}(t) \tag{6.1}$$

where $S(u(t), \dot{u}(t))$ is the restoring force, which is a function of the displacement $u(t)$ and the velocity $\dot{u}(t)$ of the filter.

6.1.2 Limit-State Function

We are interested in finding the probability that the non-linear response $u(\mathbf{X}, t)$ exceeds a level β in an interval $[0, T]$. In other words, we are interested in computing

$$\Pr\left(\min_{t\in[0,T]} g(u(\mathbf{X}, t), \beta) \leq 0\right) \tag{6.2}$$

where $g(u(\mathbf{X}, t), \beta)$, is the limit-state function at time t defined as

$$g(u(\mathbf{X}, t), \beta) = \beta - u(\mathbf{X}, t) \tag{6.3}$$

In (6.3), $\mathbf{X}$ are the independent standard normal random variables that determine the input signal (See Section 3.1) and t and β are deterministic parameters that determine respectively the time and the threshold.

In order to compute the probability (6.2), we divide $[0, T]$ in n small intervals Δt_i, $i = 1, 2, ..., n$ and choose the time points t_1, t_2, ...t_n in the middle of each interval Δt_i (See Figure 6.1). For high levels of β, the probability (6.2) can be approximated

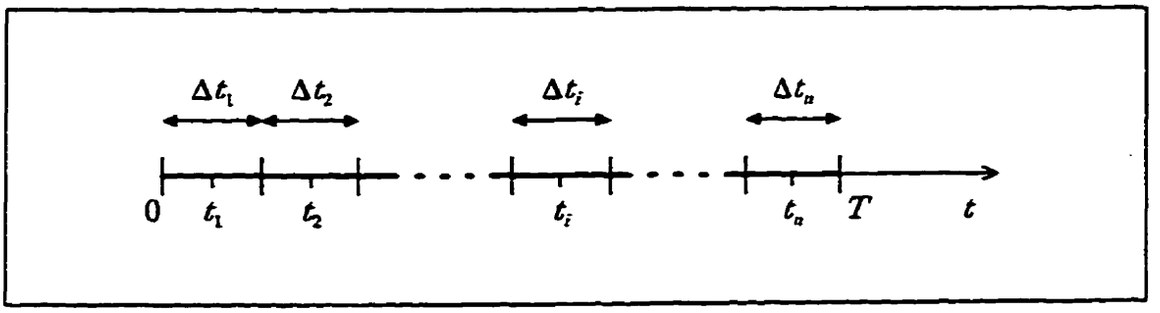

Figure 6.1: Discretization of the Interval $[0, T]$

by adding up elementary exceedance probabilities:

$$\Pr\left(\min_{t\in[0,T]} g\left(u\left(\mathbf{X},t\right),\beta\right)\leq 0\right) \cong \sum_{i=1}^{n}\Pr\left(\min_{t\in\Delta t_i} g\left(u\left(\mathbf{X},t\right),\beta\right)\leq 0\middle| t\in\Delta t_i\right) \quad (6.4)$$

$$\cong \sum_{i=1}^{n} P_i\left(\beta\right) \quad (6.5)$$

where $P_i\left(\beta\right)$ denotes the probability that the limit-state function $g\left(u\left(\mathbf{X},t\right),\beta\right)$ is negative in the interval Δt_i. This is equivalent to the probability that the non-linear stochastic response will exceed the level β in the interval Δt_i.

6.1.3 Computation of Elementary Probabilities Using Sun's Formula

It will now be indicated how the elementary exceedance probabilities in equation (6.5) can be approximated using Sun's Tube Method. For each time point t_i in the middle of the interval Δt_i, the most likely failure point $\mathbf{x}_i^*$ is computed. The most likely failure point $\mathbf{x}_i^*$ is the point on the limit state surface closest to the origin of the standard-normal domain. Since the random variables describing the input signal $X\left(t\right)$ are standard normal and independent, no transformation is needed. To find the

most likely failure point $\mathbf{x}_i^*$, the algorithm developed by Zhang and Der Kiureghian (1995) can be used. This algorithm requires repeated computations of the limit-state function $g\left(u\left(\mathbf{X},t\right),\beta\right)$. Therefore, deterministic computations of equation (6.1) and its gradients

$$\nabla_{\mathbf{x}}\left(u\left(t\right)\right)=\begin{pmatrix}\frac{\partial}{\partial x_1}\left(u\left(t\right)\right)\\ \frac{\partial}{\partial x_2}\left(u\left(t\right)\right)\\ \vdots\\ \frac{\partial}{\partial x_N}\left(u\left(t\right)\right)\end{pmatrix} \tag{6.6}$$

are required. Equation (6.1) can be solved using a Newmark Integration Method (Craig, 1981, p. 147) and the required derivatives (6.6) can be obtained directly by differentiating the discretized equations of motion (Der Kiureghian and Li, 1996). Once the most likely failure point $\mathbf{x}_i^*$ is determined, the limit state function at time t_i is linearized at the point $\mathbf{x}_i^*$ to yield

$$g\left(u\left(\mathbf{X},t_i\right),\beta\right)\simeq\beta-\left[u\left(\mathbf{x}_i^*,t_i\right)+\nabla_{\mathbf{x}}u\left(\mathbf{x}_i^*,t_i\right)\left(\mathbf{X}-\mathbf{x}_i^*\right)\right] \tag{6.7}$$

Expression (6.7) is obtained by approximating $u\left(\mathbf{X},t\right)$ in expression (6.3) by its first-order Taylor Expansion around the point $\mathbf{x}_i^*$. We now group all the terms that are constant and deterministic for a specific interval Δt_i, so that we can write:

$$g\left(u\left(\mathbf{X},t_i\right),\beta\right)\simeq\underbrace{\beta-u\left(\mathbf{x}_i^*,t_i\right)+\nabla_{\mathbf{x}}u\left(\mathbf{x}_i^*,t_i\right)\left(\mathbf{x}_i^*\right)}_{\beta_i^*}-\nabla_{\mathbf{x}}u\left(\mathbf{x}_i^*,t_i\right)\mathbf{X} \tag{6.8}$$

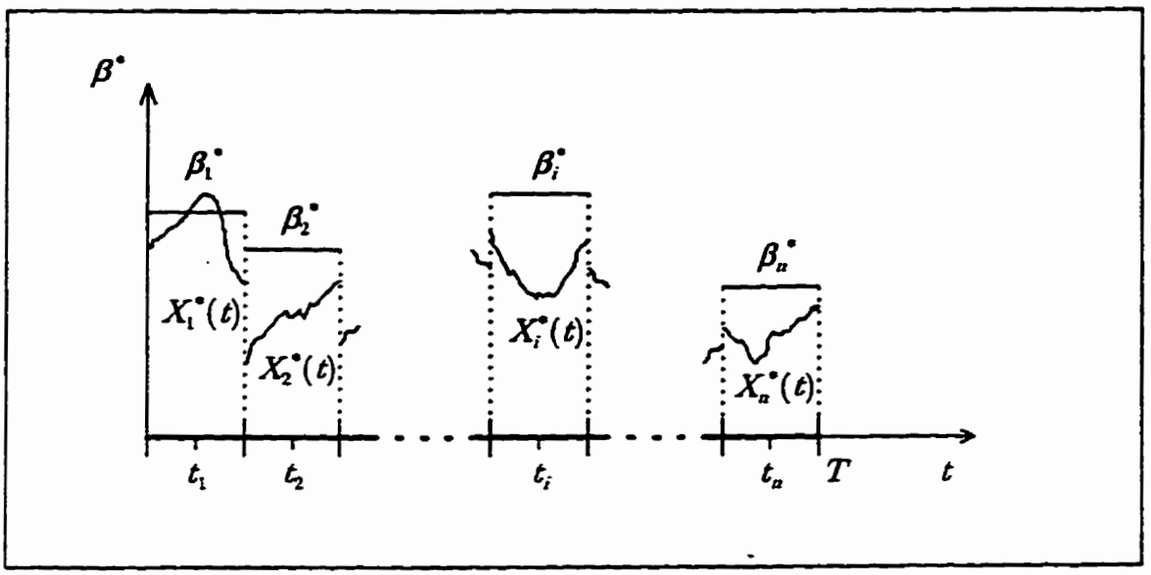

Figure 6.2: n level-upcrossing problems

Next, it is assumed that the limit-state-function $g(u(\mathbf{X},t),\beta)$ for points t sufficiently close to t_i (i.e. $t \in \Delta t_i$), can be approximated by

$$g_i(u(\mathbf{X},t),\beta) \simeq \beta_i^* - \underbrace{\nabla_{\mathbf{x}} u(\mathbf{x}_i^*,t)\,\mathbf{X}}_{X_i^*(t)} \qquad i = 1,2,...,n \tag{6.9}$$

where $g_i(\cdot)$ represents the linearized limit-state function and $X_i^*(t)$ defines a stochastic process in the interval Δt_i. Equation (6.9) shows that each probability $P_i(\beta)$ in (6.5) can be considered as the probability that a stochastic process $X_i^*(t)$ exceeds the level β_i^*(See Figure 6.2): If we insert the definition for the gradient of $u(\mathbf{x}_i^*,t)$ in the expression for $X_i^*(t)$ (6.9), the following representation is obtained for $X_i^*(t)$:

$$X_i^*(t) = \langle \nabla_{\mathbf{x}} u(\mathbf{x}_i^*, t), \mathbf{X} \rangle \tag{6.10}$$

$$= \sum_{j=1}^{N} f_j^*(t) X_j \qquad i = 1, 2, ..., n \tag{6.11}$$

where $f_j^*(t)$ is defined as

$$f_j^*(t) = \frac{\partial}{\partial x_j}(u(\mathbf{x}_i^*, t)) \tag{6.12}$$

Notice that this is the format required to apply Sun's Tube Method (See Section 3.1). Therefore, each probability $P_i(\beta)$ in (6.5) can be computed using Equation (4.57).

6.1.4 Stochastic System Parameters

The method discussed above can also be extended to the case of non-linear systems with stochastic system parameters. Let those system parameters be represented by the random vector $\mathbf{V}$. Now, the limit state function includes the set of random variable $\mathbf{V}$. A transformation will be needed to represent the system random variables $\mathbf{V}$ in the standard-normal domain. An algorithm for this transformation can be found in Hohenbichler and Rackwitz (1981). The most likely failure point will now depend on both the input and the system random variables: $(\mathbf{x}_i^*, \mathbf{v}_i^*)$. As a consequence, gradients of $u(\mathbf{x}_i^*, t)$ with respect to v will be included in the first-order Taylor Expansion of the limit-state function around the most likely failure point $(\mathbf{x}_i^*, \mathbf{v}_i^*)$. Those gradients will also be present in the definition of the stochastic process $X_i^*(t)$. However, the main steps outlined in Section 6.1.3 remain the same.

6.2 Extremes of Random Fields

While this thesis mainly focuses on the application of Sun's Method to one-dimensional random fields (i.e. stochastic processes), the method can also be applied to higher d-dimensional random fields (Sun, 1993 and Maes and Breitung, 1996). In fact, Sun's method becomes increasingly attractive as d increases, since traditional upcrossings techniques (See Section 2.1) become more cumbersome and less accurate, while Sun's approach requires little additional analytical effort.

In Section 6.2.1, the problem is reformulated for random fields of dimension 2 and higher. The fundamental ideas of Sun's method for higher dimensional random fields and the differences with the one-dimensional case are discussed in Section 6.2.2. In Section 6.2.3, the results of the two-term asymptotic approximation are given.

6.2.1 Formulation

Let T denote a compact subset of $\mathcal{R}^d$. Consider a d-dimensional Gaussian random field $Z(\mathbf{t})$ with $\mathbf{t} = (t_1, t_2, \ldots, t_d) \in T$ in the following discretized form:

$$Z(\mathbf{t}) = \sum_{i=1}^{N} Z_i h_i(\mathbf{t}) \tag{6.13}$$

The Z_i's are a set of independent standard normal random variables and the functions $h_i(\mathbf{t})$ are a set of deterministic functions, defined in the domain T. Possible discretizations include, but are not limited to, the truncated Karhunen-Loève expansion (Section 3.2) and the discretization obtained with the Expansion Linear Optimization Method (Li and Der Kiureghian (1993) or Section 3.3 of this thesis).

The objective is to obtain the extreme value distribution of this random field

$Z(\mathbf{t})$ within the domain T. More precisely, we are interested in approximating

$$P(\beta) = \Pr\left(\max_{\mathbf{t}\in T} Z(\mathbf{t}) \geq \beta\right) \tag{6.14}$$

Adler (1981) gives a one-term approximation for this probability, based on the concept of approximating the process of upcrossings by a Poisson process. Sun (1993) notes that this approximation often becomes very inaccurate for higher dimensions and is only applicable to homogeneous (i.e. stationary) random fields. Furthermore, Adler's approach of the problem cannot be used to obtain higher order approximations.

Note that due to the independence of the random variables Z_j, the autocorrelation function $R(\mathbf{s},\mathbf{t})$ can be computed as

$$R(\mathbf{s},\mathbf{t}) = \mathbb{E}\left(Z(\mathbf{s})\, Z(\mathbf{t})\right) = \sum_{i=1}^{N} h_i(\mathbf{s})\, h_i(\mathbf{t}) \tag{6.15}$$

and the variance $\sigma_Z^2(\mathbf{t})$ is simply

$$\sigma_Z^2(\mathbf{t}) = R(\mathbf{t},\mathbf{t}) = \sum_{i=1}^{N} h_i^2(\mathbf{t}) \tag{6.16}$$

Further, it is assumed that the field is scaled in such a way that this variance is less that or equal to 1 over the entire domain T and that its peak value in T is exactly equal to 1.

6.2.2 Fundamentals of Sun's Method for Random Fields

The general concept is analogous as for stochastic processes. The main ideas are given here.

The vector $\mathbf{Z} = (Z_1, Z_2, ..., Z_N)$ is written as the product of random variable R_N with a χ_N-distribution having N degrees of freedom and a random vector $\mathbf{U}$ with a uniform distribution on the N-dimensional unit sphere. This enables the computation of $P(\beta)$ by integration over all possible values of the random variable R_N:

$$P(\beta) = \int_0^\infty P(\beta | R_N = r) f_{\chi_N}(r) dr \tag{6.17}$$

where $f_{\chi_N}(r)$ is the probability density function of a χ_N-random variable. The conditional probability $P(\beta | R_N = r)$ is defined by

$$P(\beta | R_N = r) = \Pr\left(\max_{t \in T} Z(\mathbf{t}) \geq \beta \middle| R_N = r \right) \tag{6.18}$$

This conditional probability can be computed using the relative frequency approach. It can be expressed as the surface area of a subset of the N-dimensional sphere fulfilling the inequality (6.14) divided by the area of that sphere. To find an approximation for such areas, geometric results from Hotelling (1939) and Weyl (1939) about the volume of tubes around manifolds on spheres may be used. The difference with the one-dimensional case of stochastic processes lies in the fact that, we are now dealing with tubes around d-dimensional manifolds, rather than with tubes around curves.

A d-dimensional manifold $\mathcal{V}^N$ in the N-dimensional space $\mathcal{R}^N$is defined as:

$$\mathcal{V}^N = \left\{ \mathbf{v}^N(\mathbf{t}), \mathbf{t} = (t_1, t_2, ..., t_d) \in \mathbf{T}, \mathbf{v}^N(\mathbf{t}) = (v_1(\mathbf{t}), v_2(\mathbf{t}), ..., v_N(\mathbf{t})) \right\} \tag{6.19}$$

As a consequence, the geometrical interpretation of the problem is less straightforward. In the one-dimensional case, the formula provided by Hotelling (1939) for the surface area yields a one term approximation for the extreme value distribution of a stochastic process. The surface area of tubes around higher dimensional manifolds may be found in Weyl (1939). As illustrated in Sun (1993) and Maes and Breitung (1996), those expressions can be used to obtain approximation for $P(\beta)$ with any degree of accuracy. In the next section, the two term asymptotic approximation is given.

6.2.3 Two-Term Approximation of Tail Probability

First we introduce the $d \times d$ symmetric tensor matrix $G(\mathbf{t})$ which has elements g_{ij} defined as follows:

$$g_{ij}(\mathbf{t}) = \left. \frac{\partial^2 R(\mathbf{s}, \mathbf{t})}{\partial s_i \partial t_j} \right|_{\mathbf{s}=\mathbf{t}} = \mathbb{E}\left\{ \frac{\partial Z(\mathbf{t})}{\partial t_i} \frac{\partial Z(\mathbf{t})}{\partial t_j} \right\} \tag{6.20}$$

From the independence of the standard normal random variables Z_i, it follows that the i by j element of the matrix $G(\mathbf{t})$ can also be written as:

$$g_{ij}(\mathbf{t}) = \sum_{k=1}^{N} \frac{\partial h_k(\mathbf{t})}{\partial t_i} \frac{\partial h_k(\mathbf{t})}{\partial t_j} \tag{6.21}$$

d-Dimensional Random Fields

Sun (1993) lists a number of broad regularity conditions under which the tail probability (6.14) may be approximated by a two-term asymptotic expansion. The metric tensor matrix $G(\mathbf{t})$ plays a geometric key role in the two-term expansion of the tail probability (Maes and Breitung, 1996):

$$\Pr(\max_{\mathbf{t}\in T} Z(\mathbf{t}) \geq \beta) \simeq P_1(\beta) + P_2(\beta) \tag{6.22}$$

- the first term is a volume term (the volume of the manifold is simply the integral of the measure $\|G(\mathbf{t})\|^{1/2}$ over the domain T):

$$P_1(\beta) = \int_T \theta_1(\beta, \mathbf{t}) \, \|G(\mathbf{t})\|^{1/2} \, d\mathbf{t} \tag{6.23}$$

  where the function $\theta_1(\beta, \mathbf{t})$ is defined as

$$\theta_1(\beta, \mathbf{t}) = \frac{1}{2\pi^{(d+1)/2}} \Gamma\left(\frac{d+1}{2}, \frac{\beta^2}{2\sigma^2(\mathbf{t})}\right) \tag{6.24}$$

  with $\Gamma(a, u)$ the incomplete gamma function

$$\Gamma(a, u) = \int_u^\infty x^{a-1} e^{-x} dx \tag{6.25}$$

- the second term of the approximation is:

$$P_2(\beta) = \int_T \theta_2(\beta, \mathbf{t}) \left(-\frac{S(\mathbf{t})}{2} - \frac{d(d-1)}{2} \right) \|G(\mathbf{t})\|^{1/2} \, d\mathbf{t} \tag{6.26}$$

where the function $\theta_2(\beta, \mathbf{t})$ is defined as:

$$\theta_2(\beta, \mathbf{t}) = \frac{1}{4\pi^{(d+1)/2}} \Gamma\left(\frac{d-1}{2}, \frac{\beta^2}{2\sigma_Z^2(\mathbf{t})}\right) \tag{6.27}$$

$S(\mathbf{t})$ is the intrinsic scalar curvature of the manifold at point $\mathbf{t}$. For a detailed mathematical description of $S(\mathbf{t})$, we refer the reader to Kreyszig (1968, p.310).

Notice that, when $Z(\mathbf{t})$ is homogeneous, $g_{ij}(\mathbf{t})$ is the corresponding second-order spectral moment of $Z(\mathbf{t})$, which does not depend on $\mathbf{t}$. As a consequence, such a random field has zero curvature S, which means that the second term $P_2(\beta)$ of the approximation (6.22) can be combined with the first one to yield:

$$P(\beta) = \int_T \left(\theta_1(\beta, \mathbf{t}) - \frac{d(d-1)}{2}\theta_2(\beta, \mathbf{t})\right) \|G(\mathbf{t})\|^{1/2} d\mathbf{t} \tag{6.28}$$

Two-Dimensional Random Fields

Two-dimensional random fields are frequently encountered in structural reliability problems. Therefore, the asymptotic results for this case are given here.

We have that the metric tensor matrix is simply the second moment matrix:

$$G(t_1, t_2) = \begin{vmatrix} \mathrm{var}\frac{\partial Z}{\partial t_1} & \mathrm{covar}\frac{\partial Z}{\partial t_1}\frac{\partial Z}{\partial t_2} \\ \mathrm{covar}\frac{\partial Z}{\partial t_1}\frac{\partial Z}{\partial t_2} & \mathrm{var}\frac{\partial Z}{\partial t_2} \end{vmatrix} \tag{6.29}$$

The approximation for $d = 2$ becomes:

$$\Pr\left(\max_{t \in T} Z(t_1, t_2) > \beta\right) \simeq \frac{1}{(2\pi)^{3/2}} \int\int \left[\Gamma\left(\frac{3}{2}, \frac{\beta^2}{2\sigma_Z^2(\mathbf{t})}\right)\right.$$

$$+\frac{1}{2}\Gamma\left(\frac{1}{2}, \frac{\beta^2}{2\sigma_Z^2(t)}\right)\Bigg]\left(-\frac{S(t)}{2}-1\right)\sqrt{\det G(t)}dt_1dt_2 \tag{6.30}$$

Once a suitable discretization is established for the random field $Z(t)$, computation of (6.30) is straightforward. Expressions (6.16) and (6.21) indicate how $\sigma_Z(t)$ and $g_{ij}(t)$ can easily be computed using the discretization functions and their derivatives. The only difference that might arise lies in the computation of the curvature term $S(t)$. However, a more detailed study of the problem is required to determine if this will be the case. Once the integrand in (6.30) is computed for a set of points (t_i, t_j), (6.30) can be evaluated numerically.

Chapter 7

Conclusions and Recommendations

7.1 Summary and Conclusions

In the present thesis, the computation of the maxima of random fields is studied. While traditional methods are based on upcrossings, Sun's Tube method yields direct approximations of the extreme value distribution of both homogeneous and non-homogeneous discretized random fields. The present work focuses on the one-dimensional case of stochastic processes.

In Chapter 2, the traditional method to approximate the extreme value distribution of a stochastic process is explained. The technique is based on upcrossings and provides an upperbound for the exceedance probability. It is shown that there is a limited number of stationary processes for which this method provides exact closed-form solutions.

In Chapter 3, several discretization methods are discussed. The common feature of these methods is that they all yield discretized stochastic processes in the format required to employ Sun's Tube Method. Of interest are:

- the linear combination of sine and cosine functions.

  The stochastic processes obtained using this method form an instructive tool for the understanding of the geometrical concepts of Sun's Tube Method.

- the discretization of earthquake signals and seismic structural responses.

The seismic discretization methods described in the present work enable the modeling of non-stationarity in both the time and the frequency domain. Next to the ground motion process itself, any stochastic response of a linear system subject to this ground motion process can be obtained in the required discrete format.

In Chapter 4, Sun's Method is studied in detail. The stochastic process is rewritten as the scalar product of a deterministic and a random vector. In doing so, the exceedance probability can be expressed as a geometrical problem. Results from Hoteling (1939) about the volumes of tubes around curves on spheres are used for geometrical measures on the N-dimensional unit sphere. Sun's approach can be used to compute other statistics related to the extreme value distribution of a stochastic process. It is indicated how conditional probabilities of exceedance, the rate of up-crossings, the cumulative excursion time and the duration of a single excursion can be computed.

In Chapter 5, Sun's Method is applied to both stationary and non-stationary processes:

- Sun's Tube Method is applied to a stationary process consisting of two discretization functions. This simple example explains the geometrical concepts on which Sun's Tube Method is based and illustrates the problems caused by self-overlap.

- The extreme value distribution of an earthquake signal is computed. The results are in good agreement with Monte Carlo simulation. Sun's Method underestimates the log(exceedance probability) by about 2.5 %. This error can

be explained by the discontinuity in the first derivative of the discretization functions of the earthquake signal.

- The present method is used to approximate the extreme value distribution of a linear stochastic response to an earthquake signal. Comparison of the results obtained using Sun's Tube Method with simulation results show that the results are exceptionally good. Sun's Method underestimates the log(exceedance probability) by about 0.6 %. This can be explained by the fact that the discretization functions of the stochastic response now have a continuous first derivative, since they are obtained by convolution of a function with a discontinuous first derivative and a unit-impulse-response function. This accurate estimate is a very positive result, because, in engineering applications, the maxima of stochastic responses are the variables of interest in assessing safety and reliability.

In Chapter 6, two extensions of Sun's Tube Method are given. The application of Sun's Tube Method to compute the extreme value distribution of non-linear stochastic responses is discussed. It is indicated how the method can be used to approximate the maxima of higher-dimensional random fields.

The disadvantages of Sun's Tube Method are:

- The problems of self-overlap and jumps cannot be identified a priori. They can however be diagnosed
- The method is tied to discretized stochastic processes.

The main advantages of Sun's Tube Method are:

- The new approach gives direct approximations of the extreme value distribution of a stochastic process without any assumptions about point-processes and treshold crossings.
- The method is suitable for any type of stochastic process, as long as the coefficients in the discretization are standard normal random variables. This is the preferred way of discretizing anyway.
- The maxima of both stationary and non-stationary processes can be approximated.
- The method produces accurate results with little computational effort.

7.2 Recommendations for Future Research

Based on the work done in the present study, we can conclude that Sun's Tube Method has a great potential. The most important future developments should focus on applying Sun's Tube Method to the computation of:

- the distribution and moments of random variables associated with the maximum of a stochastic process
- the extreme value distribution of non-linear stochastic responses
- the maxima of higher-dimensional random fields

The Distribution and Moments of Random Variables Associated with the Maximum of a Stochastic Process

In Section 4.5, it is indicated how Sun's approach can be used to compute statistics associated with the extreme value distribution of a stochastic process. Before the concept outlined in that Section can be used, an expression has to be derived for the surface area of the intersection of two spherical caps on the unit-sphere. There are two possible ways to solve this mathematical problem. One way is to use Monte Carlo simulation to estimate the surface area of the intersection. While it is guaranteed that this approach will yield a result, it might not be a very efficient way. Preferably, a closed form expression should be derived. For this purpose, an in-depth study of the geometry in higher dimensions will be required.

The Extreme Value Distribution of Non-Linear Stochastic Responses

In Section 6.1, it is discussed how Sun's Method can be applied to approximate the extreme value distribution of non-linear responses. The quality of those approximations has to be assessed by comparing them with other existing approximation techniques or with the exceedance probabilities obtained using Monte Carlo simulation. The problem of using other approximation techniques to test the accuracy of Sun's Tube Method is that one cannot determine if differences between the two approximation methods actually mean that one method is superior to the other. Monte Carlo simulation of the maxima of non-linear stochastic responses is a computationally tedious task. The methods discussed in Section 5.4.2 to improve the efficiency of the simulation of linear stochastic responses can no longer be used, because these methods are based on the linearity of the filter. In the case of a non-linear filter, two

steps are required for the simulation of each maximum. First, a sample of the ground acceleration process has to be generated. Since the filter representing the local soil behavior is assumed to be linear, the techniques discussed in Section 5.3.2 to improve the efficiency of the simulation can still be employed. Next, the response of the non-linear filter to this input process has to be determined. This requires a deterministic solution of the equation of motion. These two steps have to be repeated for each simulation. This simulation may be cumbersome but it is the only means to assess the absolute quality of the approximations obtained by Sun's Method. However, if the degree of non-linearity is not too large, then there is no reason to believe that the application of Sun's Tube Method to compute the extreme value distribution will cause any problems.

The Maxima of Higher-Dimensional Random Fields

Another large field of further study is the application of Sun's Method to higher-dimensional random fields (See Section 6.2). The first step is to derive the expression for the intrinsic scalar curvature (6.2.3). Once this expression is established, application of Sun's formula becomes straightforward. The estimates obtained using Sun's Tube Method have to be compared with Monte Carlo simulation results or with other existing approximations.

Bibliography

[1] Abramowitz, M. and Stegun, I.A., 1972, *Handbook of Mathematical Functions.* Dover Publications, New York.

[2] Adler, R.J., 1981, *The Geometry of Random Fields.* Wiley, New York.

[3] Adler, R.J., 1990, *An Introduction to Continuity, Extrema, and Related Topics for General Gaussian Processes.* IMS, Hayward.

[4] Breitung, K., 1990, *The Extreme Value Distribution of Non-Stationary Vector Processes.* Proceedings ICOSSAR '89, 5th International Conference on Structural Safety and Reliability, Vol. II, pp1327-1332.

[5] Breitung, K., 1994, *Asymptotic Approximations for Probability Integrals.* Springer, Berlin.

[6] Breitung, K., Maes, M.A., and Huyse, L., 1995, *The Computation of Maxima of Non-Stationary Gaussian Processes*, Proceedings First Intl. Conference on Engineering Computing and Simulation, Changsha, China, November.

[7] Clough, R.W. and Penzien, P., 1975, *Dynamics of Structures.* McGraw-Hill, New York.

[8] Cramer, H. and Leadbetter, M.R., 1967, *Stationary and Related Stochastic Processes.* Wiley, New York.

[9] Der Kiureghian, A. and Li, C-C., 1996, A New Method for Seismic Reliability Assessment of Nonlinear Structures. Chapter 5 in *Reliability-Based Optimal*

Aseismic Design of Reinforced Concrete Buildings. A. H-S. Ang, et Al. (Eds.), Final Technical Report, CUREe - Kajima Research Project, Phase 2, pp101-142.

[10] Hagen, O., and Tvedt, L., 1991, *Vector Process Out-Crossing as Parallel System Sensitivity Measure*, J. Eng. Mech., ASCE, vol. 117, pp2201-2220.

[11] Hohenbichler, M. and Rackwitz, R., 1981, *Non-normal Dependent Vectors in Structural Safety.* J. Eng. Mech., ASCE, vol. 107, pp1227-1238.

[12] Hoteling, H., 1939, *Tubes and Spheres on n-spaces and a Class of Statistical Problems.* Am. J. of Mathematics, Vol. 61, pp 440-460.

[13] Johnson, N. and Kotz, S., 1972, *Continuous Univariate Distributions.* Wiley, New York.

[14] Kendall, M.G., 1961, *A Course in the Geometry of n Dimensions.* Griffin's Statistical Monographs and Courses.

[15] Kreyszig, E., 1968, *Introduction to Differential Geometry and Riemannian Geometry.* University of Toronto Press.

[16] Leadbetter, M.R., Lindgren G., and Rootzén, 1983, *Extremes and Related Properties of Random Sequences and Processes.* Springer, New York.

[17] Li, C-C. and Der Kiureghian, A., 1993, *Optimal Discretization of Random Fields.* Journal of Engineering Mechanics, 119(6), pp1136-1154.

[18] Lin, Y.K., 1967, *Probabilistic Theory of Structural Dynamics*, McGraw-Hill, New York, and Krieger Pub., Huntington.

[19] Maes, M.A., and Breitung, K.W., 1996, *Direct Approximation of the Extreme Value Distribution of Non-Homogeneous Gaussian Random Fields.* Proceedings of the 15th Intl. Conference on Offshore Mechanics and Arctic Engineering, Vol.2, pp103-109.

[20] Mura, T. and Koya, T., 1992, *Variational Methods in Mechanics.* Oxford University Press.

[21] Papoulis, A., 1991, *Probability, Random Variables and Stochastic Processes,* McGraw-Hill, New York, 3rd edition.

[22] Rice, S.O., 1944, *Mathematical Analysis of Random Noise.* Bell System. Tech. J., Vol.23, pp 282-332.

[23] Rice, S.O., 1945, *Mathematical Analysis of Random Noise.* Bell System. Tech. J., Vol.24, pp 46-156.

[24] Ross, S.M., 1990, *A Course in Simulation.* Macmillan, New York.

[25] Rubinstein, R.Y., 1981, *Simulation and the Monte Carlo Method.* Wiley, New York.

[26] Roy, R.C.Jr., 1981, *Structural Dynamics, An Introduction to Computer Methods.* Wiley, New York.

[27] Sommerville, D.M.Y., 1958, *An Introduction to the Geometry of N dimensions.* Dover Publications, New York.

[28] Sun, J., 1993, *Tail Probabilities of the Maxima of Gaussian Random Fields.* Annals of Probability, 21(1), pp 34-71.

[29] Weyl, H., 1939, *On the Volume of Tubes.* Am. J. of Mathematics, Vol. 61, pp 461-472.

[30] Zhang, Y., and Der Kiureghian, A., (1993). *Two improved algorithns for reliability analysis.* Proceedings, 6th IFIP WG 7.5 Working Conference on Structural Reliability and Optimization, Assisi, Italy, September 1994 (Rackwitz, R., G. Augusti, E. Borri, Eds.), Chapman and Hall, New York.

Appendix A

Discretization Function Obtained by Minimizing Error Variance

The expression for the error variance is

$$\mathbb{E}\left(\left|X(t)-\hat{X}(t)\right|^2\right) \tag{A.1}$$

$\hat{X}(t)$ is the filter response obtained by discretization of the white noise input (See Section 3.4):

$$\hat{X}(t) = \sum_{i=1}^{N} W_i a_i(t) \tag{A.2}$$

$$W_i = \int_{t_{i-1}}^{t_i} W(t) \qquad i = 1, 2, ..., N \tag{A.3}$$

$X(t)$ is the exact solution of the filter response to the white noise input (See Clough and Penzien, 1975):

$$X(t) = \int_0^t W(\tau)\, h(t-\tau)\, d\tau \tag{A.4}$$

where $h(t)$ is the unit-impulse-response function of the filter.

Equations (A.2) and (A.4) are inserted in the expression for the error variance

(A.1):

$$\begin{aligned} & \mathbb{E}\left(\left|X(t)-\hat{X}(t)\right|^2\right) \\ = \; & \mathbb{E}\left(\left(\int_0^t W(\tau)\,h(t-\tau)\,d\tau\right)^2\right) \\ & -2\sum_{i=1}^{N} a_i(t)\,\mathbb{E}\left(W_i\cdot\int_0^t W(\tau)\,h(t-\tau)\,d\tau\right) \\ & +\sum_{i=1}^{N} a_i^2(t)\,\mathbb{E}\left(W_i^2\right). \end{aligned} \tag{A.5}$$

In order to minimize the error variance, Equation (A.5) is derived with respect to $a_i(t)$:

$$\frac{\partial}{\partial a_i(t)}\left[\mathbb{E}\left(\left|X(t)-\hat{X}(t)\right|^2\right)\right] = 0 \tag{A.6}$$

$$\Updownarrow$$

$$-2\mathbb{E}\left(W_i\cdot\int_0^t W(\tau)\,h(t-\tau)\,d\tau\right)+2a_i(t)\,\mathbb{E}\left(W_i^2\right) = 0$$

$$i = 1,2,...,N \tag{A.7}$$

Equation (A.7) can now be solved for $a_i(t)$:

$$a_i(t)=\frac{\mathbb{E}\left(W_i\cdot\int_0^t W(\tau)\,h(t-\tau)\,d\tau\right)}{\mathbb{E}\left(W_i^2\right)} \qquad i=1,2,...,N \tag{A.8}$$

First, the denominator is calculated. Using (A.3), we have that

$$\mathbb{E}\left(W_i^2\right) = \mathbb{E}\left(\int_{t_{i-1}}^{t_i}\int_{t_{i-1}}^{t_i} W(\tau_1)\,W(\tau_2)\,d\tau_2 d\tau_1\right) \tag{A.9}$$

$$= \int_{t_{i-1}}^{t_i}\int_{t_{i-1}}^{t_i} \mathbb{E}\left(W(\tau_1)\,W(\tau_2)\right)d\tau_2 d\tau_1 \tag{A.10}$$

The autocorrelation function of white noise (Clough and Penzien, 1975) is given by

$$R(\tau) = \mathbb{E}(W(t)\,W(t+\tau)) = 2\pi\Phi_0\delta(\tau) \tag{A.11}$$

where Φ_0 is the intensity of the white noise and $\delta(\tau)$ is the Dirac impulse function defined by

$$\delta(t-\tau) = \begin{cases} 0 & t \neq \tau \\ \infty & t = \tau \end{cases} \qquad \int_{-\infty}^{\infty} \delta(t-\tau)\,dt = 1 \tag{A.12}$$

With this expression for the autocorrelation function of white noise (A.11), Equation (A.10) can be written as:

$$\begin{aligned} \mathbb{E}\left(W_i^2\right) &= 2\pi\Phi_0 \int_{t_{i-1}}^{t_i}\int_{t_{i-1}}^{t_i} \delta(\tau_2-\tau_1)\,d\tau_2 d\tau_1 \\ &= 2\pi\Phi_0 \int_{t_{i-1}}^{t_i} d\tau_1 \\ &= 2\pi\Phi_0\Delta t \end{aligned} \tag{A.13}$$

Next, the numerator of (A.8) is further examined. Using (A.3), we can write that:

$$\begin{aligned} & \mathbb{E}\left(W_i \cdot \int_0^t W(\tau)\,h(t-\tau)\,d\tau\right) \\ = \; & \mathbb{E}\left(\int_{t_{i-1}}^{t_i}\int_0^t W(\tau_1)\,W(\tau_2)\,h(t-\tau_2)\,d\tau_2 d\tau_1\right) \\ = \; & \int_{t_{i-1}}^{t_i}\int_0^t \mathbb{E}(W(\tau_1)\,W(\tau_2))\,h(t-\tau_2)\,d\tau_2 d\tau_1 \end{aligned} \tag{A.14}$$

The expression for the autocorrelation function of white noise (A.11) is inserted in

equation (A.14) to yield

$$\begin{aligned} & \mathbb{E}\left(W_i \cdot \int_0^t W(\tau)\, h(t-\tau)\, d\tau\right) \\ = \; & 2\pi\Phi_0 \int_{t_{i-1}}^{t_i} \int_0^t \delta(\tau_2 - \tau_1)\, h(t-\tau_2)\, d\tau_2 d\tau_1 \end{aligned} \tag{A.15}$$

Three different cases can be considered:

1. $t < t_{i-1}$

   In this case, the two integration intervals $[t_{i-1}, t_i]$ and $[0, t]$ in expression (A.15) do not overlap. Therefore, from the definition of the Dirac impulse function (A.12), it follows that expression (A.15) equals zero.

2. $t_{i-1} \leq t < t_i$

   In this case, the integration interval $[t_{i-1}, t_i]$ in (A.15) is split into $[t_{i-1}, t]$ and $[t, t_i]$:

$$\begin{aligned} & 2\pi\Phi_0 \underbrace{\int_{t_{i-1}}^{t} \int_0^t \delta(\tau_2 - \tau_1)\, h(t-\tau_2)\, d\tau_2 d\tau_1}_{=\int_{t_{i-1}}^{t} h(t-\tau_1) d\tau_1} \\ & +2\pi\Phi_0 \underbrace{\int_{t}^{t_i} \int_0^t \delta(\tau_2 - \tau_1)\, h(t-\tau_2)\, d\tau_2 d\tau_1}_{=0} \end{aligned} \tag{A.16}$$

3. $t \geq t_i$

   In this case, the integration interval $[0, t]$ in (A.15) is divided into three intervals

$[0, t_{i-1}]$, $[t_{i-1}, t_i]$ and $[t_i, t]$:

$$2\pi\Phi_0 \underbrace{\int_{t_{i-1}}^{t_i}\int_{0}^{t_{i-1}} \delta(\tau_2-\tau_1)\, h(t-\tau_2)\, d\tau_2 d\tau_1}_{=0}$$

$$+2\pi\Phi_0 \underbrace{\int_{t_{i-1}}^{t_i}\int_{t_{i-1}}^{t_i} \delta(\tau_2-\tau_1)\, h(t-\tau_2)\, d\tau_2 d\tau_1}_{=\int_{t_{i-1}}^{t_i} h(t-\tau_1)d\tau_1} \tag{A.17}$$

$$+2\pi\Phi_0 \underbrace{\int_{t_{i-1}}^{t_i}\int_{t_i}^{t} \delta(\tau_2-\tau_1)\, h(t-\tau_2)\, d\tau_2 d\tau_1}_{=0} \tag{A.18}$$

The above expressions for the numerator and the expression for the denominator (A.13) are inserted in (A.8). We can conclude that:

$$a_i(t) = \frac{1}{\Delta t}\int_{\min(t,\, t_{i-1})}^{\min(t,\, t_i)} h(t-\tau_1)\, d\tau_1 \qquad i = 1, 2, ..., N \tag{A.19}$$

Appendix B

Computation of Probability Associated with Endpoints and Discontinuities

In Section B.1, an expression is derived for the surface of a spherical cap on the unit-sphere. In Section B.2, this expression is used to compute the additional probability using the relative frequency approach as explained in Section 4.2.2. For simplicity of notation, the derivation is given for the additional probability at the endpoints of the process. Extension to probabilities associated with possible discontinuities in the path of the vector $\mathbf{f}(t) / |\mathbf{f}(t)|$ is straightforward.

B.1 Surface of a Spherical Cap on the Unit Sphere

Let S_θ^N, a spherical cap around a fixed point $\mathbf{y} = (y_1, y_2, ..., y_N)$ on the N-dimensional unit sphere S^N be defined as the locus of a point $\mathbf{x}$ so that:

$$S_\theta^N = \left\{ \mathbf{x} : \mathbf{x} = (x_1, x_2, ..., x_N), \sum_{i=1}^{N} x_i^2 = 1 \text{ and } \widehat{\mathbf{yx}} \leq \theta \right\} \tag{B.1}$$

where $\widehat{\mathbf{yx}}$ is the angle between the vectors $\mathbf{y}$ and $\mathbf{x}$. The angle θ denotes the angle between the centre and the border of the cap. To compute the surface area $\mathbf{A}\left(S_\theta^N\right)$ of this cap, we use the theorem (Sommerville,1958, p.138) that the surface of a variety

of revolution of species $N-2$ generated by a curve

$$x_{N-1}^2 = f(x_N) \tag{B.2}$$

rotating about the axis of x_N is given by

$$\frac{(N-1)\,\pi^{\frac{1}{2}(N-1)}}{\Gamma\left(\frac{N+1}{2}\right)} \int_\alpha^\beta \{f(x_N)\}^{\frac{1}{2}(N-2)}\, dx_N \tag{B.3}$$

In this case, the generating curve is

$$x_{N-1}^2 = 1 - x_N^2 \qquad \text{for} \qquad \cos\theta \le x_N \le 1 \tag{B.4}$$

Inserting this expression for the generating curve (B.4) in (B.3) gives the following expression for the surface area $\mathbf{A}\left(S_\theta^N\right)$ of a spherical cap with top angle θ:

$$\mathbf{A}\left(S_\theta^N\right) = \frac{(N-1)\,\pi^{\frac{1}{2}(N-1)}}{\Gamma\left(\frac{N+1}{2}\right)} \int_0^\theta \sin^{N-2} x dx \tag{B.5}$$

Using

$$\Gamma(z) = (z-1)\,\Gamma(z-1) \tag{B.6}$$

equation (B.5) can be written as:

$$\mathbf{A}\left(S_\theta^N\right) = \frac{2\pi^{\frac{1}{2}(N-1)}}{\Gamma\left(\frac{N-1}{2}\right)} \int_0^\theta \sin^{N-2} x dx \tag{B.7}$$

B.2 Probability Associated with Endpoints

Samples of the random vector **U** lying in one of the two hemi-spherical caps at the endpoints of the path of the vector $\mathbf{f}(t)/|\mathbf{f}(t)|$ will result in stochastic processes with a maximum greater than β. Therefore, the area of these two hemi-spherical caps has to be added to the area of the tube $T^N_{\beta,r}$ in equation (4.34), so that we now obtain:

$$P(\beta|\, R_N = r) = \frac{\mathbf{A}\left(T^N_{\beta,r}\right)}{\mathbf{A}\left(S^N\right)} + \frac{1}{2}\frac{\mathbf{A}\left(S^N_{\theta_0}\right)}{\mathbf{A}\left(S^N\right)} + \frac{1}{2}\frac{\mathbf{A}\left(S^N_{\theta_T}\right)}{\mathbf{A}\left(S^N\right)} \tag{B.8}$$

The top angles θ_0 and θ_T are defined by expression (4.29):

$$\theta_0 = \begin{cases} \arccos\left(\frac{\beta}{|\mathbf{f}(0)|r}\right), & (\beta/(|\mathbf{f}(0)|r)) \leq 1 \\ 0, & (\beta/(|\mathbf{f}(0)|r)) > 1 \end{cases} \tag{B.9}$$

$$\theta_T = \begin{cases} \arccos\left(\frac{\beta}{|\mathbf{f}(T)|r}\right), & (\beta/(|\mathbf{f}(T)|r)) \leq 1 \\ 0, & (\beta/(|\mathbf{f}(T)|r)) > 1 \end{cases} \tag{B.10}$$

Let $P_{add}(\beta)$ denote the additional probability associated with the endpoints. Following the same reasoning as in Section 4.2, we can write that

$$P_{add}(\beta) = \underbrace{\frac{1}{2}\int_{\beta/|\mathbf{f}(0)|}^{\infty} \frac{\mathbf{A}\left(S^N_{\theta_0}\right)}{\mathbf{A}\left(S^N\right)} f_{\chi_N}(r)\, dr}_{P^0_{add}(\beta)} + \underbrace{\frac{1}{2}\int_{\beta|\mathbf{f}(T)|}^{\infty} \frac{\mathbf{A}\left(S^N_{\theta_T}\right)}{\mathbf{A}\left(S^N\right)} f_{\chi_N}(r)\, dr}_{P^T_{add}(\beta)} \tag{B.11}$$

In this Appendix, the derivation for the computation of $P^0_{add}(\beta)$ in expression (B.11) is given. The computation of $P^T_{add}(\beta)$ is analogous. Combining expressions (B.7),

(4.9), (B.9) and (4.33) gives the following expression for $P^0_{add}(\beta)$:

$$P^0_{add}(\beta) = \frac{2^{1-\frac{N}{2}}}{\Gamma\left(\frac{N-1}{2}\right)\sqrt{\pi}} \int_{\beta/|\mathbf{f}(0)|}^{\infty} \left(\int_0^{\theta_0} \sin^{N-2} x dx \right) r^{N-1} \exp\left(-\frac{r^2}{2}\right) dr \qquad \text{(B.12)}$$

Changing the order of integration gives:

$$P^0_{add}(\beta) = \frac{2^{1-\frac{N}{2}}}{\Gamma\left(\frac{N-1}{2}\right)\sqrt{\pi}} \int_0^{\pi/2} \sin^{N-2} x \left(\int_{\beta/(|\mathbf{f}(0)|\cos x)}^{\infty} r^{N-1} \exp\left(-\frac{r^2}{2}\right) dr \right) dx \qquad \text{(B.13)}$$

First we will compute

$$\frac{d}{d\beta}\left(P^0_{add}(\beta)\right) \qquad \text{(B.14)}$$

Using

$$\frac{d}{d\beta}\left(\int_{a(c)}^{b(c)} f(x,c)\, dx \right) = \int_{a(c)}^{b(c)} \left[\frac{\partial}{\partial c} f(x,c) \right] dx + f(b,c)\frac{\partial b}{\partial c} - f(a,c)\frac{\partial a}{\partial c} \qquad \text{(B.15)}$$

we obtain that

$$\frac{d}{d\beta}\left(P^0_{add}(\beta)\right) = -\frac{2^{1-\frac{N}{2}}}{\Gamma\left(\frac{N-1}{2}\right)\sqrt{\pi}} \frac{\beta^{N-1}}{|\mathbf{f}(0)|^N} \int_0^{\pi/2} \frac{\sin^{N-2} x}{\cos^N x} \exp\left(-\frac{1}{2}\left(\frac{\beta}{|\mathbf{f}(0)|\cos x}\right)^2\right) dx \qquad \text{(B.16)}$$

Making the substitution

$$x \to v = \frac{1}{2}\left(\frac{\beta \tan x}{|\mathbf{f}(0)|}\right)^2 \qquad \text{(B.17)}$$

gives

$$\frac{d}{d\beta}\left(P^0_{add}(\beta)\right) = -\frac{\exp\left(-\frac{1}{2}\left(\frac{\beta}{|\mathbf{f}(0)|}\right)^2\right)}{\sqrt{2\pi}|\mathbf{f}(0)|^2\Gamma\left(\frac{N-1}{2}\right)} \underbrace{\int_0^{\infty} v^{\frac{N-3}{2}} \exp(-v)\, dv}_{=\Gamma\left(\frac{N-1}{2}\right)}$$

$$= -\frac{1}{\sqrt{2\pi}\,|\mathbf{f}(0)|}\exp\left(-\frac{1}{2}\left(\frac{\beta}{|\mathbf{f}(0)|}\right)^2\right) \tag{B.18}$$

By integration of $\frac{d}{d\beta}\left(P^0_{add}(\beta)\right)$, we find that:

$$P^0_{add}(\beta) = \int_{-\infty}^{\beta}\frac{d}{d\beta}\left(P^0_{add}(\gamma)\right)d\gamma + \underbrace{P^0_{add}(-\infty)}_{=1} \tag{B.19}$$

$$= -\frac{1}{\sqrt{2\pi}\,|f(0)|}\int_{-\infty}^{\beta}\exp\left(-\frac{1}{2}\left(\frac{\gamma}{|\mathbf{f}(0)|}\right)^2\right)d\gamma + 1 \tag{B.20}$$

$$= -\frac{1}{\sqrt{2\pi}}\int_{-\infty}^{\beta/|\mathbf{f}(0)|}\exp\left(-\frac{1}{2}\left(\frac{\rho}{|\mathbf{f}(0)|}\right)^2\right)d\rho + 1 \tag{B.21}$$

$$= -\Phi\left(\frac{\beta}{|\mathbf{f}(0)|}\right) + 1 \tag{B.22}$$

$$= \Phi\left(-\frac{\beta}{|\mathbf{f}(0)|}\right) \tag{B.23}$$

In a similar way, it can be proven that

$$P^0_{add}(\beta) = \Phi\left(-\frac{\beta}{|\mathbf{f}(T)|}\right) \tag{B.24}$$

B.3 Probability Associated with Discontinuities

The derivation of the expression for probabilities associated with discontinuities is analogous to the proof in Section B.2.